Maskless Parallel Patterning with Zone Plate Array Lithography (ZPAL)

by

Darío Gil

B.E, Stevens Institute of Technology, 1998

Submitted to the Department of Electrical Engineering and Computer Science in partial fulfillment of the requirements for the degree of

Master of Science in Electrical Engineering and Computer Science

at the

MASSACHUSETTS INSTITUTE OF TECHNOLOGY

June, 2000

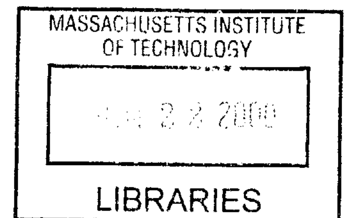

©2000 Massachusetts Institute of Technology
All rights reserved

Author.........................
Department of Electrical Engineering and Computer Science
April.19 , 2000

Certified by...............
Henry I. Smith
Keithley Professor of Electrical Engineering
Thesis Supervisor

Accepted by...........
Arthur C. Smith
Chairman, Department Committee on Graduate Studies

Maskless Parallel Patterning with Zone Plate Array Lithography (ZPAL)

By

Darío Gil

Submitted to the Department of Electrical Engineering and Computer Science
on April 19, 2000 in partial fulfillment
of the requirements for the degree of
Master of Science

Abstract

The ever increasing demand in lithography for finer features while increasing the throughput is pushing the level of complexity and the cost of lithography tools to unprecedented levels. The work presented in this thesis, Zone-Plate-Array Lithography (ZPAL), is a promising maskless technology that should be capable of reaching the limits of the lithographic process, while maintaining the cost of the tool at reasonable levels. An experimental ZPAL system at UV wavelengths has been constructed and used to simultaneously expose nine different patterns with a 3X3 array of zone plates in a quasi-dot-matrix fashion. The design and construction of the UV-ZPAL system is described in detail, as well as the theory and fabrication of zone plate arrays. In addition, a parallel confocal microscope employing the same array of zone plates used for exposing patterns has been built, and images have been taken with it. The microscope has added significant functionality to the system, enabling accurate control of the separation between the zone-plate array and the wafer, as well as providing the possibility of level-to-level alignment. Future areas of development for ZPAL are also addressed, with special emphasis on micromechanics and system optimization.

Thesis Supervisor: Professor Henry I. Smith
Title: Keithly Professor of Electrical Engineering

Acknowledgments

First and foremost I want to express my gratitude to Professor Henry Smith for believing in me from the beginning. His contagious enthusiasm is both motivational and inspirational. For the past two years he has always been supportive in all the matters that I presented to him, always encouraging me to work with joy and pride. It is truly an honor to be part of his laboratory. I greatly appreciate his constant flow of novel ideas, and look forward to the remaining years of my graduate studies to continue my education under his supervision.

The project described in this thesis, ZPAL, is very much a team effort, comprised of David Carter, Rajesh Menon and myself. I can not thank Dave enough for all I have learned from him in the past years. He is a terrific engineer with a great breath of knowledge that he is always willing to share with others. I will forever remember that night in May 99, a week prior to 3Beams, trying to get results at three in the morning listening to Sinatra in the lab to try to remain awake. I know we both felt ecstatic when the patterns came out and we looked at them in the SEM at 7 am. That morning, while biking home, I felt that all the hard work of the previous year had finally paid off.

It has always been a pleasure to work with Rajesh Menon. His achievements in simulations have been terrific, but above all, I am grateful for having become his friend. I particularly enjoy our late afternoon tea breaks, as well as our almost daily discussions of the news. I am looking forward to having many more of them.

Todd Hastings and Mike Walsh have been great office-mates. It was always great to have our conversations about what is like to be graduate students, what we like, what we don't, what needs to be changed, etc. It is through sharing thoughts like these that I felt I was not alone in this endeavor, realizing that the good and the bad times are also shared by many others.

I thank Tim Savas for his always excellent advice about the many optics questions that I have asked him in the past two years. I thank Paul Konkola for sharing with the ZPAL team his expertise in mechanical engineering. I have always thought Tom Murphy deserves an extra pay for his outstanding job in maintaining the Nano-server and solving

the daily storm of computer questions from all of us. Thank you very much for your patience and help.

I'd like to express my thanks to the staff members of the NSL. It has been a pleasure to work with them. I especially would like to thank Mark Mondol for helping me write the zone plates that were used to obtain the results presented in this thesis. I particularly appreciate his good nature and his constant willingness to help to make things better for all of us. I also would like to thank Jim Daley and Jimmy Carter for all their advice, training and help offered to me in the past two years. My gratitude also goes to James Goodberlet for his always helpful comments. Keinchi Murooka was a great asset to the group during his stay at MIT. He provided me with help that ranged from solid-state physics, to circuit design, to optical design, always with a smile on his face. Thanks also go to Cindy Lewis for her efficient administration.

NSL is a great laboratory with terrific students. Interactions with Maya Farhoud, Mike Lim, Alex Bernshteyn, Carl Chen, Euclid Moon, Feng Zhang, and Mark Finlayson have been instrumental in the achievements reported in these pages. A word of gratitude goes to Ihsan Djomehri for his transfer of ZPAL knowledge to me when I arrived to MIT. Special thanks go to Juan Ferrera for his kind advice and for the many conversations we had in the past year. I no longer have anyone to talk to in Spanish, and that is a loss.

From my *alma matter* my thanks and my appreciation go to Prof. Traugott Fischer for introducing me to the wonders of research. His support was instrumental in my coming to MIT, for which I will be forever grateful.

MIT wouldn't have been nearly as enjoyable without my great friend Paul Herz. Through the many classes taken together and an unforgettable trip to Spain I have gotten to know him and value his generosity and kind spirit.

To my friend and soul mate Dave Grewal I don't have enough words to express how happy I am we are such good friends. I am glad we can now see each other frequently. Our common love for books and bookstores, for classical music and good conversations makes me feel very fortunate to have a friend that shares so many of my passions.

I am very grateful for having a wonderful family that has supported me throughout my entire life. The hardest part of being at MIT has been, without question,

being away from them. I miss them terribly. I miss their never-ending joy and passion for life. I wish we could see more of each other.

To all the Godsoes and Rathbuns I thank you for all the support you have provided me while being away from home. I am very happy to be a member of your family.

But above all, I want to thank my wonderful wife Amanda. She is the best thing that has ever happened to my life, the reason for my happiness. If there is something that excites me more than our past together, it is the great future that is ahead of us. Whether is in our loved New York, or in Madrid or in Rome, it won't matter as long as we are together. I love you very much.

A La Tejera,

por su Vía Láctea

Contents

Preface **19**

1 Next Generation Lithographies (NGL's) **21**

1.1 The present...23

1.2 The economics...24

1.3 The future...24

1.4 Extreme Ultra Violet Lithography (EUVL)...25

1.4.1 EUVL Exposure Tool...29

1.5 From electron beam lithography to SCALPEL...30

1.6 SCALPEL...31

1.6.1 Commercialization of SCALPEL...34

1.7 X-ray lithography...34

1.8 Conclusions...37

2 Zone Plate Array Lithography (ZPAL) **39**

2.1 Introduction...39

2.2 The radiation source...40

2.3 The micromechanics...43

2.4 Zone plates....44

2.5 The stage....45

3 Zone Plates **47**

3.1 A brief history of zone plates....47

3.2 Zone plate theory....51

3.2.1 Geometry of zone plates....51

3.2.2 Zone plate design....52

3.2.2.1 UV zone plate design....53

3.3 Zone plate fabrication....56

3.2.1 Fabrication of UV-zone plates - Calculations....58

3.2.2 Fabrication of UV-zone plates - Processing....62

3.4 Zone Plate Efficiencies, Background and the Need for Stops....65

3.4.1 The effect of stops....71

4 ZPAL System Design and Construction **75**

4.1 System Components....75

4.2 The laser....76

4.2.1 The right polarization for ZPAL....77

4.2.2 Power stabilization....79

4.2.3 Cleaning and expanding the beam....82

4.3 The micromechanics....85

4.3.2 Electronic Operation....86

4.3.3 Addressing....87
4.3.4 Gray scaling....90
4.4 Projection optics: achieving a 1 to 1 mapping of micromirrors to zone plates....94
4.5 Making the Zone-Plate-Array parallel to and properly spaced from the substrate....94
4.5.1 The white light Michelson interferometer....95
4.5.2 Capacitive gapping....97
4.5.3 Gapping with Zone Plates....100
4.6 Scanning the substrate....104
4.7 Conclusion....105

5 Pattern exposures and microscopy results 107

5.1 Finding the right dose....107
5.2 Design and implementation of the experiment to produce arbitrary patterns...108
5.3 Exposure results....110
5.4 UV-Microscopy with a zone-plate array....114
5.4.1 Microscopy results....115
5.4.2 Speed....119
5.4.3 Applications of the Zone-Plate-Array Confocal Microscope....119

6 Optimization and Extendibility of ZPAL 123

6.1 Modeling the throughput of ZPAL....123

6.1.1 Increasing throughput by increasing the number of zone plates...........128

6.1.2 Increasing throughput by faster addressing of the micromechanics......129

6.2 Extendibility of ZPAL: the move to shorter wavelengths.........................132

7 Conclusions and Future Work **137**

Appendix A Zone Plate Fabrication **141**

References **147**

List of Figures

Figure 1- 1. Exposure tool cost vs. time 22

Figure 1- 2. Semiconductor Industry Association (SIA) National Roadmap for Lithography 1999. 25

Figure 1- 3. Multilayer mirrors 27

Figure 1- 4. Standing wave field 28

Figure 1- 5. EUV projection system 29

Figure 1- 6. Scalpel schematic 31

Figure 1- 7. SCALPEL principle of operation 32

Figure 1- 8. The SCALPEL mask 33

Figure 1- 9. X-ray lithography 35

Figure 2 - 1. ZPAL schematic 40

Figure 2 - 2. Role of micromechanics in ZPAL.. 43

Figure 2 - 3. Shutters as a multiplexing scheme for ZPAL 44

Figure 2 - 4. A zone plate 45

Figure 3 - 1. The Fresnel Zones 48

Figure 3 - 2. Zone plate schematic 50

Figure 3 - 3. Zone plate geometry 51

Figure 3 - 4. 3D mesh of Outer Zone Width vs. Focal length vs. Number of zones 55

Figure 3 - 5. Contour plots for UV-Zone Plate Design 57

Figure 3 - 6. Phase Zone Plate 59

Figure 3 - 7. Need for Chrome.. 61

Figure 3 - 8. Process flow of UV Zone Plates 63

Figure 3 - 9. Scanning Electron Micrographs of Zone Plate Set 3 from Table 3- 1 (PMMA on quartz).. 64

Figure 3 - 10. Zone Plate Orders 66

Figure 3 - 11. Worst Case Contrast 68

Figure 3 - 12. Zone Plate with Stops 72

Figure 3 - 13. Contrast vs. normalized stop height, *l*, for amplitude and phase zone plates 74

Figure 4- 1. He-Cd Laser Schematic 77

Figure 4- 2. 1/4 wave plate 78

Figure 4- 3. Circular polarization detection scheme 80

Figure 4- 4. Optics for laser power control. 81

Figure 4- 5. Block diagram of power feedback 82

Figure 4- 6. Gaussian profile of 442nm He-Cd laser 82

Figure 4- 7. Measured beam profile of He-Cd laser @ λ=442 nm 83

Figure 4- 8. Spatial filter and expansion optics 84

Figure 4- 9. Micromechanics for UV-ZPAL 86

Figure 4- 10. TI DLM Technology........ 87

Figure 4- 11. Addressing of TI micromirrors........ 89

Figure 4- 12. Gray scaling for ZPAL........ 90

Figure 4- 13. Pulse Width Modulation (PWM)........ 92

Figure 4- 14. Low bandwidth PWM scheme for TI micromirrors........ 93

Figure 4- 15. Images of UV-zone plates as illuminated from the back with 442 nm light reflected off the micromirror array and imaged onto the zone plates........ 95

Figure 4- 16. Michelson interferometer as a gap setting technique........ 96

Figure 4- 17. Mask layout for capacitive gapping technique........ 98

Figure 4- 18. Capacitance gapping results........ 99

Figure 4- 19. Capacitance noise measurements........ 100

Figure 4- 20. Confocal gapping technique........ 101

Figure 4- 21. Axial response of a zone plate compared to a theoretical model........ 102

Figure 4- 22. Gap detection by calculating the Center of Gravity (CoG) of the axial response........ 103

Figure 4- 23. Picture of the UV-ZPAL apparatus........ 105

Figure 5- 1. SEM of single spot exposures of a single zone plate for dose optimization 108

Figure 5- 2. Left- SEM of the outer zones of the zone plates. Right- Spot size at the optimum dose........ 109

Figure 5- 3. Configuration of optics for illuminating the zone plates with the TI micromirrors........ 110

Figure 5- 4. SEM of nine different patterns exposed in parallel with the UV-ZPAL system. 111
Figure 5- 5. SEMs of top center and the top right patterns from Figure 5- 4 112
Figure 5- 6. SEM of nested-L pattern. 113
Figure 5- 7. Confocal microscopes 114
Figure 5- 8. First image scanned with the zone-plate array confocal microscope… 116
Figure 5- 9. Cause of interference fringes on the images obtained with the zone-plate microscope. 116
Figure 5- 10. Images of SiO_2 substrate with grating lines of different periods etched 1 μ m deep, coated with aluminum 117
Figure 5- 11. Confocal images of an IC at increasing resolution 118
Figure 5- 12. Level to level alignment scheme.. 120
Figure 6- 1. ZPAL's throughput 127
Figure 6- 2. Zone plate illumination uniformity 131
Figure 6- 3. Optical solution to zone plate illumination non-uniformities. 132
Figure 6- 4. Thin-film micromirrors manufactured by Daewoo Electronics 133
Figure 6- 5. Shutters for ZPAL as multiplexing elements 134
Figure 6- 6. Scanning electron micrographs of MIT Lincoln Labs Shutter Arrays. 135
Figure A- 1. Spin curve for 3.5% PMMA 142
Figure A- 2. Quartz etch depths w/ CHF_3 for inner lab RIE 145
Figure A- 3. Average ebeam errors encountered while writing zone plates 146

List of Tables

Table 1- 1. Devices fabricated with x-ray lithography in recent years 36

Table 3- 1. Design parameters of fabricated zone plate arrays for UV-ZPAL 64

Table 4- 1. The effect of grayscaling on throughput 91

Table A- 1. Etch depths for quartz w/ CH F_3 144

Preface

Lithography is clearly a cornerstone of the semiconductor industry and the information revolution. High-resolution lithography is crucial to a wide variety of devices, from chips for computers, to filters for optical communication, to high-density magnetic information storage. In the 21st century we will see lithography impacting flat-panel displays, information-storage systems, molecular biology, and the chemical industry through the control of catalysis and molecular manipulation. Applications unforeseen at this time will no doubt emerge, particularly if relatively inexpensive techniques for sub-100 nm lithography are developed [1]. This is the goal of this thesis.

The concept of a nanolithography system comprised of a short wavelength radiation source, an array of Fresnel zone plates and a multiplexing element has been proposed earlier as a means to achieve sub-100 nm resolution [2]. A subsequent set of preliminary experiments with 193 nm radiation were performed showing the focusing capabilities of zone plates [31-32]. This thesis presents the extension of the preliminary deep UV system into a fully operational maskless lithography tool at UV wavelengths capable of writing arbitrary patterns with 350 nm features. In addition, as a natural extension to the system, a parallel confocal microscope has been implemented using the same zone plate array employed for exposing patterns.

Chapter 1 provides a summary of the future needs for lithography and the contenders to satisfy these needs. These competing technologies are usually labeled as Next Generation Lithographies (NGL's).

Chapter 2 describes what is Zone Plate Array Lithography. The discussion briefly covers all the components of a ZPAL system: source, micromechanics, zone plates, writing strategy and wafer stage requirements. A more detailed description of each component is provided in Chapter 4.

Chapter 3 details on the theory, design, and fabrication of zone plates. The discussion includes phase and amplitude zone plates (zp), as well as zp efficiencies and the need for stops to improve contrast.

Chapter 4 elaborates on the design and construction of a fully operational UV ZPAL system. The chapter deals with all major components of the system: laser source, optics, micromirrors, UV-zone plates, stage and software.

Chapter 5 provides a detailed description of the experiment that produced arbitrary patterns written simultaneously with the UV ZPAL system. An analysis of the results as well as the system's capabilities is included. The chapter also includes a description of the zone plate array confocal microscope that was built, and images obtained with such a microscope are presented.

Chapter 6 analyzes the optimization and the extendibility of ZPAL. In particular the means of improving the system's throughput are carefully described. Alternative micromechanics that would allow the system to operate at x-ray wavelengths are presented.

Chapter 7 summarizes the concepts of ZPAL and explores the reasons why Zone Plate Array Lithography might prove to be of great importance for a variety of fields.

Chapter 1

Next Generation Lithographies (NGL's)

The tremendous growth of the semiconductor industry since its inception has been fostered by a number of engineering advances that reduce the cost per function of integrated circuits by about 25-30% a year. The industry has been able to maintain such an extraordinary pace due to advancement in equipment performance, throughput and uptime; by improving product yields, quality and reliability; and by increasing wafer size. However, the most significant contributor to keeping on the historic productivity curve has been the ability to shrink integrated circuit feature sizes through advances in lithography.

Although the semiconductor industry has been its main beneficiary, improvements in lithography have enabled in the past the creation of new fields, such as MEMS, as well as advances in other scientific fields, including astronomy, through the fabrication of interferometrically generated gratings for X-Ray telescopes [3], and optical communications [4]. There is no reason to expect that this trend will not continue, and there is little doubt that new applications and industries will emerge as lithographic techniques become more mature and advanced.

There is a caveat though, to this '*everybody wins situation*'. Because it's the semiconductor industry, with its incredible resources and brutal competition, that has in the past, and will in the future, push high volume lithography to its limits, the technology they develop, although appropriate for their needs, will no longer be suitable for other emerging fields due to prohibitive cost and some degree of inflexibility. The race they have entered to shrink devices further and further while increasing productivity has raised the costs of the tools to unprecedented levels.

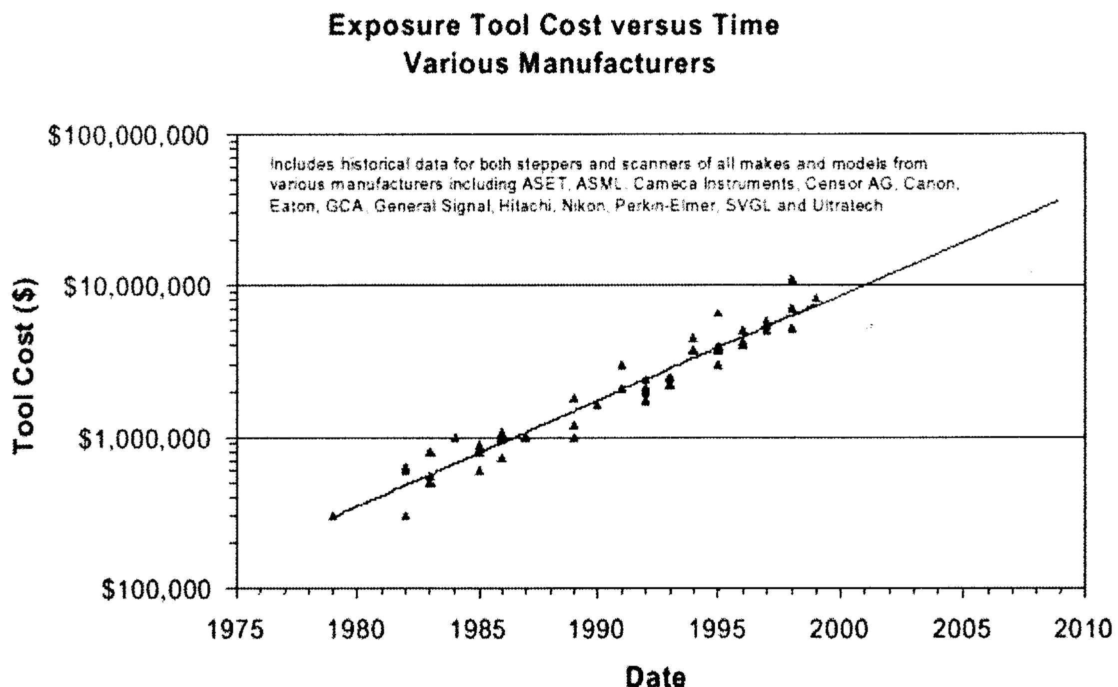

Figure 1- 1. Exposure tool cost vs. time

The current trend has produced exposure tool costs in excess of $10M (Figure 1-1). If we add to this the cost of masks, which can go as high as $80K for a single mask, it is evident why the creation of other industries besides that of semiconductors may be severely limited. But even if companies are willing to pay the price, optical projection lithography, the technology of choice of the semiconductor industry for the past three decades, is reaching its theoretical limits, and sometime before 2005 a new paradigm in lithography will have to take on the challenge of printing features to the limits of the

lithographic process. There are hence two separate potential markets for new lithographic technologies to exploit. Both require high-resolution lithography, but they differ in the throughput requirements and in their cost. The work done in this thesis tackles both requirements with a flexible scalable technology: Zone Plate Array Lithography. But before we get into details of what ZPAL is and its merits, it is of critical importance to see where this technology fits in context with the proposed lithographic solutions of major corporations and research institutions around the world.

1.1 The Present

Optical lithography has been the technology of the industry for more than 30 years, taking the feature sizes from 10 microns in the late 1960's to present production feature sizes of 0.18 microns (180 nm). Currently the most advanced lithographic tools used in high-volume manufacture employ deep ultra violet (DUV) radiation with a wavelength of 248 nm to print features that have line widths as small as 180 nm. While further improvements are expected in optical lithography, by using 193nm radiation or even 157-nm radiation, this technology is not expected to take feature sizes below100nm. The industry is aggressively searching for a lithography solution which will be capable of printing chips for the 100 nm-device generation and below. The exact time for transition to the new imaging technology is uncertain, but it is anticipated that production with 100 nm features will begin in the year 2005. It is then when the so-called Next-Generation Lithographies will be required. They are successors to optical projection lithography, and hence they are also referred to by many as "post-optical". The list of contenders for the golden spot varies according to personal biases, but there seems to be a consensus that the main candidates are Extreme Ultraviolet Lithography (EUV), X-Ray Lithography, and SCALPEL (a form of e-beam projection lithography). We hope to include Zone plate Array Lithography as a possible contender in the future.

1.2 The Economics

The $8 billion lithography industry is the cornerstone of the $140 billion world semiconductor industry. The lithography industry is projected to grow to more than $25 billion by the year 2005. New semiconductor fabrication facilities cost between $1 and $3.5 billion, and the cost of lithography equipment constitutes from 25% to 35% of the cost of these facilities. Building new facilities and upgrading existing facilities is the driving force behind the semiconductor lithography equipment industry. [5]

1.3 The Future

The standard by which the semiconductor industry measures itself and tries to remain competitive is referred to as Moore's Law [6] which states that on average, the number of transistors in a state-of-the-art integrated circuit doubles every 18 months. According to this well known "law", a Roadmap is put together every three yeara and updated regularly by the Semiconductor Industry Association (SIA) [7], setting the goals that are to be achieved by companies if they are to remain competitive. The roadmap covers a huge variety of areas across many technical fields, but because lithography has been the key area responsible for the past successes of the industry, the lithography roadmap is the most widely cited. It is the one that concerns us in this analysis. Figure 1-2 shows the 1999 roadmap along with the possible technologies that will be able to meet the demands at each technology node. It seems plausible that we will get to the 100-nm node with optical lithography, either with 193 or 157-nm radiation, but we can see that the 100-nm node will very likely require a new technology. Let's analyze each one of the contenders.

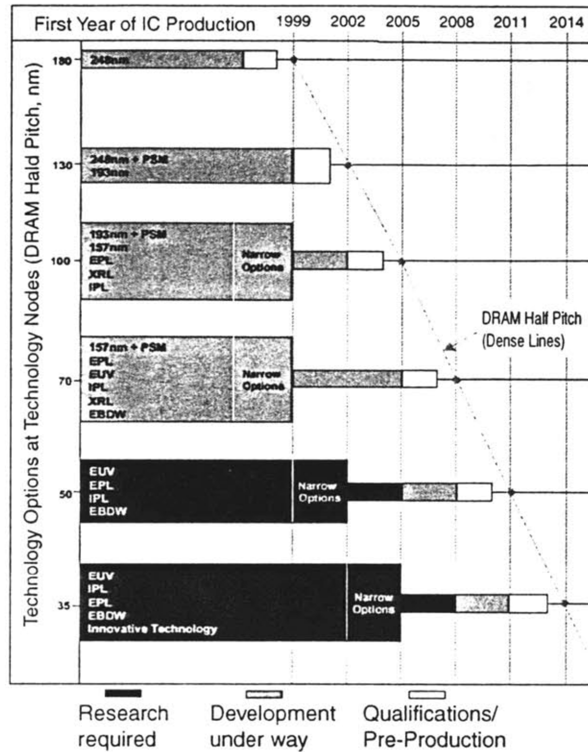

Figure 1- 2. Semiconductor Industry Association (SIA) National Roadmap for Lithography 1999.

1.4 Extreme UltraViolet Lithography (EUVL)

EUVL, or soft x-ray projection lithography for the politically incorrect, is a relatively new form of lithography that uses EUV radiation with a wavelength in the range of 10 to 14 nm to carry out projection imaging. Defenders of the technology claim that it's a natural extension to optical lithography, since it uses short wavelength radiation to carry out projection imaging. Many researchers find this claim a stretch, since the properties of the materials that are to be used in the EUV portion of the electromagnetic spectrum are so different from those in the visible and UV regimes.

There is a simple and plausible reason for drastically reducing the wavelength of an imaging system that is to be used for high-resolution lithography. The reason becomes evident if we look at the equations that describe two of the most fundamental

characteristics of an imaging system: its resolution and depth-of-focus. These equations are usually expressed as

$$\text{Min Linewidth} = k_1 \cdot \frac{\lambda}{NA} \quad \textbf{1-1}$$

$$DOF = k_2 \cdot \frac{\lambda}{NA^2} \quad \textbf{1-2}$$

where λ is the wavelength of the radiation used and NA is the numerical aperture of the imaging system. What's apparent from these equations is that we can improve the resolution of an optical system by decreasing the wavelength and increasing the NA. But we can also see that if we do so we have to pay a price for it, that is, the reduction of the depth-of-focus. The case $k_1=1/2=k_2$ corresponds to the usual definition of diffraction limited imaging. But because of aberrations, errors in lens manufacturing, non-uniform illumination over the field, the contrast of the resist being used and many other factors, the k factors have historically fell short of the theory. Values of k_1 and k_2 greater than 0.6 have been used comfortably in high-volume manufacturing, but recently it has become necessary to reduce these values to improve the resolution of the optical system while tightening process control.

The question of how much one should reduce the radiation's wavelength is the source of much controversy. The first thing to consider is what optics can be used as we move to shorter wavelengths. Every material becomes absorbing for wavelengths shorter than 110 nm [8]. This absorption decreases gradually toward shorter wavelengths, while at the same time the refractive index approaches a value close to 1. These facts eliminate the possibility of using refractive optical elements, such as lenses and transmission masks at EUV wavelengths, making it necessary to have the imaging system entirely reflective and carried out in vacuum.

But even reflective surfaces are a tremendous challenge at these wavelengths, and to achieve a reasonable reflectivity, multilayer structures have to be used. These structures consist of a large number of alternating layers of materials having dissimilar optical constants at the wavelength of interest, and they provide a resonant reflectivity

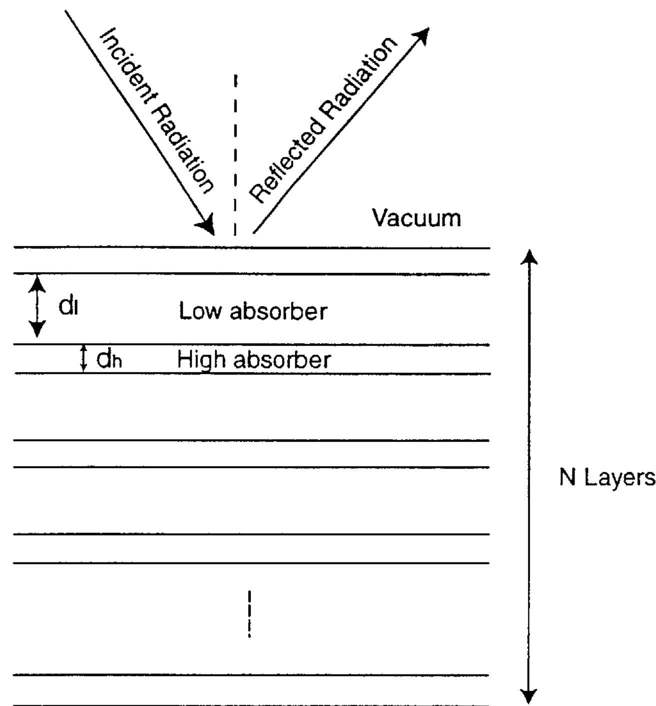

Figure 1- 3: Multilayer mirrors

when the period of the layers is approximately λ/2. This is the key technology that enables EUVL, as well as its major hurdle.

High reflectivity multilayer mirrors are obtained when all boundaries, or at least all periods, add in phase with the reflected wave. Multilayer mirrors consists of alternate layers of materials with high and low absorption (Figure 1- 3). The periodicity of the structure is $d = d_h + d_l$, but the thicknenesses d_h and d_l need not be constant as functions of z, the depth of the multilayer, so long as d remains constant. As previously mentioned, the purpose of using multilayers is to get around the strong absorption that all materials exhibit at low wavelengths. To minimize the detrimental effect of absorption, the standing wave field that gets produced within each coating of the multilayer can be utilized advantageously. The basic idea is to position the highly absorbing material in very thin layers into the nodes of the standing wave field, and fill the remaining space with a material with very low absorption. The standing wave field is produced due to superposition of the incident and reflected waves. By placing thin absorbers at the nodes of the standing-wave (see Figure 1- 4), the small contributions from all these thin films

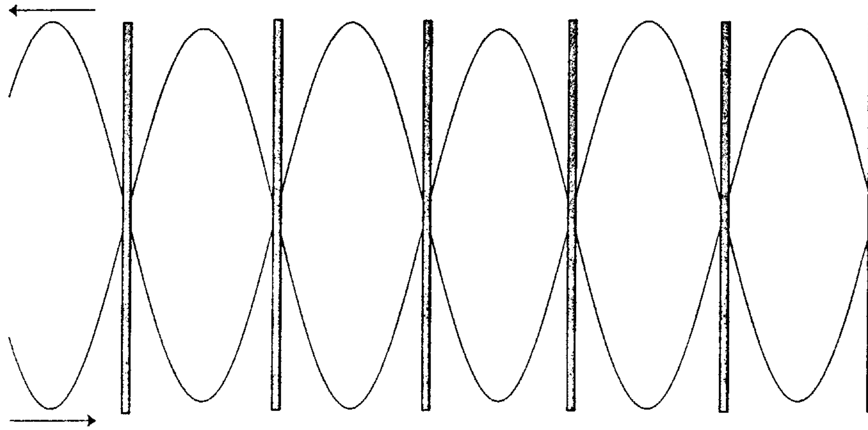

Figure 1- 4. Standing wave field

will add in phase with the reflected wave. In the limit of very thin films, and very large number of periods, the absorption losses approach zero and the reflectivity 100% [9]. Even though in theory reflectivities of 100% are possible, the measured performance of a multilayer is much lower than this value due to errors in layer thickness, contamination, uncertainties in the optical constants and quality of the boundary, just to name a few parameters. As a consequence, EUV researchers are required to fabricate multilayer mirrors with unprecedented perfection.

Surface figure errors on the mirrors must be within 0.25 nm rms [10], and the roughness of the substrate must be better than $1/10^{th}$ of the period (Period = $\lambda/2$=6.75 nm) [11]. Until recently, achieving this kind of surface figure accuracy was out of the question, but there seems to be great progress towards getting close to the figures required for the mirrors.

We have gotten to the point were we can partially reason out why 13.5 nm was the wavelength of choice for EUVL. Multilayer coatings can work at a great range of wavelengths by careful design and appropriate choice of materials, however the efficiencies of the mirrors also vary widely depending on the materials used. Through careful analysis of the possible materials, LBNL and Sandia National Laboratory decided to go with Mo-Si and Mo-Be multilayer coatings. Mo-Si and Mo-Be multilayers that peak at 13.5 nm have achieved reflectivities in excess of 68%, making them the highest near-normal-incidence reflectivity of any multilayer x-ray mirror [10,11].

1.4.1 EUVL Exposure Tool

A schematic representation of an EUV projection system is shown in Figure 1- 5. The key components are: an EUV source (generally a laser plasma source, although there has been some talk about using a synchrotron), a patterned reflective mask, a 4X reduction camera consisting of 4 mirrors (although some schemes use 6 mirrors) and a EUV sensitive

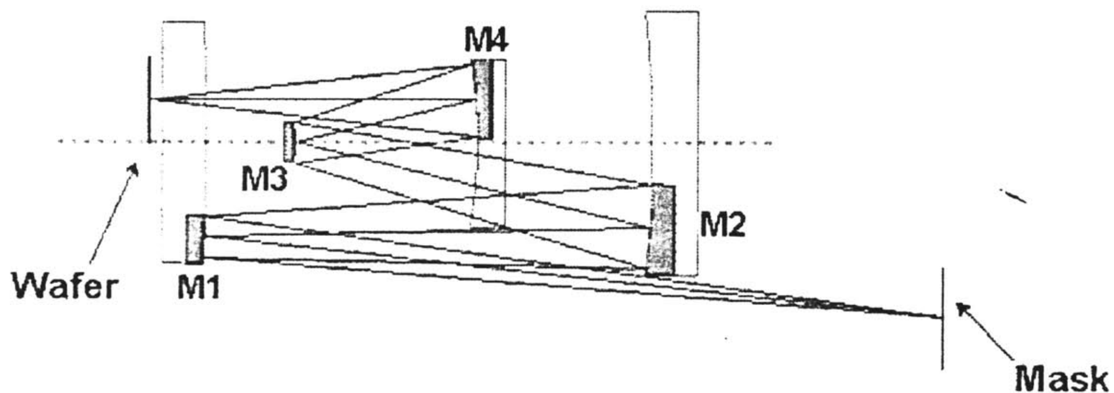

Figure 1- 5: EUV projection system

resist. In actual operation, the mask and the wafer are simultaneously scanned in opposite directions, with the mask moving four times faster than the wafer.

The EUVL masks are, like the rest of the system, reflective. They consist of a patterned absorber of EUV radiation placed on top of a multilayer reflector. The reflectance spectrum of the mask must be matched to that of the multilayer coated mirrors in the camera [10]. A huge problem that EUVL faces is the fact that there is no known method for repairing the masks once they are patterned, and they are neither inexpensive nor easy to manufacture. A 1998 study by International Sematech [12] estimates the cost of a single mask between $60,000 and $75,000, and that is assuming that the technology will be mature enough for a mask to achieve 60% yields in manufacturing. If the yield drops to ~40% the cost goes up to $180,000. The mask's reliability issue only gets aggravated by the fact that the pellicles that are used to protect masks from contamination

in current practice can not be used because of the undesirable absorption that would be encountered.

Despite all the problems, and to no small part due to a $250M investment just in the last three years [13], results have been finally obtained, and a team from Sandia National Laboratory was able to print 90 nm nested L's with a 4X reduction camera. The technology is in principle expected to support the shrinking of features down to the 30nm node [14]. It is worth noting that the initial estimate of the cost of a EUVL tool is $15.2M [12].

1.5 From electron beam lithography to SCALPEL

Electron-beam lithography has long been considered a potential solution for high-resolution lithography. However, despite its high resolution, good depth of focus, and flexibility as a direct-write tool, conventional e-beam technology has fallen further and further behind other technologies, mainly because of throughput. Throughput in electron-beam lithography is fundamentally limited by a combination of beam current and resist sensitivity [16].

Current state-of-the-art systems have currents between 2 and 5 nA and the best resist sensitivities available are around 2 μ C/cm^2. This means a state-of-the-art ebeam system can write 1 cm^2 in 400 seconds (6 min and 40 sec). Were we to write an entire 8" wafer it would take 36 hours. Being more realistic, and assuming less than 1/2 of the actual wafer is actually written, and neglecting overhead, we get a half day per wafer. It seems obvious why, when industry standards are looking for a technology that can pattern 40 or more wafers per hour that e-beam is simply not an alternative for high volume manufacturing. The problems with e-beam throughput have been apparent for many years, and many new schemes have been proposed that use electrons as a source while circumventing the problem of throughput. The best known alternatives are SCALPEL, which will be analyzed in the next section, and a variety of multiple beams techniques. These tools minimize space charge effects by spreading out the electrons over a larger volume of space. The multiple beam approaches can be further subdivided into two categories: multisource [17], where multiple beams are generated in a single

optical column, and multicolumn [18], where each beams has its own individual micro-column.

1.6 SCALPEL

SCattering with Angular Limitation Projection Electron-beam Lithography (SCALPEL), being developed by Lucent Technologies, is another leading candidate for next generation lithography. SCALPEL is a reduction image projection technique which uses 100 keV electrons to produce images by scattering contrast. Figure 1- 6 shows a schematic representation of the SCALPEL system.

In the SCALPEL system, a mask consisting of a low-atomic-number membrane covered with a layer of a high-atomic-number material in which the pattern to be printed is defined, is illuminated with high energy electrons.

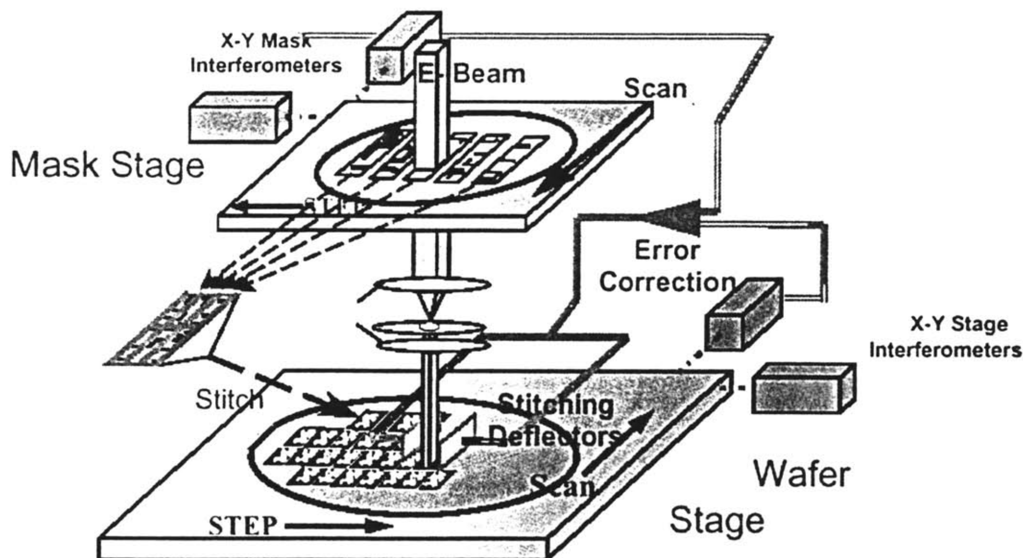

Figure 1- 6. Scalpel schematic

Because of the extremely short wavelength that the system utilizes and the fact that the membrane is relatively thin, the entire mask structure is essentially transparent to the electron beam, and very little of its energy is deposited there. The portions of the

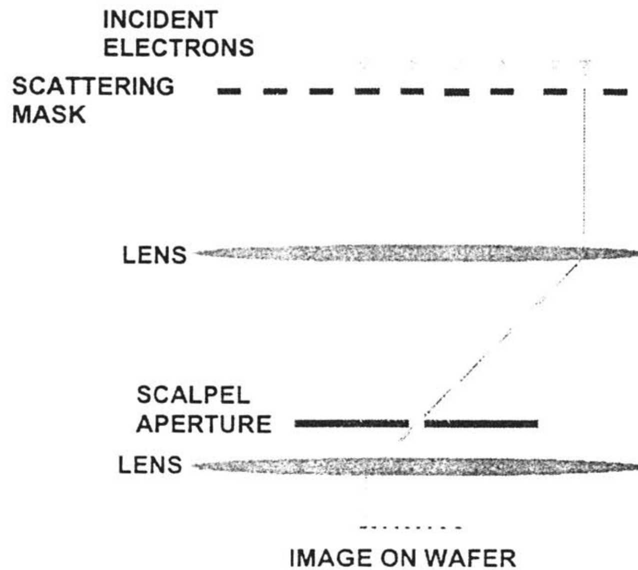

Figure 1- 7. SCALPEL principle of operation

beam that pass through the high-atomic-number pattern layer are scattered through angles of a few milliradians. Contrast is generated by using an aperture (see Figure 1- 7) in the back focal plane of the projection lens system to filter out the scattered electrons [15].

The key component of the system is, without doubts, the scattering mask. The silicon nitride membrane that SCALPEL uses as a mask is too fragile to span the large areas required for a typical die, so an arrangement of supporting struts is used to divide the membrane into smaller and more robust areas, as can be seen schematically in Figure 1- 8. The mask employs a 100nm thick SiNx membrane layer on top of Si. A 30 nm Cr/W bilayer, which will serve as the scatterer that allows image formation, is then deposited. The rest of the process involves the formation of the struts, 100 μm wide and 350μm deep, by dry etching, followed by the patterning of the bilayer with the features to be printed. The system is designed to provide a 4X reduction. Finally, to produce the desired pattern on the wafer, the mask is mechanically scanned parallel to the struts in synchrony with the wafer.

One of the major areas of concern for all types of lithographies based on electron beams is pattern distortion due to proximity effects. This refers to the tendency of scattered electrons to expose nearby areas that are not intended for exposure. This effect

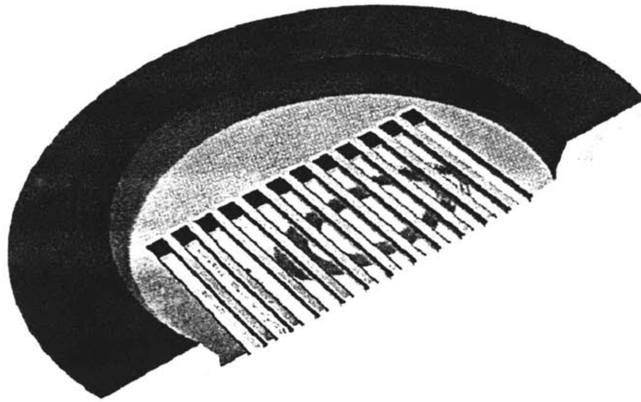

Figure 1- 8. The SCALPEL mask

is severe for high-energy electron beams.

But perhaps the two areas of biggest concern for SCALPEL are beam blur and wafer heating. Beam blur is an uncorrectable "smearing" of the sharpness of the image that is to be printed caused by charged particle interactions. In some ways it is analogous to the effect of an optical lens with finite numerical aperture on an aerial image. Throughput for any charged-particle lithographic technique is a strong function of beam current. SCALPEL obviously would like to maximize the current, however, increasing the current increases the stochastic blur of the system due to an increase in the number of charged particle in the column.

Wafer heating arises due to the high power density deposited in the relatively small area of the wafer that is being exposed at any given time. The high power density will cause the wafer's temperature to rise, and hence, to locally distort *while* the patterns are being written. When the area exposed cools off, errors have been introduced in the placement of the features. Wafer heating is a serious problem to which there are no easy solutions. A possibility is to lower the power into the area exposed by allowing multiple passes, hence causing a much smaller temperature gradient on the wafer. The penalty is, once again, throughput.

1.6.1 Commercialization of SCALPEL

SCALPEL is being actively developed by Lucent Technologies, and in November 1999, a group of semiconductor device and equipment manufacturers announced a joint agreement aimed at accelerating the development of SCALPEL technology into production. Participants in the program include: eLith LLC, a joint venture of Applied Materials, Inc. and ASM Lithography Holding N.V.; Lucent Technologies Inc.; Motorola Semiconductor Products Sector; Samsung Electronics Co., Ltd.; and Texas Instruments Incorporated (TI).

Also in 1999, SEMATECH decided that the only two options they would actually pursue and fund for Next Generation Lithographies would be EUV and SCALPEL.

1.7 X-ray lithography

X-ray lithography was first suggested by Spears and Smith in 1972 [19,20]. The principle of operation is relatively simple. The technique is a shadow printing scheme, in which a source of radiation (x-rays in this case, with wavelengths between 6 and 14 Å) is shaped by a mask to produce the desired pattern on a resist sensitive to the radiation utilized (Figure 1- 9). Unlike the situation for electrons and optical photons, it is very difficult to construct any type of optics for x-rays, and as a consequence, the x-ray exposure setup employs a 1X mask. That is, no reduction is performed by the tool.

The mask and the wafer are maintained in close proximity, typically a distance on the order of 10 μ m. The resolution, or more precisely the minimum printable line width W, is dominated, to first order, by diffractive blurring at the finite wavelength $\lambda$and gap G [21]. The relationship between mask-substrate gap G and the minimum feature size W is given by

$$G = \alpha \frac{W^2}{\lambda} \qquad \textbf{1-3}$$

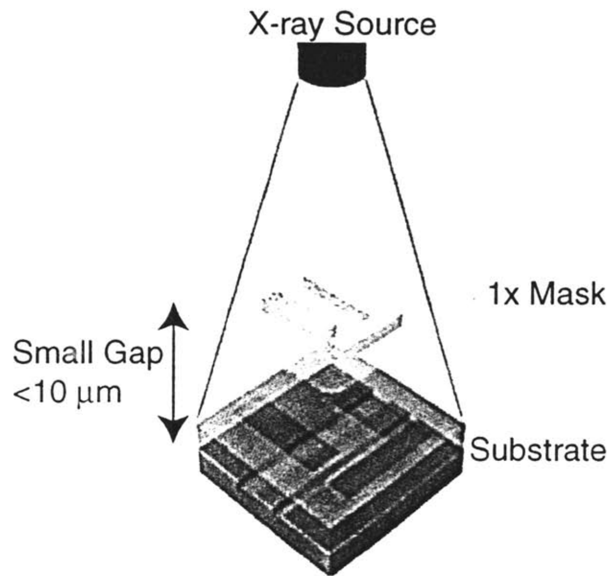

Figure 1- 9. X-ray lithography

where α is typically in the range 1-1.5 [22-24]. For feature sizes below 50 nm, the gap must be below 4 μ m. The small gap, although not a problem for research, has traditionally been a cause of great concern for the semiconductor industry. The small gap is probably not unfeasible for manufacturing, but it is certainly a limitation of the technology.

The 1X mask is the heart of the x-ray lithography process, and it consists of an absorber pattern on a thin membrane. The mask structure is dictated by the optical properties of the x-rays. The membrane must be transparent enough to allow for fast exposures, and yet be able to withstand handling and radiation damage. In general, the membrane will be on the order of 1 to 2 μm thick, and be made of low-Z materials for high transmission. Currently used mask membranes are fabricated with silicon, silicon nitride, or silicon carbide, while high Z materials such as gold, tantalum, and tungsten, are used as absorbers [25].

Since exposure is a 1X process, the placement accuracy of the pattern must be within the bounds dictated by the error allocation budget. This implies that the membrane must be rigid enough so that no distortion of the pattern is induced by the handling and exposure process. The membrane is not self-supporting, so it must be fastened to some

support to provide the necessary rigidity. The support structure is usually a Pyrex ring. In general, the mask is fabricated starting from a 3" or 4" silicon wafer, using a variety of techniques, but the fundamental structure of a mask is the same: a thin, uniform membrane is mounted on a structurally rigid holding frame. The pattern is applied on the membrane, typically by means of electron-beam lithography.

Pattern distortion is a serious problem in x-ray masks. The distortions are present not only from the writing of the mask via e-beam, but also due to the built-in stress in the absorber. At the NanoStructures Laboratory at MIT, an effort is underway in correcting for such distortions by means of localized heat correction techniques. The mathematical problem of determining the heat input required to cancel out a given distortion is a very difficult problem that remains to be solved.

Despite these limitations, x-ray lithography is by far the most mature of all the so-called New Generation Lithographies. The technology is well advanced in many fronts, with a substantial industrial infrastructure. An impressive list of IC devices have been fabricated for many years now, some of which are summarized in Table 1- 1.

Since the mid 1970's X-Ray Lithography (XRL) has been considered a promising candidate for implementation in the "next generation" of IC manufacturing. Today, 20 years later, such implementation has still not taken place. The manufacturing entrance point of the technology has continued to slip as improvements in UV optics and extensions to DUV, enhanced by clever optical and processing techniques, have postponed the need for a post-optical advanced lithography.

Device	Density	Feature Size	Date	Origin	Reference
CMOS logic	6M xistors	0.2 μm	1994	IBM	[26]
DRAM	64 Mb		1995	IBM	[27]
DRAM	1 Gb (test)	0.14μ m	1995	Mitsubishi	[28]
CMOS	16ps/stage	0.10μ m	1995	IBM	[29]
DRAM	4 Gb (test)	0.12μ m	1996	Toshiba/NTT	[30]

Table 1- 1. Devices fabricated with x-ray lithography in recent years

An issue that has also scared the semiconductor industry in the past is the need to use a synchrotron as the radiation source for x-ray lithography. Synchrotrons are feared mainly because of their cost and because they represent a major fixed facility. EUVL also shares the need for a source of short wavelengths and high power, and much development is under way to develop alternatives to a synchrotron.

Although the US semiconductor industry has decided, through SEMATECH, not to pursue x-ray lithography as an alternative to optical lithography, the technology is still alive in Japan, where much work is under way to continue the development of the infrastructure needed to insert the technique when the end to optical lithography is reached.

1.8 Conclusions

Optical lithography still remains the lithographic technology of choice for the semiconductor industry. It is believed that 157 nm technology will be able to satisfy the needs of the industry down to the 100 nm node. However, what will replace optical lithography once its limits have been reached is still unclear. Each of the technologies has strong regional support, with X-ray being championed in Japan, while the US supports EUV, in conjunction with Europe and some localized efforts also in Japan, and SCALPEL. Technological soundness, money, and a certain degree of politics, will determine the winner.

Regardless of who the winner is (it is highly unlikely that it will be the kind of situation that "winner takes all" anyhow) lithography is a larger field than what the semiconductor industry uses it for. As mentioned in the introduction of this chapter, lithography is a key enabler of optical integrated circuits for optical communications, MEMS, high-density magnetic storage, and biological research. It is highly unlikely that SCALPEL or EUV will provide the lithography technology needed for these other applications, either because of tool cost, inflexibility, insufficient feature-placement accuracy, or spatial coherence. Hence, it is important to recognize the need for a

bifurcation in the development of lithographic technologies for the future: one branch addressing the needs of the semiconductor industry, the other branch addressing the requirements of the non-semiconductor industry applications.

The ambition of the project described in this thesis is to create a technology that will potentially be able to satisfy the needs of both branches. But to motivate why a maskless approach is the right approach for the future of lithography, let's finish with a quotation from the 1999 International Technology Roadmap for Semiconductors published by Sematech:

> "*Breakthroughs in direct-write technologies that achieved high throughput would be a significant paradigm shift [in lithography]. It would eliminate the need for masks, offering inherent cost and cycle-time reductions*".

Chapter 2

Zone Plate Array Lithography (ZPAL)

2.1 Introduction

ZPAL is depicted schematically in Figure 2 - 1. An array of Fresnel zone plates focuses incident radiation into an array of spots on a substrate. The spot size is approximately equal to the minimum feature size of the zone plate (i.e. the outer zone width). By using micromechanics to independently turn on or off the radiation to each zone plate, and simultaneously scanning the substrate in a raster pattern through a zone-plate-unit cell, arbitrary patterns can be generated. ZPAL combines the advantages of maskless lithography with the high throughput of parallel writing provided by an array of zone plates.

ZPAL was first proposed by Smith in 1996 [2] in a paper which detailed the basic writing strategy and presented an analysis which indicated that a ZPAL system utilizing 4.5 nm radiation from an undulator on a compact synchrotron should be capable of producing ~25 nm feature sizes at a throughput of 1cm^2/sec. Subsequent work presented resist exposures using phase zone plates in the deep UV (λ =193 nm) [31-32] and

demonstrated rudimentary parallel patterning with a zone-plate array. The work presented in this thesis greatly extends the original deep UV ZPAL setup into a system that includes the micromechanics, the software, and the stage needed for writing arbitrary patterns simultaneously.

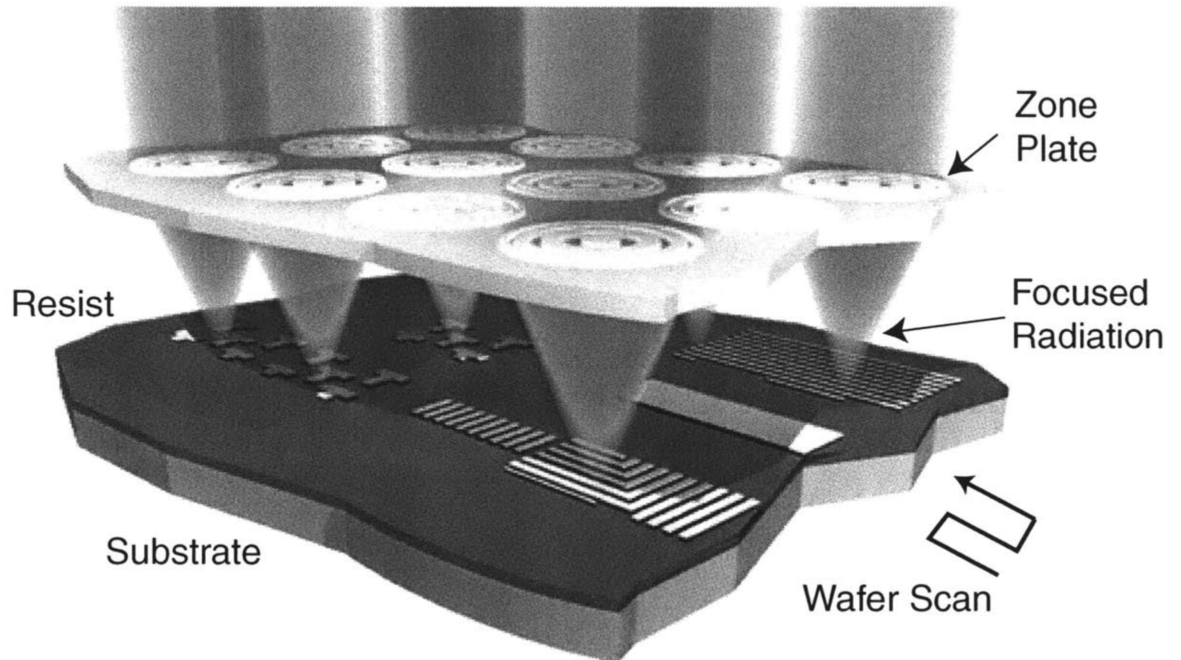

Figure 2 - 1: ZPAL schematic

The resulting ZPAL system is comprised of four major components: a radiation source, micromechanics, a zone plate array and a moving stage. The rest of the system (optics and software) simply provides the means for these key components to interact effectively. Let's take a closer look at each one of these elements (a much more detailed analysis will be undertaken in Chapter 4).

2.2 The Radiation Source

An essential characteristic of zone plates is that, with proper design and fabrication, they work at **any** wavelength. As a matter of fact, they even work with neutral atoms [33]. As a consequence, a ZPAL system is flexible enough to offer the unique opportunity of choosing which radiation we want to use for lithographic purposes by

simply designing the appropriate array of zone plates for it. That brings up the question of what is the best radiation for lithography. Although there are some engineering tradeoffs that arise with this choice, we do indeed have a great deal of flexibility when picking the radiation that we want to work with. The question of what's the best radiation for lithography always provokes a great deal of scientific controversy, but it is an important issue that is worth analyzing.

We saw in the review of Extreme Ultraviolet Lithography (EUVL) in Chapter 1, that there was a limitation in how low a wavelength could be used for EUVL, and that the restriction was imposed due to the need of having acceptable reflectivity values for the multilayer mirrors that provide the focusing of the EUV system. The reason for going to very short wavelengths became apparent in the review, but the question of whether 13.5 nm is the best radiation to use for lithography went unanswered. If the shorter the wavelength the higher the resolution, why not reduce it even further? That way it will not be necessary to use thin resists that only adds steps to the already complex lithographic process. However, we don't want to go to too low a wavelength to avoid too energetic photons damaging sensitive substrates.

From decades of research at the Nanostructures Laboratory at MIT, and supported by the results of Flanders et al almost 20 years ago [35], in which sub-20 nm patterning was achieved, we believe that the 4.5 nm photon is the best photon for lithography. It offers the optimal combination of minimal proximity effects and absence of backscattering, short enough wavelength to enable large depth-of-focus, sufficient penetration to eliminate the need for surface-interaction resists, and low enough energy to avoid damage to sensitive electronic substrates. In addition, the 4.5 nm photon allows for exposure in a helium atmosphere, thus simplifying the exposure apparatus and improving thermal management of the system. This assumes that we want to push lithography to its absolute limits. This distinction is important, because for many applications there is not a need for ultra-high resolution lithography, and other techniques are hence applicable. We can make an analogy with cars, noting that not everybody needs, nor can afford, a Ferrari, and despite its excellent features and high performance for many situations, it's not necessarily the most convenient car. Using the 4.5 nm photon for ZPAL will enable the

system to reach its ultimate performance in terms of resolution, but not necessarily in terms of cost-of-manufacturing, cost-of-ownership and ease of use.

The long standing search for an efficient, reliable and affordable source for the soft x-ray regime has still not been fulfilled, and the available options only satisfy one, or at most two, of these requirements. If we want high throughput, the options are pretty much reduced to using a synchrotron, with a cost in the order of $20 M!! There are other options that use lasers to excite plasmas that provoke the emission of soft x-rays, but, being pulsed sources, they are not the best option for ZPAL if we are interested in high throughput. For low cost and low throughput, a bombardment source could be used, and for the purposes of our research, this is the source of choice in our laboratory.

The important thing to realize is that ZPAL is flexible enough to allow other options in terms of sources if we are willing to compromise somewhere else. This possibility became apparent to us from the very beginning, and as a consequence, two lines of research were started. One involved the design and construction of an Ultra Violet (UV) ZPAL system, and the other, the construction of an X-ray system. The concept is the same, and both systems share the four main components that were mentioned in the Introduction, but they differ in the radiation that is used, and therefore in resolution. The UV-ZPAL system uses a He-Cd laser at 442 nm. The laser is CW, easy to use and it's very reasonably priced. Future research will be directed at reducing the wavelength of the laser used to the 200's nm regime. With this sources we expect to have a resolution in the order of 150 - 170 nm. With soft x rays, the resolution can be pushed to the sub-50 nm regime.

As a summary, the key concept to remember about the source for ZPAL is that it depends on the intended purpose of the system. If a small bio-tech company is interested to have a lithography tool that has high resolution (< 1 μ m), but they don't need very high throughput, they can choose to have a very inexpensive and reliable laser as a source. If, however, the company is Intel, and their interest is ultra-high resolution and very high throughput, they also have the option of a much more expensive source that will satisfy their needs.

2.3 The Micromechanics

It is apparent from Figure 2 - 1 that if we want each zone plate to write independently we have to be able to control the illumination of each zone plate. This control is provided by upstream micromechanics. The reason we need micromechanics is because the area of a unit cell, which is the square area over which we want to control the illumination, ranges from 10 to 100 μ m on an edge. There are a variety of options available, but the two main ones are the use of micromirrors, and the use of micro-shutters.

The use of mirrors is depicted schematically in Figure 2 - 2. The idea is to place a micromirror array in the path of the radiation beam. With proper alignment and use of optics, each mirror will be responsible for the illumination of an individual zone plate.

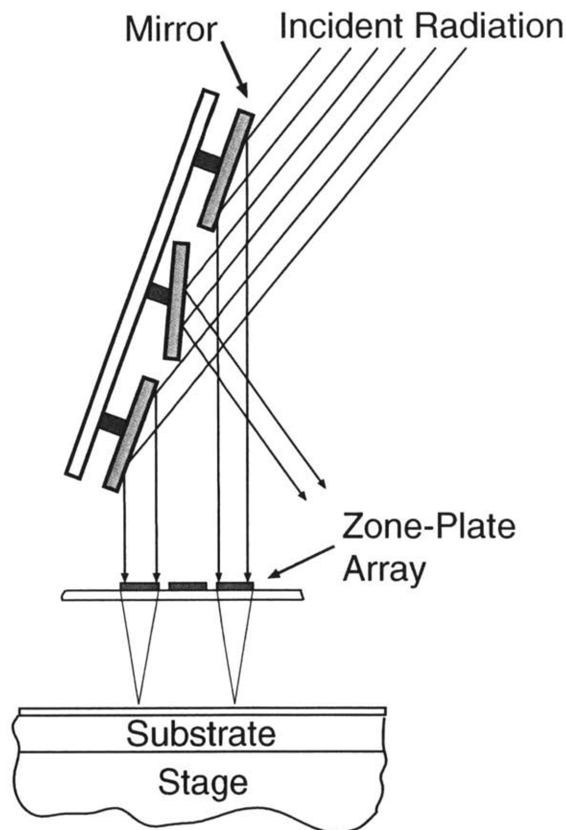

Figure 2 - 2. Role of micromechanics in ZPAL. Radiation is modulated by means of micromirrors, which can tilt to two angles by means of electrostatic deflection.

This is possible because the mirrors can tilt to two positions responding to the control of a computer, and hence, when they are latched in one position the light will be reflected to the appropriate zone plate, and when in the other, the radiation will be deflected out of the imaging system.

The other possibility is to use shutters as illustrated in Figure 2 - 3. The concept is to place a shutter above each zone plate to allow the incident radiation to pass or not depending on whether it's open or closed. Each shutter is actuated electrostatically. The micromechanics will be examined in greater detail in Chapters 4 and 6.

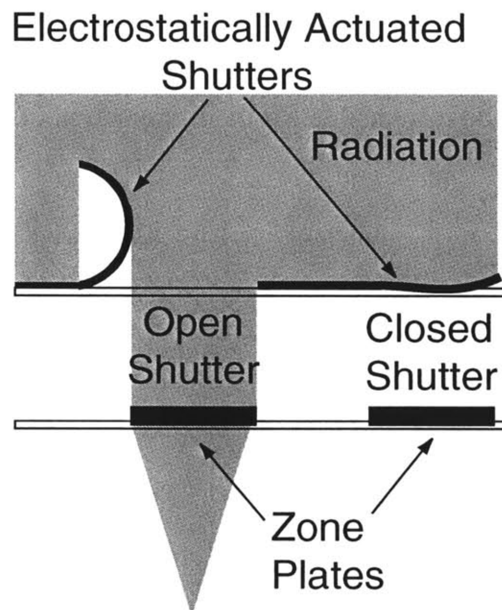

Figure 2 - 3 : Shutters as a multiplexing scheme for ZPAL

2.4 Zone Plates

Although the next chapter will deal exclusively with zone plates, their theory, design and fabrication, it is worth giving a brief definition for the sake of completeness of all the major components of ZPAL.

A zone plate is a diffractive optical element of circular symmetry in which the local spatial period depends on the radius in such a way, that the first order diffracted radiation from any radius value crosses the axis at the same point, the focal length. This concept is

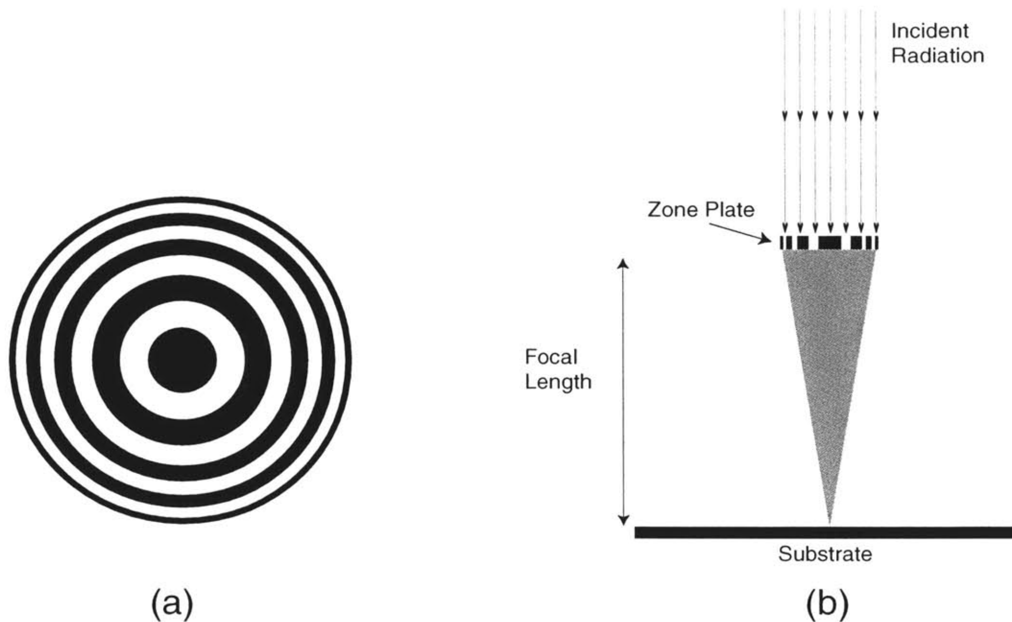

Figure 2 - 4 : A zone plate. (a) Top view (b) Cross section

illustrated in Figure 2 - 4. It goes without mention that the zone plates are the core of ZPAL, and that they are the innovative idea in terms of a complete new paradigm in lithography. Zone plates enable the use of any portion of the spectrum of radiation, from microwaves to x-rays.

2.5 The Stage

The last of the four major components of ZPAL is a precision movable stage. Its function is to raster scan the substrate over a zone plate unit cell in order to produce the desired patterns. A useful analogy is to think that there are two ways to write a pattern on a piece of paper: we can do it by keeping the pen steady (the focused beamlet from a zone plate) and then move the paper (the substrate) underneath, or we can move the pen and keep the paper still.

An important issue that's worth noticing at this point is the importance of synchronization between the micromechanics and the stage, a must if we want to obtain nanoaccuracy in the placement of the features on the substrate. This level of placement

accuracy is achieved through sophisticated software control, as well as a state-of-the-art flexure stage with sub 4 nm resolution.

Chapter 3

Zone Plates

3.1 A Brief History of Zone Plates

The invention of zone plates originates from the work of Fresnel (1788-1827) on diffraction. In 1808 the Paris Academy proposed the theme of diffraction for a prize, and Fresnel presented a paper [36] synthesizing Huygens's (1629-1695) principle and Young's (1773-1829) Principle of Interference. The resulting theory is now known as the Huygens-Fresnel Principle. Despite strong opposition from Poisson, a member of the jury and an ardent critic of the wave theory of light, Fresnel won the prize from a jury also composed of Pierre Laplace, Jean B. Biot, Dominique F. Arago, and Joseph L. Gay-Lussac[37].

The paper is worth examining, for it presents the foundations necessary for zone plates to be invented. The most important concept that concerns us in Fresnel's paper is the idea of what later would be called Fresnel Zones. Let's examine where they come from.

Fresnel's treatment of diffraction was based on the idea of Huygens principle, in which every point on a wavefront is assumed to be the center of a system of secondary waves, or wavelets, and the new wavefront is the common tangent of these waves. The breakthrough came from the realization that by taking into account the mutual interference that takes place between these secondary waves, diffraction effects could be explained. It is in the theoretical development of this explanation of diffraction that the Fresnel Zones arise, and as an extension, the Fresnel zone plate.

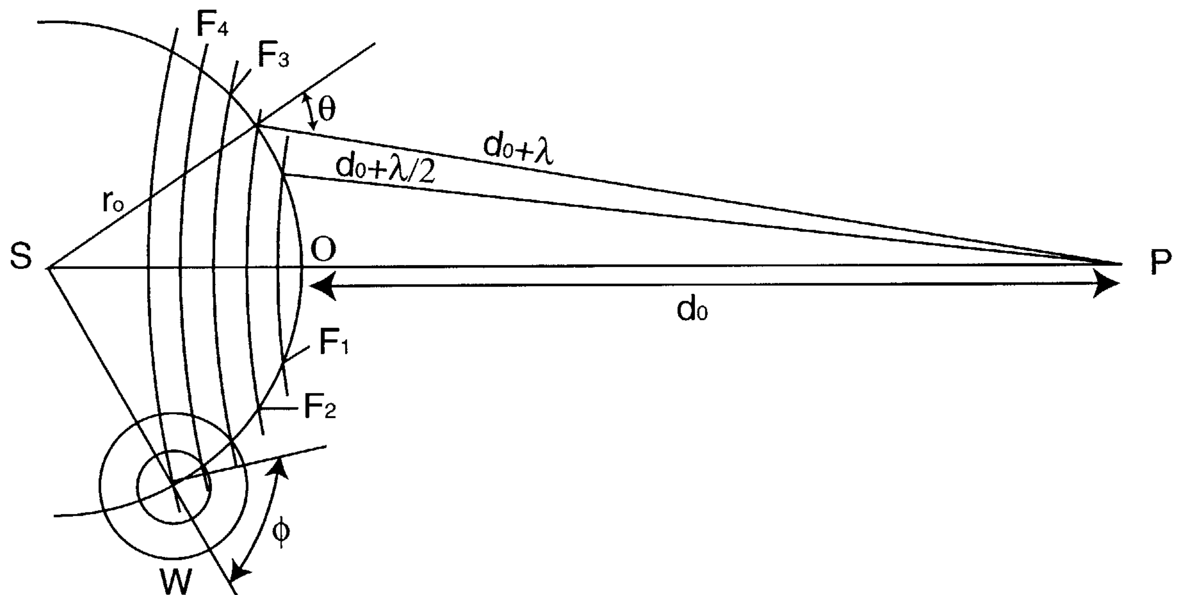

Figure 3 - 1: The Fresnel Zones

Figure 3 - 1 shows a wavefront arising from a point source at S. Fresnel maintained that the effect of the point source at a point where the light disturbance is to be determined, P, could be found either by allowing this wavefront to proceed until it reaches P, or by dividing the wavefront into small areas so that each one can be assumed to generate one wavelet (see W in the graph). Each of these wavelets then produces an effect at P, which can be summed according to the principle of superposition to give the total effect at P of the point source. Obviously, these two methods should yield identical results, but the second allows the calculation of the effect at P if parts of the wavefront are obscured by edges or apertures.

Going back to Figure 3 - 1 we can see that the shortest distance between the wavefront and P is d_0 (=OP). Other parts of the wavefront will cause disturbances at P which are out of phase with that produced by the nearest part (at O) due the difference in length that the light has to travel. This can be analyzed by constructing a set of concentric spheres centered at P with radius $d_0+n\,\lambda/2$, with n = 1,2,3,... These spheres cut the wavefront at F_1, F_2, F_3, etc. Let's focus on the first of these circles, F_1. Within this circle the phase of the disturbances arriving at P varies between 0 an π. If we now look at circle F_2 we see that the disturbances arriving at P from the area between these two circles (F_1 and F_2) will have a phase that will vary between π and 2π.

Further annuli or zones can be constructed, each having an effect at P varying by 180° of phase. These hypothetical zones are known as **Fresnel zones**. The size of these zones is dependant upon the wavelength of the light used as well as the distance to the point P. It's easy to prove that when we have a spherical wavefront, and the wavelength of the light used is small compared to d_0, the areas of the zones are all very nearly equal to $\pi d_0 \lambda$ and the radii of their boundaries are proportional to the square roots of natural numbers.

As the areas of these zones are equal, we can assume that they produce the same number of secondary wavelets from equal element areas. However, Fresnel had to introduce a correction here. If each wavelet radiated uniformly in all directions, in addition to generating a forward traveling wave, there would also be a reverse wave traveling back towards the source. No such wave is found experimentally, so the radiation pattern of the secondary waves had to be modified. Fresnel introduced an *obliquity* or *inclination factor*, which is a function of θ (see Figure 3 - 1), in order to describe the directionality of the secondary emissions. To be historically correct, Fresnel postulated the need for it, but it was Kirchoff who provided an expression for it [37].

We are now at a position to deduce what happens at P. We had assumed that each zone produces the same number of secondary wavelets since they all have equal areas, but, taking into account the obliquity factor, which increases as we go out from the central zone, we can see that the amplitude at P due to the zones will gradually diminish from the central zone outwards. From the way in which the zones have been constructed,

it follows that the effect at P from any one zone is exactly opposite in phase from that of an adjacent zone.

With these concepts in mind, and avoiding the analytical work in favor of doing it just for zone plates in the following section, we are ready to make the jump to the concept of a zone plate. In the previous considerations it was noted that successive Fresnel zones nullify each other due to variations in phase. If we prevent the light propagation from alternate zones from reaching P, that from the remaining zones, since they will all arrive with the same phase, will add up constructively and produce a greatly increased illumination at this point. This concept is illustrated in Figure 3 - 2.

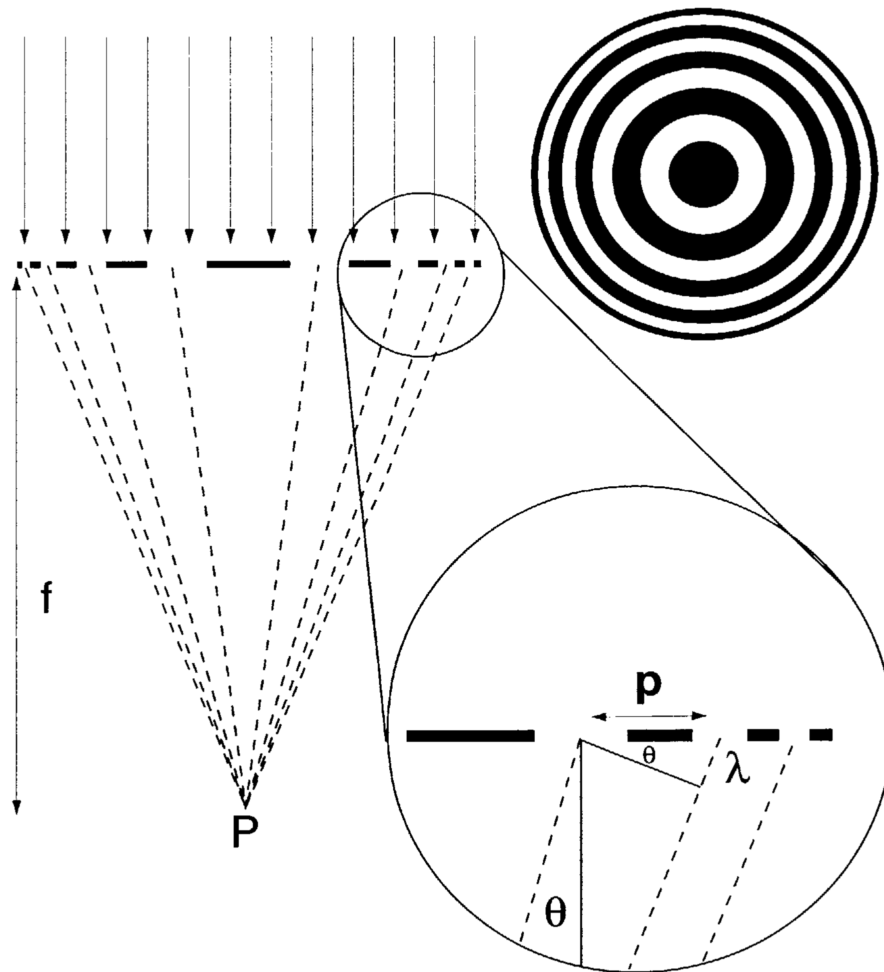

Figure 3 - 2. Zone plate schematic

An even higher increase in light concentration would be obtained if, instead of blocking alternate zones (amplitude zone plate), the phases of the wavelets from these zones were change by π. The disturbances from all zones would then arrive at P with the same phase. This is called a phase zone plate.

Let's now take a look in a more quantitative manner at how a zone plate works.

3.2 Zone Plate Theory

3.2.1 Geometry of Zone Plates

Consider the schematics shown in Figure 3 - 3.

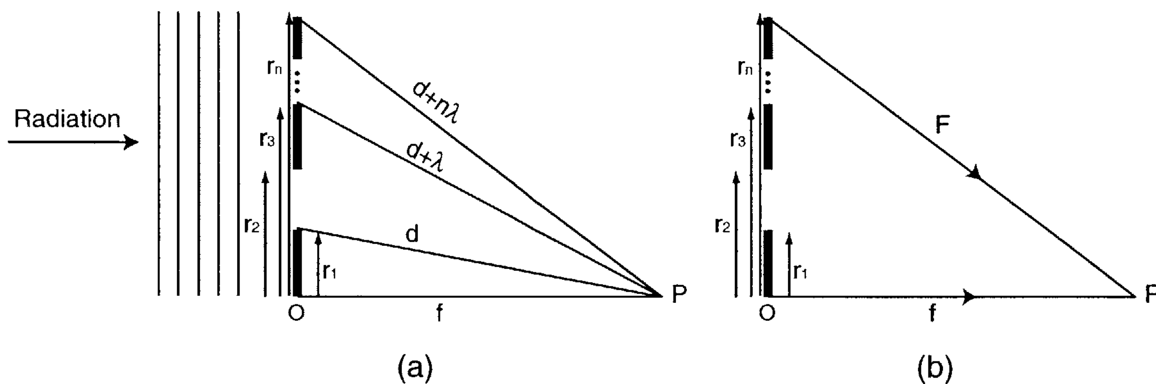

Figure 3 - 3. Zone plate geometry

It presents the cross section along a zone plate radius, with a ray diagram indicating the lengths of possible light paths from an incoming plane wave to P. The objective is to derive the necessary expressions for the radii of the zone boundaries. Since we are trying to model a zone plate, we will assume that the total optical path to P via the nth zone differs by $\pm\lambda/2$ from the path through the corresponding point on a neighboring zone. To avoid confusions, it should be noted that zones are constituted both by open and closed annuli. If the zone plate is to work efficiently, the difference in path

length between any point in an open zone and the corresponding point in the next open zone should be equal to the wavelength of the light used, λ

We determine the values of r_n by demanding that the optical paths F and f (see Figure 3 - 3) differ by $\frac{n\lambda}{2}$, so

$$F = f + \frac{n \cdot \lambda}{2} \qquad \textbf{3 - 1}$$

Since $r_n^2 = F^2 - f^2$, we find that

$$r_n = \sqrt{n \cdot \lambda \cdot f + n^2 \cdot \frac{\lambda^2}{4}} \qquad \textbf{3 - 2}$$

If $f >> \frac{n\lambda}{4}$, which is generally a good approximation if x-ray zone plates are used, the radius of the nth zone is expressed as

$$r_n \cong \sqrt{n \cdot \lambda \cdot f} \qquad \textbf{3 - 3}$$

Rearranging, we find the approximate expression for the focal length of a zone plate

$$f = \frac{r_n^2}{n \cdot \lambda} \qquad \textbf{3 - 4}$$

3.2.2 Zone Plate Design

There are a few independent variables to choose from that influence the performance of a zone plate. The important variables are the wavelength, the number of zones, and the outer zone period. There are, however, many tradeoffs involved in the selection of these variables, especially when zone plates are integrated in a lithographic system such as ZPAL.

For instance, the wavelength can be chosen at will, however, as discussed previously, in practice one is restricted due to the availability of laser lines (for UV ZPAL) and soft x-ray sources of reasonable cost (for X-ray ZPAL). The choice of wavelength can also be restricted due to the micromechanics that modulate the light impinging upon the zone plates, for reasons that will become apparent in the following chapter. Ultimately, the wavelength limits the resolution of the system, the cost and the ease of use.

Once the wavelength is selected, the next step is to choose the number of zones. This parameter is intimately linked with the source bandwidth, limiting the number of zones per zone plate. The number of zones is also limited by practical considerations, such as the actual size of the zone plate. Because a ZPAL system will be limited either by either the frequency of the micromechanics or the repetition rate of the laser, whichever is smaller, the bigger the zone plate, the bigger the unit cell (defined as the area of the substrate that each zone plate is responsible for exposing), and as a consequence, the lower the throughput.

The third parameter of importance is the outer zone period. When a zone plate focuses radiation to its first order focus, it does so to a spot whose size is approximately equal to the outer zone width of the zone plate. The period of the zone plate is approximately twice the outer zone width, so therefore, by choosing the period, we are fixing the minimum linewidth we are going to be able to write in a substrate with ZPAL.

3.2.2.1 UV Zone Plate Design

The zone plates for our UV setup were designed for 442 nm radiation. This choice was made exclusively due to the micromechanics used, i.e.,the Texas Instruments Micromirrors. These micromirrors are packaged in a glass cage that absorbs all radiation below ~350 nm. As a consequence, a He-Cd laser with λ=442nm was used.

Because zone plates are based on diffraction they are subject to chromatic aberration. That is, different wavelengths are focused at different axial distances. A zone

plate will produce a diffraction-limited focal spot only for radiation in a bandwidth (BW) given by

$$BW < \frac{1}{N} \qquad \textbf{3 - 5}$$

where N is the total number of zones [2].

Equation 3 - 5 tells us that if the bandwidth of the source is not small enough, we might be limited in the number of zones we can have, which can severely impact the performance of the zone plate. Fortunately, this is not a problem with a laser, but it will be a problem with certain x-ray sources. The Liconix HeCd laser we use for our experiments has a bandwidth of 3 GHz. Expressing bandwidth as

$$BW = \frac{\Delta v}{v} = \frac{3GHz}{\left(\frac{3\times 10^{8}\,{}^{m}\!/_{s}}{442nm}\right)} = \frac{1}{226,244} \qquad \textbf{3 - 6}$$

therefore,

$$\frac{1}{226,244} < \frac{1}{N} \Rightarrow N < 226,244 \text{ zones}$$

This is certainly not a restriction for ZPAL, where we will always be dealing with zone plates with less than 100 zones.

The next step in zone-plate design is to calculate the zone plate radii for a given number of zones, while letting the resolution and the focal length vary. This last parameter, the focal length, is important for practical reasons, since it determines the gap between the zone plate array and the substrate. The gap distance between masks (the zone plate array in our case) and substrates in lithography can be critical, especially if the gap gets smaller than 20 μm. Too small a gap can cause problems for high volume manufacturing, so it's important to design a zone plate with a focal length that's greater than 20 μm.

It is not possible to solve explicitly for all these parameters, so a numerical solution was implemented using Matlab. The key concept is to realize that the outer zone width (OZW) is approximately equal to half the outer zone period, that is:

$$OZW = r_N - r_{N-1} = \frac{P\min}{2} \qquad \textbf{3 - 7}$$

Expanding r_N and r_{N-1} from equation 3 - 2,

$$OZW = \sqrt{f \cdot n \cdot \lambda + \frac{n^2 \cdot \lambda^2}{4}} - \sqrt{f \cdot (n-1) \cdot \lambda + \frac{(n-1)^2 \cdot \lambda^2}{4}} \qquad \textbf{3 - 8}$$

where f is the focal length, n is the number of zones, and $\lambda$is the wavelength.

This equation can now be solved iteratively with λ fixed and f and n varying to obtain the plot shown in Figure 3 - 4. The plot shows how the outer zone width, which is an indication of the resolution of the ZPAL system, varies as the focal length and the

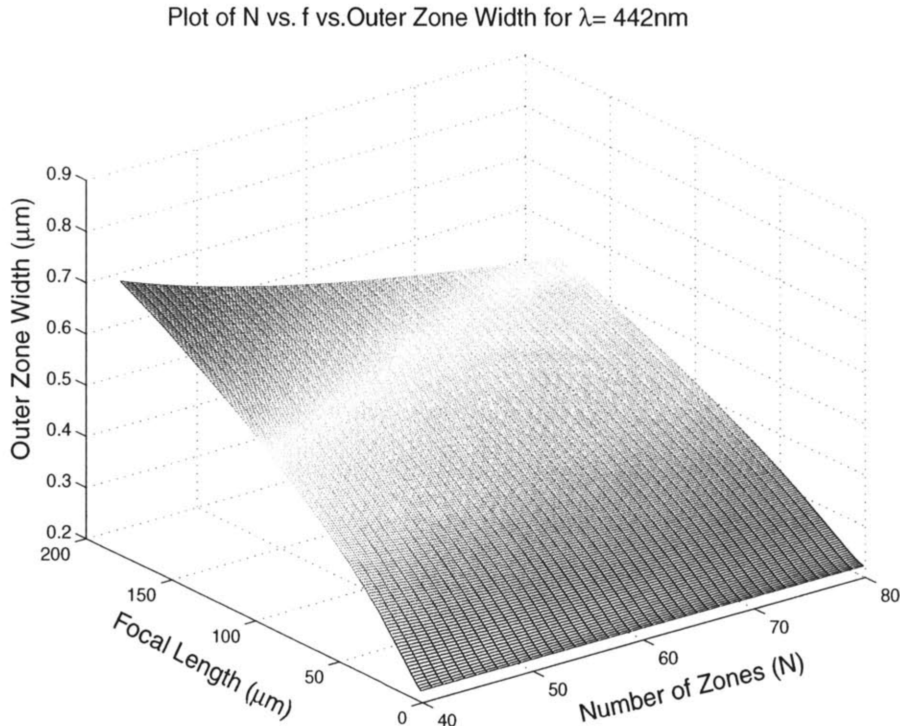

Figure 3 - 4: 3D mesh of Outer Zone Width vs. Focal length vs. Number of zones

number of zones are changed. We can see that as we increase the focal length, and therefore make the gap between the zone plates and the substrate bigger (a big plus!), the resolution decreases. But, looking at the curvature of the plot, it's apparent that this effect can be somewhat palliated by having a sufficient number of zones.

It is more convenient, however, to take contour plots of the solutions and plot them in two graphs as shown in Figure 3 - 5. These two graphs provide the guidelines for designing zone plates for 442 nm radiation. Figure 3 - 5 (a) is a contour plot of the outer zone width plotted versus the focal length and the number of zones. Figure 3 - 5 (b) plots the outer radius versus the number of zones and the focal length. One design criteria was to have a relatively large gap between the zone plates and the substrate, in excess of 40 μ m. We can see from Figure 3 - 5 (a) that the smallest outer zone width (best resolution) with this kind of focal length is 336 nm, provided we have more than 70 zones. In order to have some increased flexibility in terms of gap we chose to have 76 zones. We can then draw a line that extends from graph (a) into graph (b) as shown in the figure, and hence obtain at the crosspoint of Figure 3 - 5 (b) the radius of the zone plate: 44.6 μ m. The radii for each of the zones are calculated according to Equation 3- 2.

These are all the parameters we need to proceed to the fabrication of the zone plate arrays.

3.3 Zone Plate Fabrication

The first zone plates for visible light were made in the 19th century by Lord Rayleigh, Soret, and Wood by photographically demagnifying drawings of zone plates [38]. Through decades of research and improvements in fabrication techniques, zone plates capable of focusing light at almost all ranges of the electromagnetic spectrum, including soft x-rays, were fabricated. It was Baez in 1961 [39] who first constructed zone plates capable of working with extreme ultra-violet and soft x-ray radiation. Because at these wavelengths radiation is absorbed by photographic plates, it was necessary for Baez to either fabricate unsupported zone plates, or support them on very

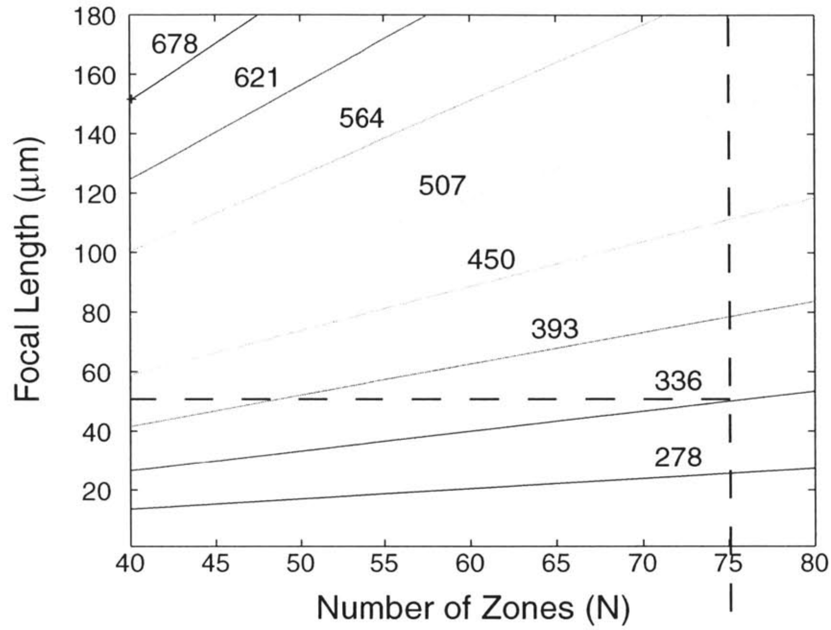

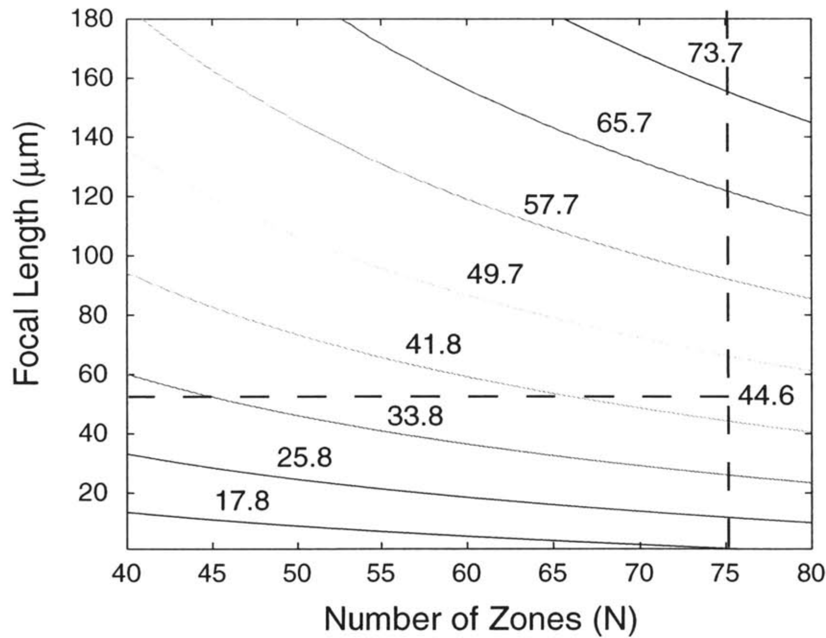

Figure 3 - 5 : Contour plots for UV-Zone Plate Design

thin transmitting membranes. He was able to fabricate unsupported zone plates for imaging for 253.7 nm radiation. The zone plates consisted of 19 rings of gold with a diameter of 2.6 mm, an outer zone width of 17 μm, and a focal length of 15 cm.

However, it soon became apparent that other techniques besides photo-reduction and mechanical ruling were necessary to fabricate high-resolution zone plates capable of operating at such short wavelengths. The challenges for the fabrication were twofold: the smallest linewidth desired was (and still is) beyond the resolution of optical projection systems, and the number of zones could sometimes be very large. Another important aspect is the placement of the features. For diffraction limited performance, the errors in the positioning of the each section of each ring has to be a small fraction of the zone period. Baez proposed holography in 1961 to produce zone plates with large number of zones [39]. However, lasers were not yet available at this time, and the requirements for spatial and temporal coherence reduced the intensity of conventional sources too much to be of practical use for the production of high quality zone plates. Holography became an easy method only after high-quality laser sources became available, and interference patterns with huge number of fringes could be produced routinely.

Electron beam systems for the fabrication of fine microcircuit patterns were first developed in the 1960s, and zone plates were often used as test patterns to demonstrate the resolution. Ever since, with holography still being the choice for certain applications, electron beam lithography has been the main tool for the fabrication of zone plates. The strength of holography is the large field; the strength of ebeam systems, the high resolution and the flexibility [40].

3.3.1 Fabrication of UV Zone Plates - Calculations

Because of the reasons explained in the previous section, and the need to fabricate arrays of zone plates and not just individual ones, the UV zone plates were fabricated with an ebeam system. Fortunately for us, we have an ebeam available in house, well capable of achieving the resolution and placement accuracy needed to fabricate UV zone plates.

In Section 3.1 it was mentioned that there are two types of zone plates: amplitude zone plates and phase zone plates. Amplitude zone plates are much less efficient than phase zone plates, focusing approximately 10% of the incident radiation into the first-order focus, whereas phase zone plates can have up to 40% efficiencies. Phase zone plates also have the advantage of eliminating the zero order, hence eliminating deleterious background radiation that is potentially damaging for lithography. The issue of background will be analyzed in Section 3.4.

Because of the better efficiency, it was decided to fabricate phase zone plates for UV-ZPAL. Due to its well characterized optical properties and availability, we used fused quartz substrates as the material of our zone plates.

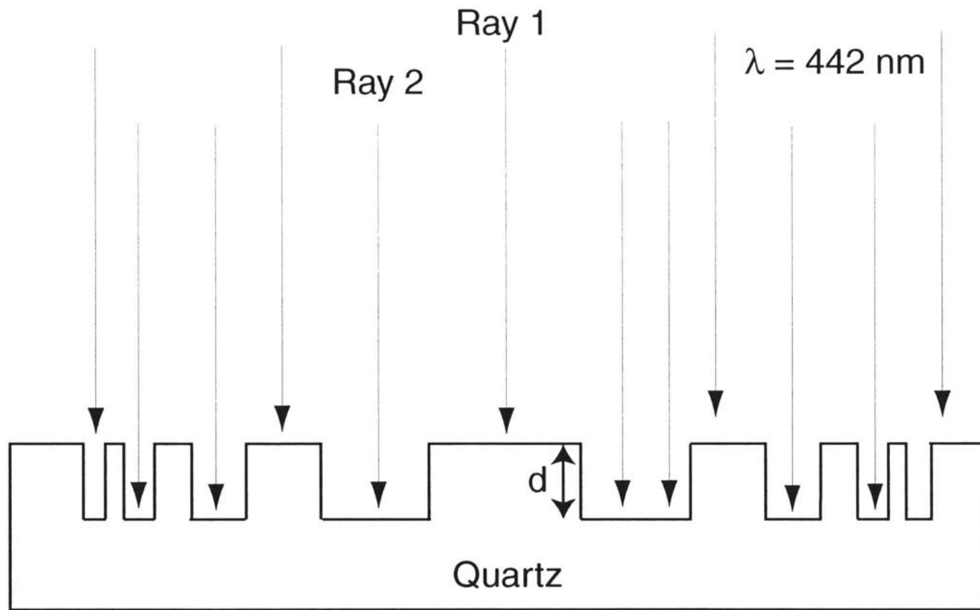

Figure 3 - 6: Phase Zone Plate

The first parameter that needs to be calculated prior to proceeding to fabricate the zone plates is the depth of the quartz etch, *d* (see Figure 3 - 6), that will provoke a π phase shift between adjacent zones. Still referring to Figure 3 - 6, we can model the light form our laser impinging upon the zone plate as a plane wave, with a wavefunction Ψ. Therefore, we can write

$$\Psi = A \cdot e^{i \cdot \vec{k} \cdot \vec{r}} \qquad \textbf{3 - 9}$$

$$\text{where } k = \frac{2\pi}{\lambda} \cdot n$$

and n is now the index of refraction of the material (at $\lambda = 442$ nm the index of refraction of fused quartz is $n_r = 1.466287$ at 18°).

Let's see what happens to light as it goes through paths 1 & 2 in Figure 3 - 6. For path 1, light goes through quartz a distance d, and the wavefunction for light can be written as:

$$\Psi_1 = A \cdot e^{i \cdot \vec{k} \cdot d} = A_1 \cdot e^{i \cdot \frac{2\pi}{\lambda} \cdot n_r \cdot d} \qquad \textbf{3 - 10}$$

Light going through path 2 will only travel in air, so n = 1.

$$\Psi_2 = A \cdot e^{i \cdot \vec{k} \cdot d} = A \cdot e^{i \cdot \frac{2\pi}{\lambda} \cdot d} \qquad \textbf{3 - 11}$$

At depth d, we want a π shift between the light that traveled path 1 and the light that did traveled path 2, therefore:

$$\Delta\Theta = \pi = \frac{2\pi}{\lambda} \cdot n_r \cdot d - \frac{2\pi}{\lambda} \cdot d = \frac{2\pi}{\lambda} \cdot d \cdot (n_r - 1) \qquad \textbf{3 - 12}$$

Solving for d:

$$d = \frac{\lambda}{2} \cdot \frac{1}{n_r - 1} \qquad \textbf{3 - 13}$$

Since λ= 442 nm and n_r= 1.466287,

d = 474 nm = Etch Depth

On the substrate holding the zone plates, we want to block all the incident radiation that is not going through the zone plate. Thus, we deposit a layer of Cr around

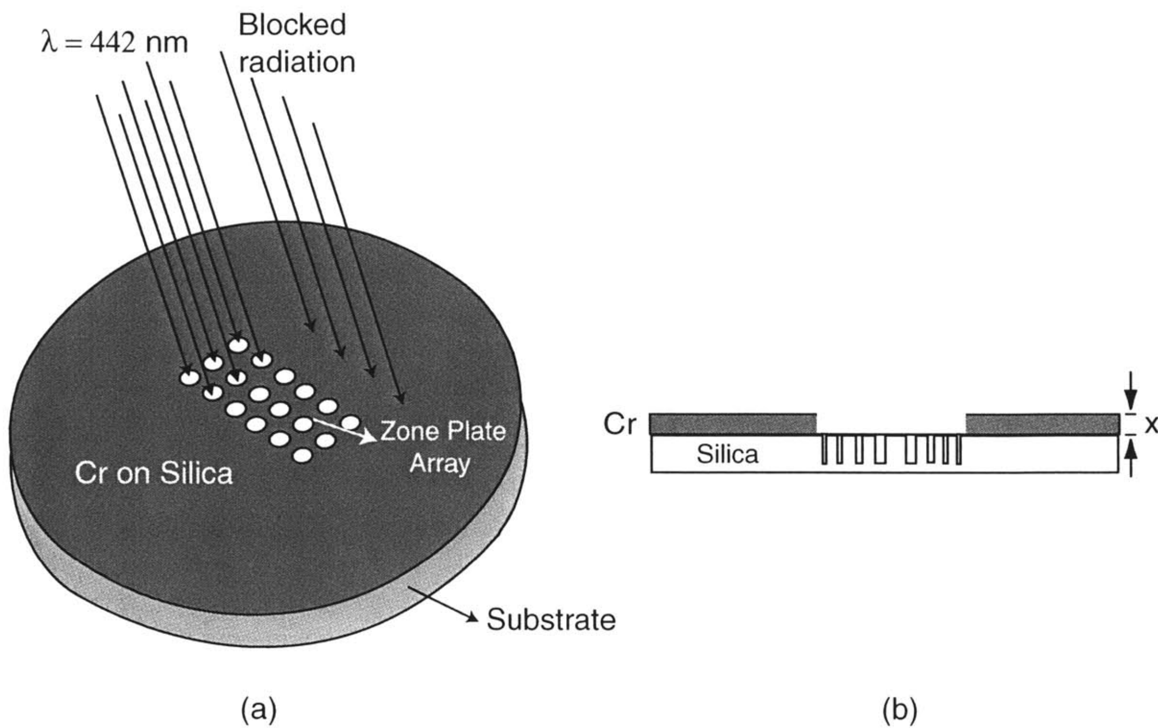

Figure 3 - 7. Need for Chrome. (a) Three dimensional view of the zone plate array and the substrate underneath. A layer of an absorbing material surrounding the zone plates, Cr in this case, is needed in order to prevent undesired radiation from exposing the substrate. (b) Side view of the fused silica wafer with a zone plate etched into it.

the zone plates as illustrated in Figure 3 - 7.

We use the skin depth as the criterion to determine the thickness of the Cr layer that needed. The skin depth tells us when the incident radiation has been attenuated by 1/e due to absorption in the material through which light is propagating .

Again, we can model the incident radiation as:

$$\Psi = e^{i \cdot \vec{k} \cdot x} \qquad \textbf{3 - 14}$$

Since we are now considering attenuation we want to use the imaginary part of the index of refraction. We get:

$$\Psi = e^{i \cdot \vec{k} \cdot x} = e^{i \cdot \frac{2\pi}{\lambda} \cdot i \cdot n_i \cdot x} = e^{-\frac{2\pi}{\lambda} \cdot n_i \cdot x} \qquad \textbf{3 - 15}$$

Rearranging to put it in terms of the skin depth:

$$\Psi = \left(\frac{1}{e}\right)^{\frac{2\pi}{\lambda}\cdot n_i \cdot x} \qquad 3-16$$

If we want to attenuate the incident radiation by 5 skin depths:

$$\left(\frac{1}{e}\right)^5 = \left(\frac{1}{e}\right)^{\frac{2\pi}{\lambda}\cdot n_i \cdot x} \qquad 3-17$$

therefore,

$$5 = \frac{2\pi}{\lambda}\cdot n_i \cdot x \rightarrow x = \frac{5}{2\pi}\cdot\frac{\lambda}{n_i} \qquad 3-18$$

For λ= 442 nm , n_r = 4.06

X = 5 x Skin Depth = **86.633 nm**

Therefore, the Skin Depth = 17.317 nm.

3.3.2 Fabrication of UV Zone Plates - Processing

The fabrication of UV zone plates involves significant ebeam writing time and some cleanroom processing, of which the reactive ion etching (RIE) step is the most critical, and the one that requires careful monitoring. The process flow of the fabrication procedure is outlined in Figure 3 - 8.

The main steps of the process are the following:

- Defining the areas in which the zone plates are going to be placed.
- Surrounding these areas with a Cr layer of the thickness calculated in the last section.
- E-beam write the actual zones inside the clear circles.
- Reactive ion etch the wafer to provide the desired π phase shift.

PROCESS FOR MAKING UV ZONE PLATES

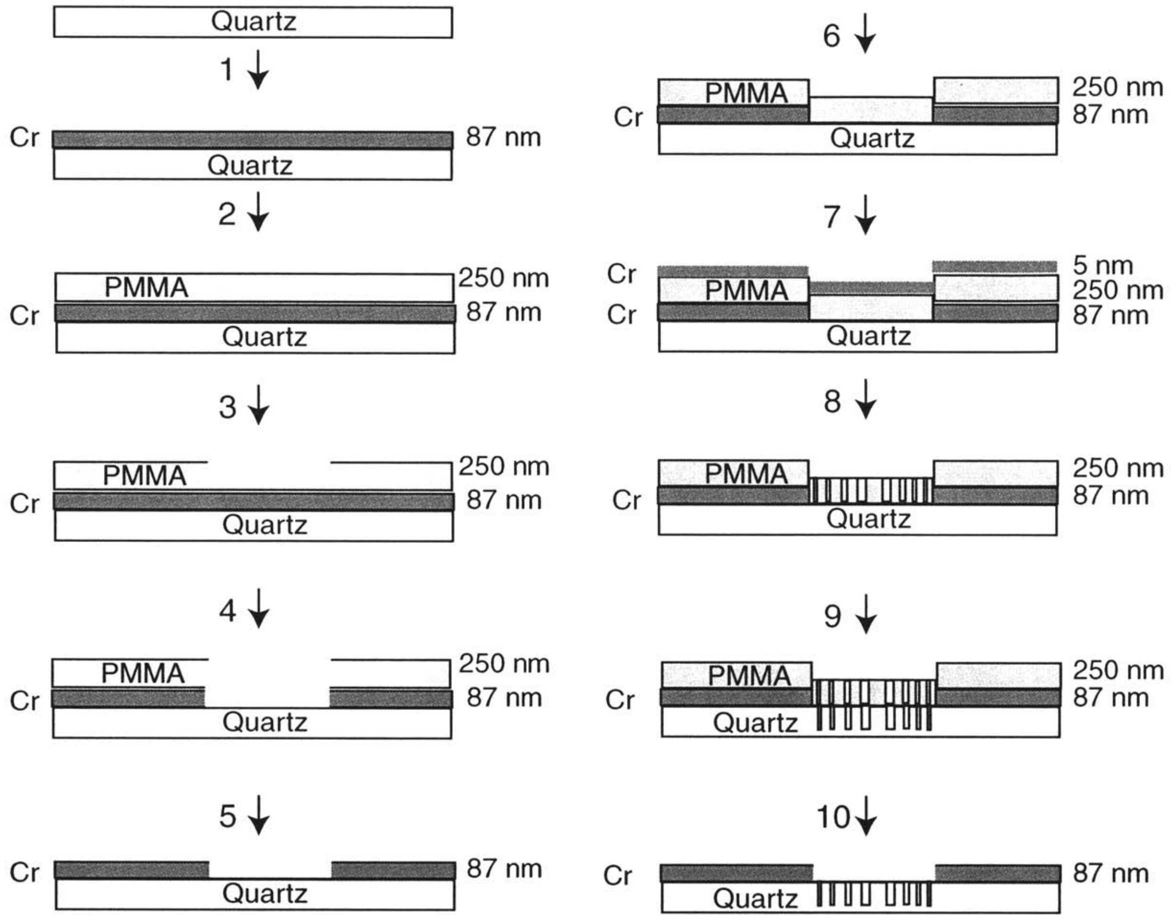

Figure 3 - 8: Process flow of UV Zone Plates

Detailed fabrication steps, including ebeam writing techniques, are included in Appendix A.

Four 3X3 arrays of zone plates were fabricated with various design parameters, as indicated in Table 3- 1. The objective in having many different arrays was to explore how high in numerical aperture (NA) the zone plates could be pushed for a particular wavelength (λ= 442 nm in this case). Figure 3 - 9 shows two scanning electron micrographs of Set 3 (PMMA on quartz). They corresponded to Step # 8 in Figure 3 - 8.

The Moire effect present in the left image is due to a beating between the periodicity of the zone plate and the periodicity of the pixels on the SEM TV screen. Figure 3 - 9 (b)

shows a detail of the outer zones. Notice the excellent agreement to the intended outer zone width of 336 nm.

	SET 1	SET 2	SET 3	SET 4
OZW (nm)	280	500	336	620
N	76	68	76	50
R_n(μ m)	34.26	64.27	44.64	59.67
f (μ m)	26.54	129.93	50.94	155.60
NA	0.79	0.44	0.65	0.79

Table 3- 1. Design parameters of fabricated zone plate arrays for UV-ZPAL[1]

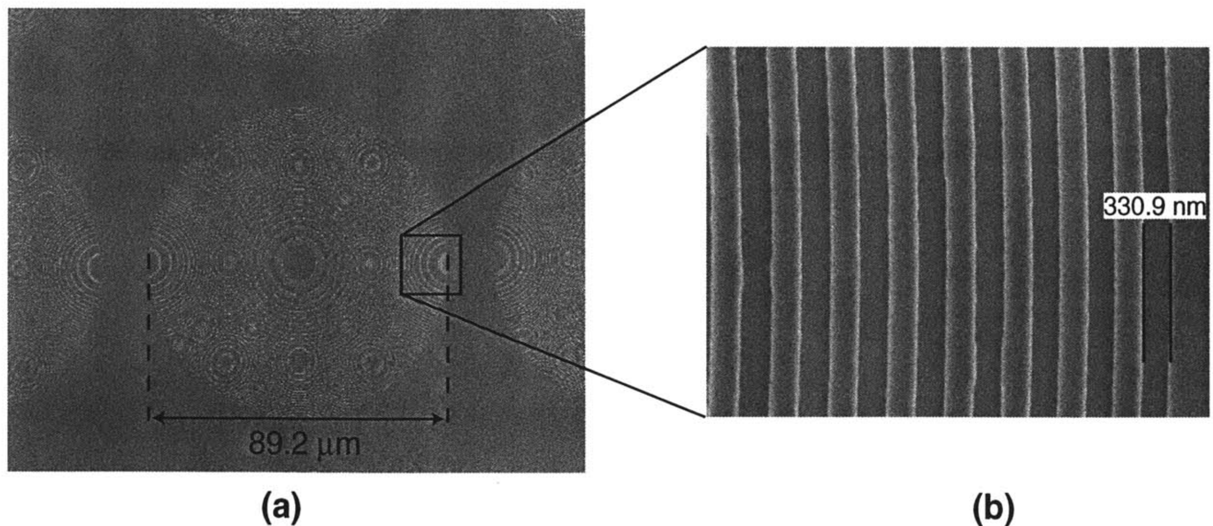

Figure 3 - 9. Scanning Electron Micrographs of Zone Plate Set 3 from Table 3- 1 (PMMA on quartz). (a) View of complete zone plate. The Moiré effect present in the image is due to a beating from the periodicity of the zone plate and the periodicity of the pixels on the SEM TV screen. (b) Detail of the outer zones. The intended outer zone width was 336 nm.

[1] Notation for Table 3- 1: OZW = Outer ZoneWidth, N = Number of Zones, R_n=Radius, f = focal length

3.4 Zone Plate Efficiencies, Background and the Need for Stops

The fact that we are using zone plates for lithographic purposes and not for imaging makes it necessary to pay attention to certain issues that traditionally have been somewhat overlooked in the zone plate community, such us image contrast, depth-of-focus and minimum feature size.

Lithography is all based on the ability to produce sufficient image contrast in a resist sensitive to the radiation used. Ideally, we would have a pattern that we want to reproduce, we would then put it through a black box (the perfect lithography tool), and obtain instantaneously the desired pattern printed on a substrate at the desired scale. Life, however, is not so sweet, and of the many issues that prevent us from achieving this lithographic nirvana is the issue of background. Background is present in all lithographic systems in one form or another. In optical lithography, there will be some diffraction of the image as the light propagates from the mask to the substrate, causing undesired exposures in areas that were not intended to receive radiation. In e-beam lithography, although the electrons might initially be aimed at the proper area on the substrate, forward scattering in the resist and backscattering from the substrate will tend to distribute the electrons in the resist. These effects will lead to a reduced volume dose contrast in the resist - the "unexposed" areas may be dosed somewhat, and the dose in the exposed regions may be reduced [41].

In ZPAL the problem of background is very significant due to the diffractive nature of zone plates. Because a zone plate is a form of diffraction grating, there will be more than one diffracted order. Whenever the optical path difference between rays passing consecutive zone boundaries is $m\lambda/2$ (for integer m), the zone plate will focus the radiation. Figure 3 - 10 shows schematically the ray paths for the first and third order foci that result when a zone plate is illuminated with a monochromatic plane wave. There will also be negative diffracted orders, corresponding to the radiation diverging from virtual foci. In theory a zone plate can have an great number of focal lengths

$$f_m = \frac{f}{m} \quad \textbf{3 - 19}$$

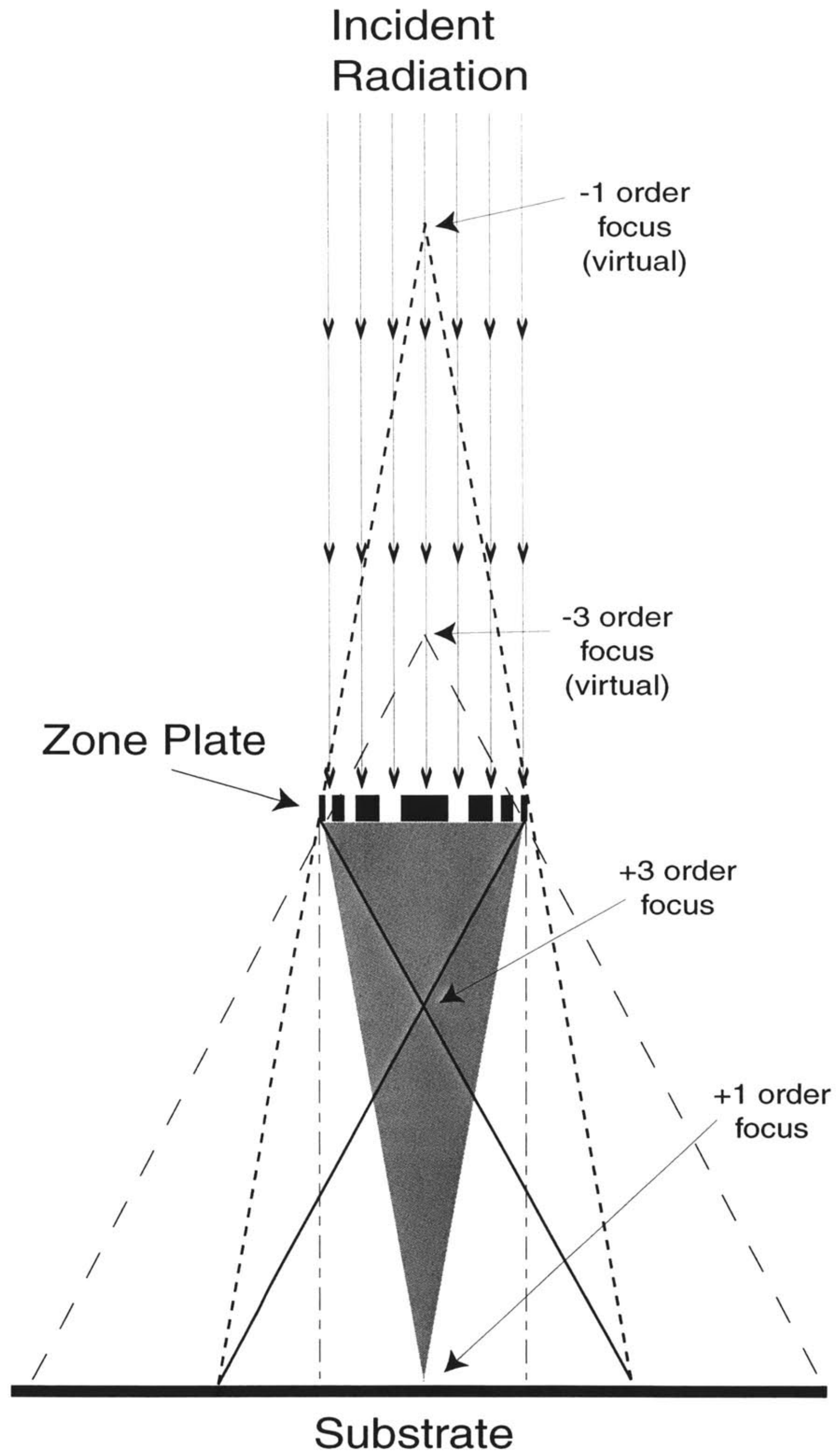

Figure 3 - 10: Zone Plate Orders

where m is an integer and $f \equiv f_1$ is given by Equation 3 - 4. However, not all these foci necessarily exist in practice, since some high orders of diffraction are cut off and the efficiency of diffraction of the various orders must be taken into account. For example, in the case of an amplitude zone plate the resultant amplitudes in all even-order foci are zero. Only odd-order foci ($m = \pm1, \pm3, \pm5...$) and zero-order (undiffracted) radiation are produced [42].

It's apparent from Figure 3 - 10 that any incident power which does not go into the positive first-order focus goes into the background. This background power, although of the same order of magnitude as the first-order power, is spread over a large area. If we were interested in exposing only a single pixel, or perhaps a few pixels in a field, the background would have little or no effect on the final pattern. However, the background from each exposed pixel in a field will add. The "worst-case" exposure would be if a field were to be fully exposed except for one unexposed pixel. This is shown schematically in Figure 3 - 11.

It is possible to analyze the effect of zone-plate design on contrast in the worst-case exposure. The background intensity distribution will be stepped and repeated across the unit cell of a zone plate, thus leaving behind an average intensity distribution from each diffracted order. This average intensity will be equal to the power into the order divided by the projected area of the order at the focal plane.

The single-spot contrast, $K^{\sin gle-spot}$, will be the +1-order intensity divided by the sum of the intensities from all the other diffracted orders. The worst case contrast, $K^{worst-case}$, will be the single-spot contrast divided by the number of pixels in a unit cell (equal to $16N^2$) [1].

Let's proceed to a more quantitative approach to analyze the issue of contrast and to explore the feasibility of producing a pattern as shown in Figure 3 - 11.

The calculation of zone-plate diffraction efficiencies is analogous to that for linear gratings, except that the zone plate structure is periodic in r^2 rather than in r. The period of a zone plate, p, can be approximated by

$$p \equiv r_n - r_{n-2} \qquad \textbf{3 - 20}$$

The mth-order diffraction efficiency for a Fresnel zone plate with a rectangular profile as shown in Figure 3 - 6 can be proven [43] to be

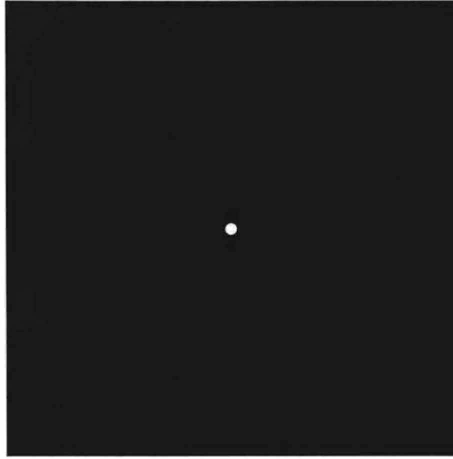

Figure 3 - 11: Worst Case Contrast

$$\varepsilon(m) = \left[A_1^2 + A_2^2 - 2A_1A_2\cos(\phi_2 - \phi_1)\right]\cdot\frac{\sin^2\left(m\pi g/p\right)}{m^2\pi^2} \qquad \textbf{3 - 21}$$

where p is the (unitless) period (=1), g is the duty cycle, A_n is the transmission amplitude through a segment, and ϕ_n is the phase shift through a segment

An ideal Fresnel zone plate has A_1=0, A_2=1, $g=p/2$ and $\phi_1 = \phi_2 = 0$, so that

$$\varepsilon(m) = \frac{\sin^2\left(m\pi/2\right)}{m^2\pi^2} \qquad \textbf{3 - 22}$$

From Equation 3 - 22 we can obtain the efficiencies of the various diffracted orders

$$\varepsilon(0) = 0.25 \text{ and } \varepsilon_m = \frac{1}{m^2\pi^2} \text{ for } m = \pm1, \pm3, \pm5, \ldots$$

and

$$\varepsilon(m) = 0 \text{ for } m = \pm2, \pm4, \pm6, \ldots$$

If we deal with amplitude zone plates then half of the zone plate area is opaque, absorbing half of the incident radiation. The most efficient focus is clearly the first order, with $\varepsilon(1) \approx 10\%$.

For phase zone plates, the condition is that $\phi_2 = \phi_1 + \pi$, and assuming that $A_1=A_2$ we get

$$\varepsilon(m) = \frac{4A_1^2 \sin^2\left(\frac{m\pi g}{p}\right)}{m^2\pi^2} \qquad \textbf{3 - 23}$$

which gives a maximum first-order efficiency of 40% when g/d=1/2 and $A_1 = 1$.

If the incident intensity is one, then the intensity, I, for the +1 order focus (focused to one pixel) at the focal plane a distance f from the zone plate will be

$$I^{+1} = \varepsilon_1^+ \cdot 16N^2 \cdot \left(\frac{\pi}{4}\right) \qquad \textbf{3 - 24}$$

The factor of π/4 comes from the area difference between the square unit cell and the circular zone plate, and 16 N^2 is the ratio of zone plate area to pixel area.

From the negative first order, which has a virtual source at -f, the same amount of energy will be spread out over four times the area of the zone plate (since the distance from virtual source to zone plate is half that from virtual source to focal plane). We therefore expect the background intensity from the -1 order radiation to be:

$$I^{-1} = 1 \cdot \varepsilon_1^- \cdot \left(\frac{\pi}{4}\right)\left(\frac{1}{4}\right) \qquad \textbf{3 - 25}$$

The positive and negative third-order foci will also contribute background. The +3 order focus occurs at $f/3$, and the -3 order occurs at $-f/3$. The +3 order focus will have a geometrical intensity reduction of 1/4, since the primary focal plane is two focal lengths away from the +3 focus. The -3 order will have a reduction of 1/16, since the primary focal plane is four focal lengths away from the -3 focus. So we have:

$$I^{+3} = 1 \cdot \varepsilon_3^+ \cdot \left(\frac{1}{4}\right) \qquad \textbf{3 - 26}$$

$$I^{-3} = 1 \cdot \varepsilon_3^- \cdot \left(\frac{1}{16}\right) \qquad \textbf{3 - 27}$$

The total background is therefore:

$$I^{bkgnd} = z + \varepsilon_1^-\left(\frac{\pi}{4}\right)\left(\frac{1}{4}\right) + \varepsilon_3^\pm\left(\frac{\pi}{4}\right)\left(\frac{1}{4} + \frac{1}{16}\right) + \ldots = z + \varepsilon_1^-\left(\frac{\pi}{16}\right) + \varepsilon_3^\pm\left(\frac{5\pi}{64}\right) + \ldots \qquad \textbf{3 - 28}$$

where z is the zero order intensity.

If we assume a pure amplitude zone plate and plug in for $\varepsilon_n^\pm$ from above, we get:

$$I^{bkgnd} = 0.25 + 0.1\left(\frac{\pi}{16}\right) + 0.011\left(\frac{5\pi}{64}\right) + \ldots = 0.272 \qquad \textbf{3 - 29}$$

$$I^{spot} = \varepsilon_1^+ \cdot 16N^2\left(\frac{\pi}{4}\right). \qquad \textbf{3 - 30}$$

This makes our contrast (for N=50):

$$K^{\text{single}} = \frac{I^{\text{spot}}}{I^{\text{bkgnd}}} = \frac{\varepsilon_1^+ \cdot 16N^2\left(\frac{\pi}{4}\right)}{0.25 + 0.1\left(\frac{\pi}{16}\right) + 0.011\left(\frac{5\pi}{64}\right) + \ldots} \cong \frac{3142}{0.272} = 11{,}550 \qquad \textbf{3 - 31}$$

This is for a single shot exposure. In the worst case (a single exposed spot surrounded by a ring of unexposed spots surrounded by a fully exposed field), this contrast is reduced by approximately $16N^2 = 40{,}000$, so the worst-case contrast is $\frac{K^{\text{single}}}{40{,}000} = 0.288$, which is clearly not sufficient.

3.4.1 The Effect of Stops

The contrast will improve if we add stops to prevent some of the unwanted radiation from making it to the substrate that is to be exposed. We will first consider the case of a pair of stops, as illustrated in Figure 3 - 12. The outer stop is placed between the zone plate and the substrate, and a complementary central stop is placed on the zone plate. This combination will totally block the zero-order. For the worst case scenario the blockage of the zero order yields a contrast of 3.5.

However, the stops also help in other ways. In addition to eliminating z in the above calculation, the pair of stops also decreases both the unwanted background radiation and some of the desired focused radiation. Let us examine this more closely for the case of an amplitude zone plate.

To better understand the effect of stops, we examine the expression for the worst-case contrast with no zero-order component. Written in symbolic form, it is:

$$K^{\text{worst case}} = \frac{I^{\text{spot}}}{16N^2 I^{\text{bkgnd}}} = \frac{\varepsilon_1^+ \cdot 16N^2\left(\frac{\pi}{4}\right)}{16N^2\left(\varepsilon_1^-\left(\frac{\pi}{16}\right)+\varepsilon_3^\pm\left(\frac{5\pi}{64}\right)+\ldots\right)} \qquad \textbf{3 - 32}$$

We now consider the effect of the stops. Let us define l as the fraction of f above which the outer stop lies above the substrate (see Figure 3 - 12). As l decreases, the outer stop moves closer to the substrate and the circular hole through which radiation passes gets smaller. As l increases, the outer stop moves closer to the zone plate and its hole gets larger. Since the central stop is complementary to the inner stop, as l decreases, the size of the central stop (and the fraction of the zone plate which is blocked) decreases. As l approaches one, the zone plate approaches being fully covered by the central stop. Obviously there will be some tradeoff between a small l, which will give better contrast at the expense of a smaller outer-stop-to-substrate gap, and a large l, which will give a

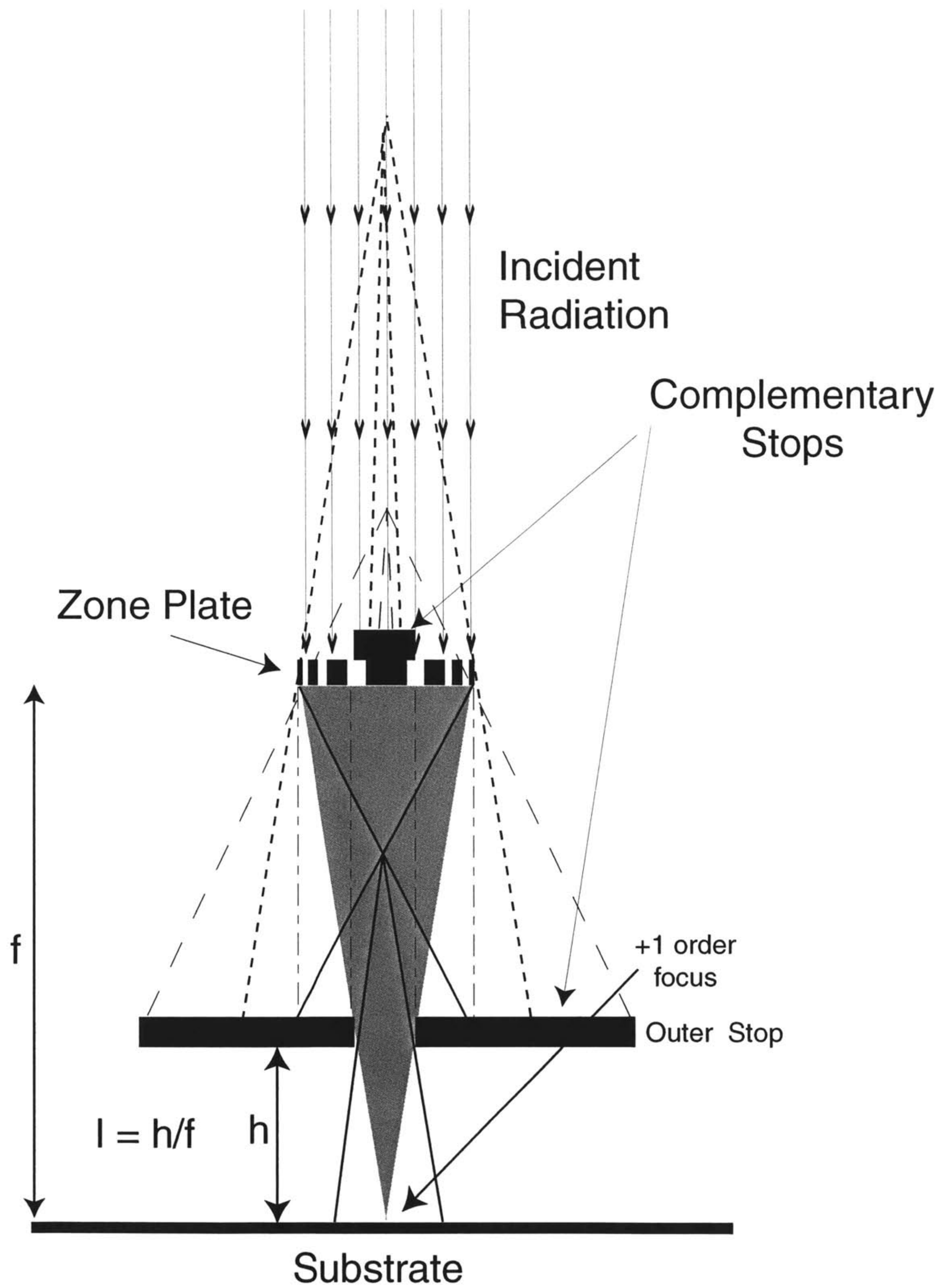

Figure 3 - 12: Zone Plate with Stops

larger gap (which reduces contrast), but which will prevent much of the incident radiation from reaching the substrate.

The areal fraction of the zone plate which is covered by the central stop equals l^2. The areal fraction which transmits is $1-l^2$. This will decrease the focused power and reduce the throughput of the ZPAL system. Since all the orders will have their power reduced by the same factor, we will neglect the effect of the central stop for the rest of this calculation, with the caveat that increasing l will impact throughput, which may need to be factored in with any contrast optimization in a full system design.

The combination of inner and outer stops eliminate zero-order radiation . In the case of a phase zone plate, the inner stop would not be needed, since the zero order would be cancelled by design. A significant amount of additional contrast improvement comes from the reduction of other radiation orders by the outer stop.

The outer stop improves worst-case contrast by blocking off background radiation from pixels which are far from the center pixel in the worst-case scenario previously described (Figure 3 - 11). Since all of the diffracted radiation reaches either the substrate or the stop, only the background radiation will be reduced by a factor equal to the fraction of the area which is covered by the outer stop.

The areal fraction which is left open is simply l^2. The expression for worst-case contrast therefore becomes

$$K^{\text{worst case}} = \frac{\varepsilon_1^+\left(\frac{\pi}{4}\right)}{l^2\left(\varepsilon_1^-\left(\frac{\pi}{16}\right)+\varepsilon_3^\pm\left(\frac{5\pi}{64}\right)+\ldots\right)} \tag{3 - 33}$$

Figure 3 - 13 plots contrast vs. l for the cases of an amplitude and a phase zone plate. Even with conservative stop heights which will yield large gaps, contrasts above ten can be obtained. Note that in state-of-the-art photolithography for VLSI manufacturing, a contrast of 3 is considered sufficient. The ability to work at such low contrasts is due to the high contrast of modern resists.

The analysis presented above is clearly a simple geometrical approach to a very real problem that deserves to be treated more rigorously by means of simulations. Still,

despite its limitations, the analysis provides a basic understanding about the need for stops and how they can help achieve excellent contrast in patterning with zone plates.

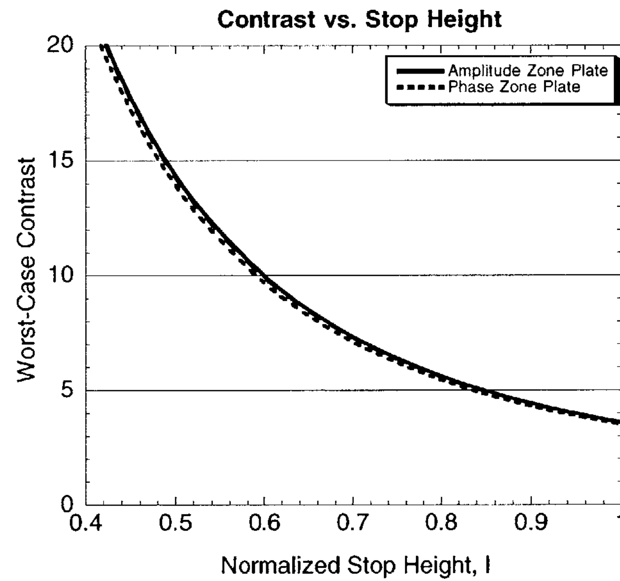

Figure 3 - 13. Contrast vs. normalized stop height, *l*, for amplitude and phase zone plates.

Chapter 4

ZPAL System Design and Construction

This chapter presents the work done to design and build a complete UV-ZPAL system capable of writing arbitrary patterns on resist.

4.1 System Components

As described in Chapter 2 a ZPAL system is comprised of 4 key components:

- A light source
- Micromechanics
- A Zone-Plate array
- A high-precision scanning stage

The successful integration of all these components is the key to the success of the technology, since all four elements have been proven to work well independently. It is therefore worth taking a closer look at the remaining elements that have not been

analyzed so far in the previous chapters (i.e. the laser, the micromechanics and the stage) to achieve the necessary understanding needed to optimally couple the different technologies. To provide a structure in the description of the ZPAL system, the next sections will cover, step by step, the "journey" of the photons from the time they are generated in the laser to the time they get absorbed in the resist. As explained, the polarization of the laser beam will be changed, the beam will be stabilized, filtered and expanded. It will be reflected off a micromirror array, then go through beam shaping optics to finally be focused by the zone-plate array. Lets proceed then with how the photons were generated for the experiments performed.

4.2 The Laser

The zone plates for the UV-ZPAL system were designed for 442 nm radiation. This choice was made exclusively due to the micromechanics that were used, the Texas Instruments Micromirrors. These micromirrors are packaged in a glass enclosure that absorbs all radiation below ~350 nm. As a consequence, a He-Cd laser operating at λ=442nm was used.

The HeCd laser (Figure 4- 1) is a member of the same laser family as the HeNe, and is the only relatively economical, continuous-wave source for violet (442 nm) and ultraviolet (325 nm) output. The lasing element in the HeCd laser is cadmium. At room temperature, cadmium is a metal. For lasing to occur, the metal must be evaporated from a reservoir, and then the vapor must be distributed uniformly down the laser bore. All gas lasers have the need, and hence the problem, of maintaining the correct distribution of vapor in the tube to optimize the output power. Under normal conditions the ionized cadmium atoms, which provide the energy levels between which laser action takes place, drift towards the anode. This phenomenon is known as cataphoresis and tends to produce a gradient in the ion concentration so that at only one point along the length of the tube is the concentration optimized. If the tube is wide enough, diffusion will oppose this effect and prohibit the build up of large concentration gradients. A fairly uniform distribution is accomplished by flowing cadmium down the tube towards the cathode thus counteracting

cataphoresis. The gas tube itself is made hot enough by the discharge to prevent condensation of the cadmium vapor. The end of the life of the laser typically occurs after 10,000 hours when the cadmium is depleted from its reservoir.

A schematic diagram of a HeCd laser is shown in Figure 4- 1. The HeCd laser used for the UV-ZPAL system is dual-wavelength (λ=442nm and λ=325nm) and it's manufactured by LICONIX (currently a part of Melles-Griot). It has an output power of P=45mW @ λ=442nm and P=11mW @ λ=325nm. The beam diameter is 1.3mm (at $1/e^2$) and the divergence is 1 mR (at $1/e^2$).

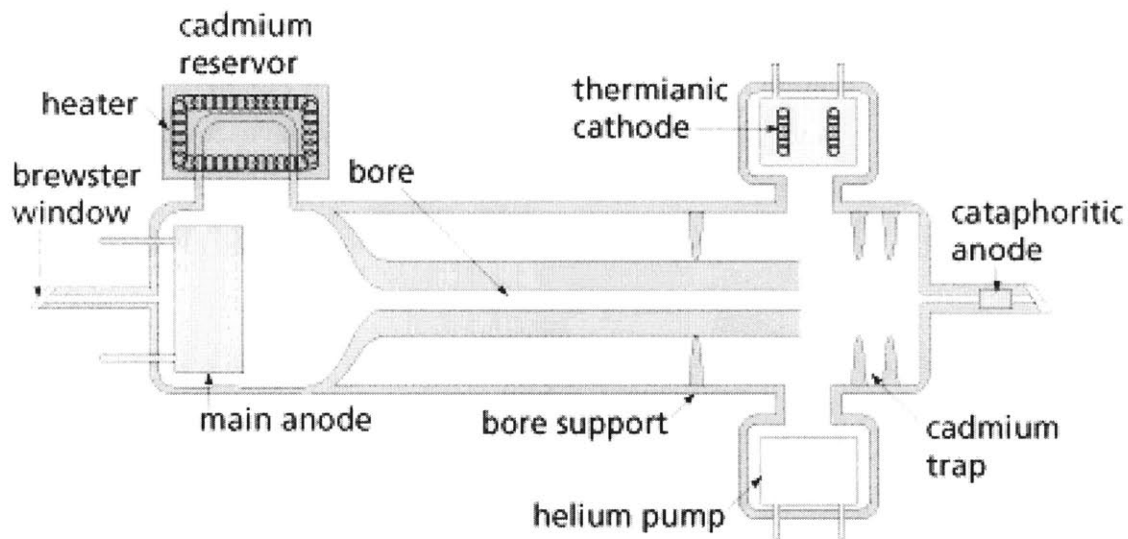

Figure 4- 1. He-Cd Laser Schematic

There are two issues that have to dealt with before the laser output can be used for ZPAL exposures: the polarization of the laser light and the power fluctuations of the beam.

4.2.1. The right polarization for ZPAL

Polarization studies for zone-plates is an area that has not been significantly studied in the past, so without constructing a rigorous vector model it's difficult to assess

the impact of polarization on zone plate performance[1]. However we can try to make preliminary arguments about what the right polarization should be for ZPAL. Because zone-plates are circularly symmetric diffractive structures, it seems plausible that if we want to prevent astigmatism in the focused spot the light illuminating the zone-plates should be circularly polarized. The astigmatism arises due to the fact that gratings (locally we can always think of a zone plate as a grating) have different efficiencies depending on the direction of polarization with respect to the orientation of the grating [44]. The He-Cd laser has a Brewster window at the output, making the beam linearly polarized. To convert the light's polarization from linear to circular a 1/4 wave plate is used. Figure 4- 2 shows a linearly polarized beam of light falling on a transparent anisotropic crystal so that the vector $\vec{E}$ is at an angle of 45° to the optical axis of the crystal. The ordinary and the extraordinary waves at entry have equal phases and amplitudes. The thickness of the crystal is chosen so that the phase difference between the ordinary and the extraordinary waves equal to $\pi/2$ when they exit the crystal.

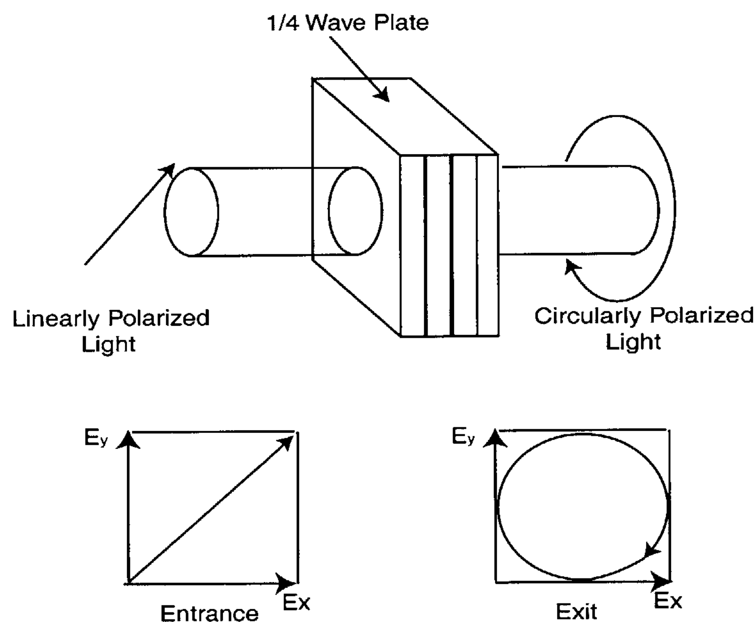

Figure 4- 2. 1/4 wave plate. The transformation of linear polarization of light to circular polarization

[1] This area will be explored by Rajesh Menon's Masters Thesis "ZPAL: Simulations and System Design"

This shift correspond to a path difference equal to $\lambda/4$ (hence the name of 1/4 wave plate). The amplitudes of these waves thus remain equal, and the light leaving the crystal is circularly polarized

A practical question arises when using a 1/4 wave plate. The plate is typically mounted on a rotary stage so that it can be rotated to have the incoming beam at a 45° angle to the orientation of the crystal. The question is how to figure out when have we reached the right angle. To solve this problem the method illustrated in Figure 4 -3 can be used. Linearly polarized light passes through a beam splitter cube making it polarized in the P direction (I am picking a direction for simplicity only, it could be S as well). The light then passes through the 1/4 plate. At this point, depending on the rotational position of the quarter wave plate the light will be either elliptically polarized (most likely) or circularly polarized. To figure out what state the light is we let it reflect off a mirror, reversing the handedness of the polarization. The light goes again through the 1/4 wave plate, becoming linearly polarized again (it is a reversible optical system after all). This time however the direction of polarization will be different. If the plate was perfectly aligned the light will be polarized in the S direction. If, as it is more probable, the plate was somewhat misaligned the light will be in a combination of S and P polarization. In either case, we let the light go through the polarizing beam splitter again, and we look at the power reading of the detector as illustrated in Figure 4 -3. The beamsplitter will select what polarization can go through (the P) and which will be reflected towards the detector (the S). It's is now apparent what we should do. We should rotate the 1/4 wave plate until we maximize the power reading. When this occurs, the plate is aligned correctly and the light is circularly polarized.

4.2.2 Power Stabilization

To have a stable laser power is critical for ZPAL, since fluctuations in power will impact the spot size and hence the minimum feature size that the system is capable of. The system has not been characterized enough to know with precision how much process latitude we have in power fluctuations, but from the exposures performed it seems that

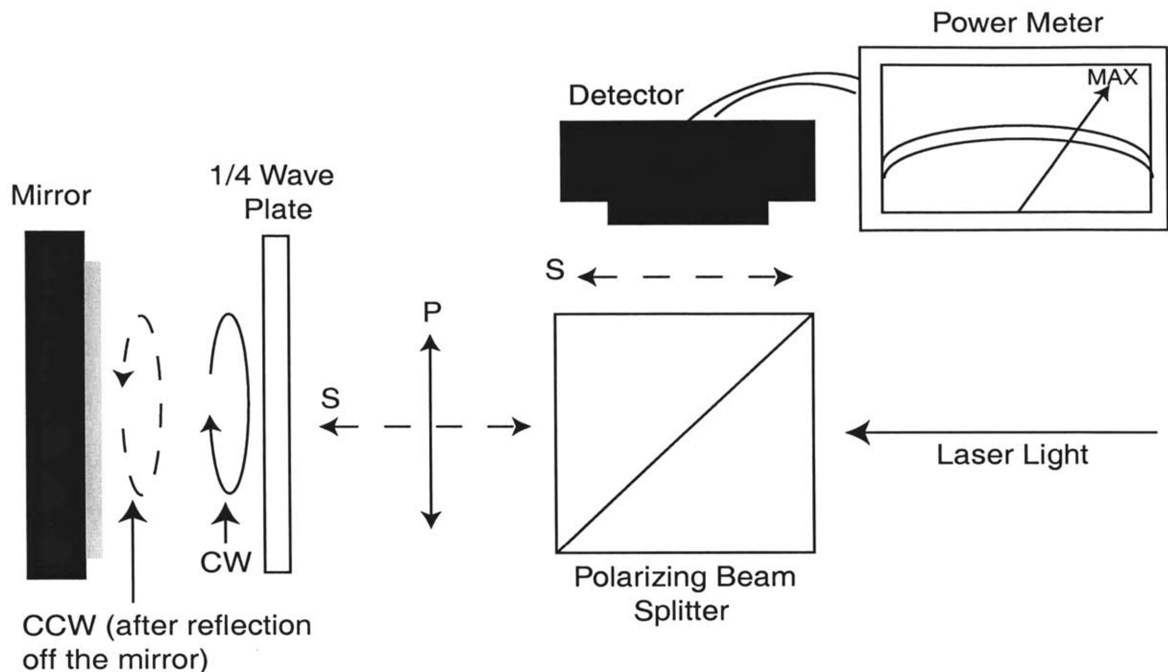

Figure 4- 3. Circular polarization detection scheme

this number should be under 1%. The He-Cd laser does not meet this criteria, with ~4.5% drift over the course of 2 hours. This implies that we must have an active power correction scheme with feedback. The way this is achieved is by means of a 1/2 wave plate and a polarizing beam splitter, as illustrated in Figure 4- 4.

A 1/2 plate has the effect of rotating the polarization of the incident beam by 90°. The concept is similar to the 1/4 wave plate except for the fact that the phase difference that the plate induces is π, instead of $\pi/2$. By using a polarization beam splitter we can decouple the S polarization from the P polarization. This is achieved by having a multilayer dielectric coating on the hypotenuse face of one of the prisms (the cube is made out of two prisms bonded together). The reflection from each layer is partially polarized and the cumulative effect of the multilayer coating produces transmitted and reflected beams that are highly polarized. The transmitted beam is P polarized and the reflected S polarized. The two prisms are bonded together with an index matching cement. All sides of the cube are coated with an antireflection coating.

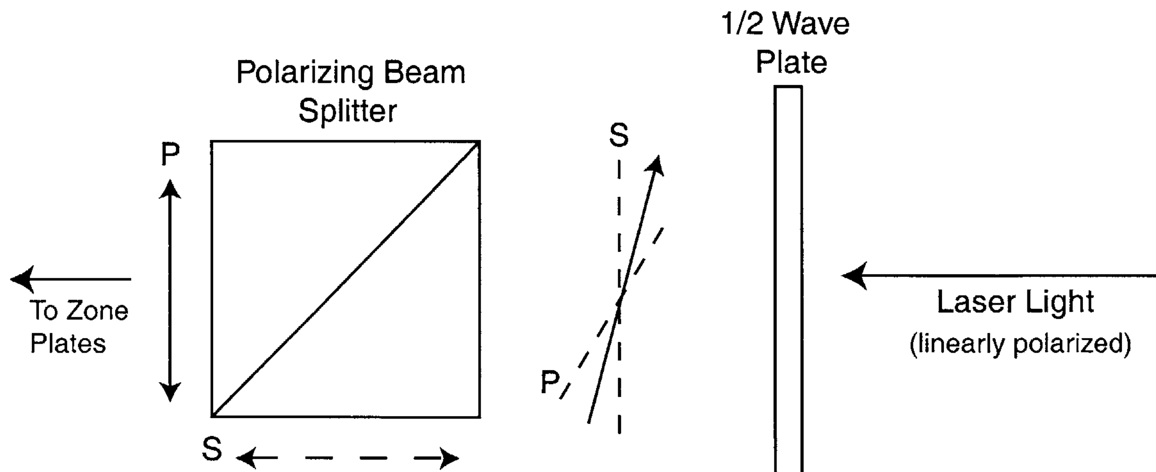

Figure 4- 4. Optics for laser power control.

The power of the laser beam is controlled in the following manner. The1/2 wave plate is mounted on a controllable rotary stage. The beam incident upon the plate is linearly polarized. By rotating the 1/2 wave plate the direction of the polarization angle with respect to the optical axis will change. If it is rotated so that the transmitted beam is lined up with the P direction, the beam splitter will allow all the light to go through (this is the direction of interest, the one that goes to the zone plate array) and the power will reach a maximum. If, on the other hand, the plate is rotated so that the beam is now lined up with the S axis, the beam splitter will deflect the light out of the desired path and the power will reach a minimum. By means of an active feedback system that will give a control signal to the rotating 1/2 wave plate, power fluctuations can be corrected. The block diagram of the feedback mechanism is illustrated in Figure 4- 5.

The 1/2 wave plate is rotated by means of an actuator (a Picomotor, manufactured by New Focus) that moves in response to a pulse. The feedback control is implemented via software (LABVIEW), with the intention of replacing it with a circuit box in the near future. Its basic mechanism of operation is to compare the current power with a desired power, and if the difference is larger than a user-specified threshold value, correct for it by rotating the 1/2 wave plate in the correct direction.

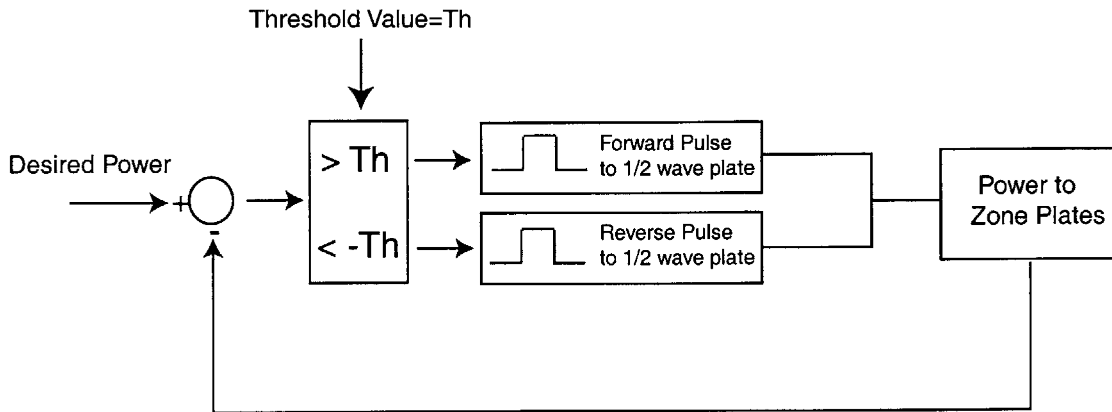

Figure 4- 5: Block diagram of power feedback

4.2.3 Cleaning and expanding the beam

The beam, after going through the steps described in the previous two sections, now has the right polarization (circular) and the right power. There is one more prerequisite that the beam has to satisfy prior to illuminating the zone plates. As shown in Figure 4- 6, the 1.3 mm beam has a gaussian profile with a 90% clipping level that corresponds to a spatial extent of 331.4 μm.

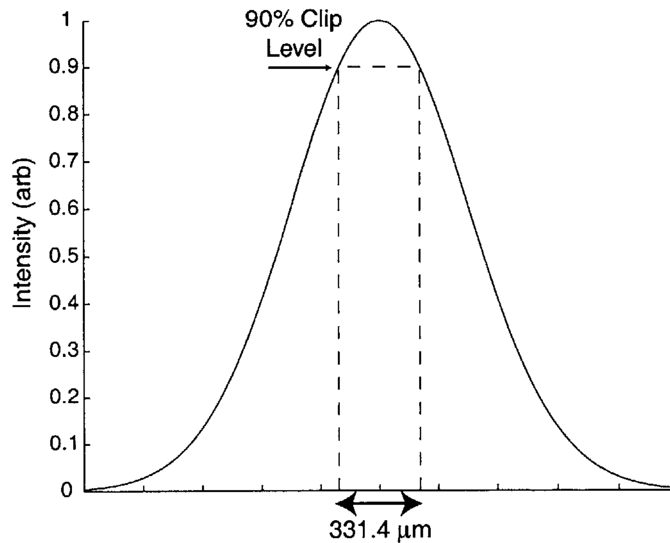

Figure 4- 6. Gaussian profile of 442nm He-Cd laser

If all zone plates are to have the same baseline for exposures the beam phase front must be uniform, with constant power delivered throughout the extent of the zone plate array. The array size for the experiments performed was 3x3, which corresponds to a 450x504 μm area. In order to have a power variation of less than 1% over this area the beam was expanded 33.3 times, so that the beam profile had a spatial extent of 0.5 cm for the 95% clipping level (=5% threshold), as shown in Figure 4- 7(b).

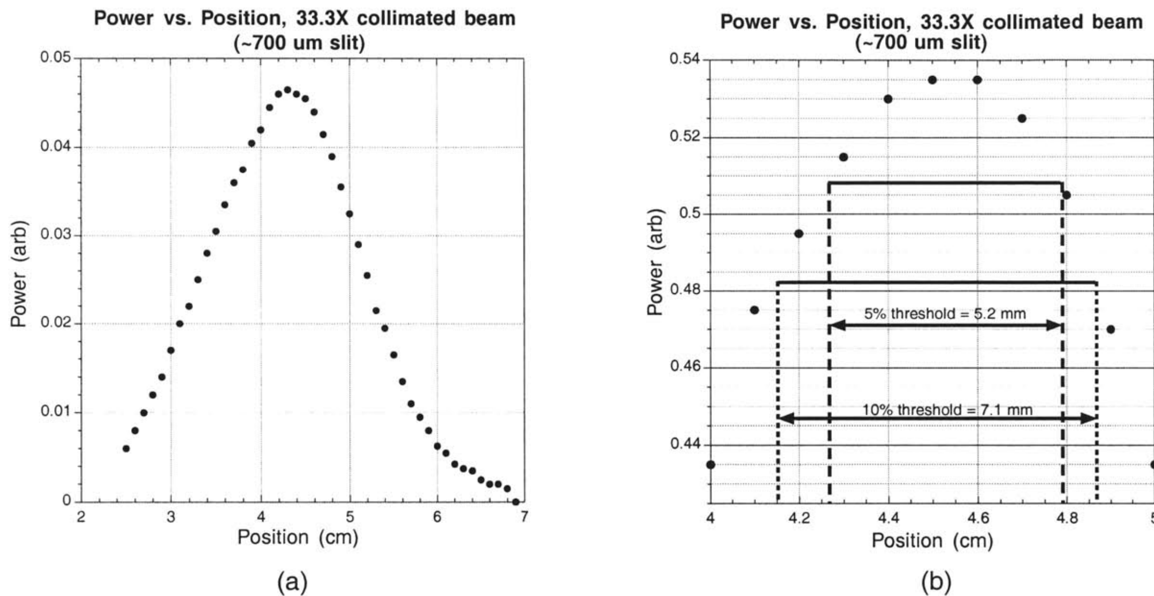

Figure 4- 7. Measured beam profile of He-Cd laser @ λ=442 nm. (a) Power vs. position after a 33.3X expansion, (b) 5% and 10% threshold values.

The beam was expanded and cleaned by means of a spatial filter in conjunction with a lens. The reason for using a spatial filter is to get rid of the spatial noise caused by the intensity variations from scattering by optical defects and particles in the air. The spatial filter will pass only the fundamental Gaussian mode of the laser cavity. Figure 4-8 schematically depicts the optics needed to clean and expand the beam.

When a Gaussian beam passes through a converging lens, the minimum beam diameter at the focal spot is limited by diffraction effects. The diffraction-limited spot size that the objective lens will form is given by

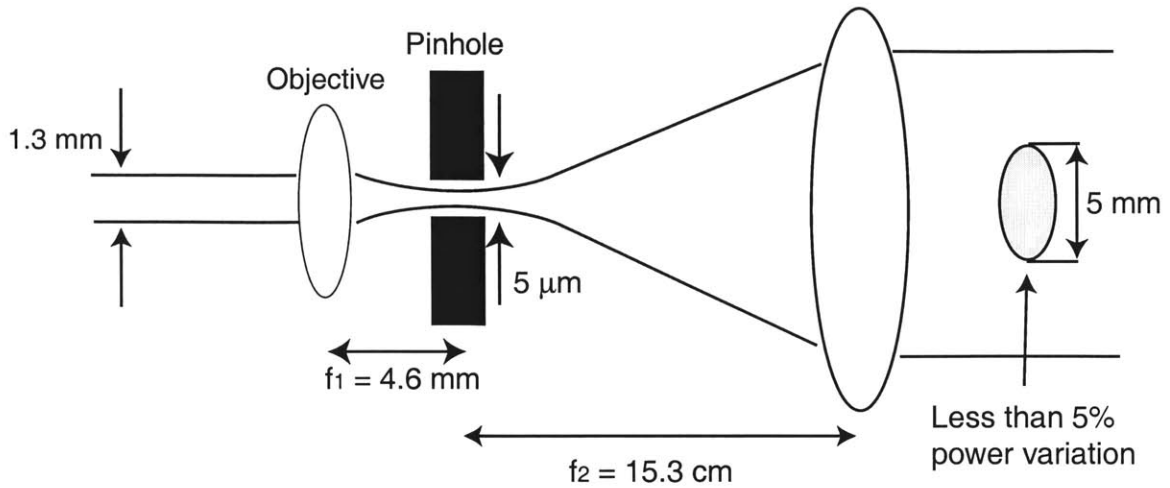

Figure 4- 8. Spatial filter and expansion optics

$$w_0 = \lambda \cdot f/\# \quad \textbf{4-1}$$

where λ is the wavelength and f/# is the f-number of the lens used to focus the beam into the pinhole (the objective lens). The f-number is defined as

$$f/\# = \frac{f}{D} \quad \textbf{4-2}$$

with *f* being the focal length of the lens and D its diameter. However, when calculating the f/# it is important to use the effective diameter of the lens, given by the actual area that illuminates the lens. For an f_1=4.6mm (40X objective with NA=0.66) the f/# is then

$$f/\# = \frac{f_1}{D_{effective}} = \frac{4.6mm}{1.3mm} = 3.54$$

where 1.3 mm is the laser beam diameter. This corresponds to a NA

$$NA = \frac{1}{2 \cdot f/\#} = 0.1413 \quad \textbf{4-3}$$

The diffraction limited spot size is then

$$w_0 = \lambda \cdot f/\# = 442nm \cdot 3.54 = 1.564\mu m \qquad \textbf{4-4}$$

Care should be taken in cutting off the beam with a small aperture. The source distribution would no longer be Gaussian, and the far-field intensity distribution would develop zeros and other non-Gaussian features. However, if the aperture is at least three or four w_0 in diameter, these effects are negligible. Hence, the pinhole size was chosen to be

$$Pinhole = 3 \cdot w_0 \approx 5\mu m$$

To obtain a 33.3X magnification

$$f_2 = 33.3 \cdot f_1 = 33.3 \cdot 4.6 = 153.18mm \qquad \textbf{4-5}$$

At this point all that remains to be done prior to the light being focused by the zone plates is to shape the beam into multiple beams (as many as there are zone plates) by means of micromechanics.

4.3 The Micromechanics

The current micromechanics of choice for UV-ZPAL are the Texas Instruments DLM (Digital Light Modulators) micromirror array[45]. They are used in the configuration shown schematically in Figure 4- 9. The TI micromirrors (Figure 4- 10) are a MEMS structure that is fabricated by CMOS-like processes over a CMOS memory. Each aluminum mirror, 16 μm^2, can reflect light in one of two directions depending on the state of the underlying memory cell. With the memory cell in the (1) state, the mirror rotates to +10 degrees. With the memory cell in the (0) state, the mirror rotates to -10 degrees. The mirrors are rigidly connected to an underlying yoke. Through the use of six photomask layers (see Figure 4- 10), the structure is formed with alternating layers of aluminum for the address electrode, hinge, yoke, and mirror layers and hardened

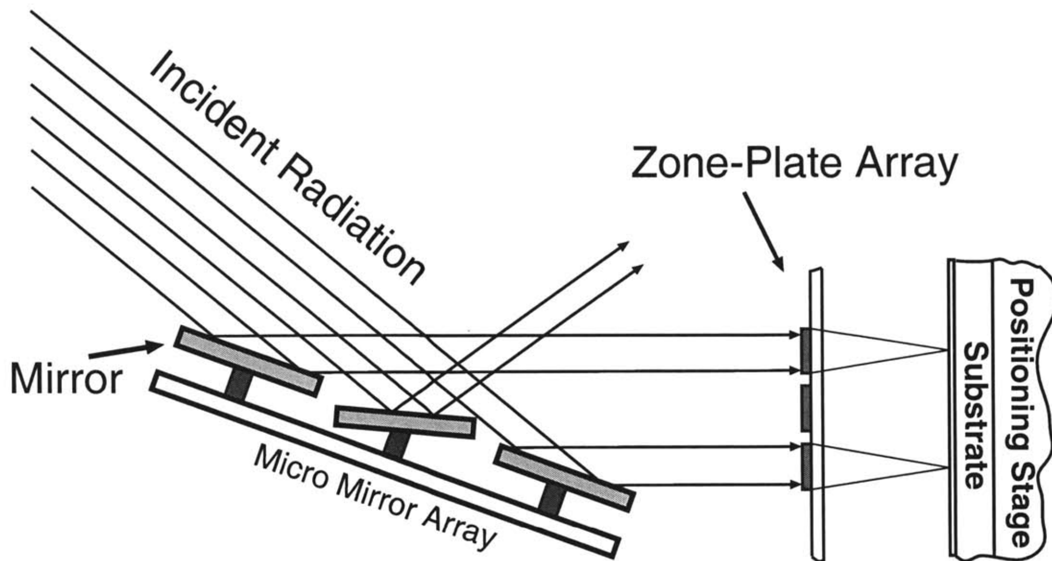

Figure 4- 9. Micromechanics for UV-ZPAL

photoresist for the sacrificial layers that form the two air gaps. The air gaps free the structure to rotate about two compliant torsion hinges. [46]

TI claims that the lifetime of the micromirrors is in excess of 100,000 hours (11.4 years) [47].

4.3.1 Electronic Operation

Each time the mirrors are to be addressed to new rotation states, the following address sequence is performed:

1. Turn off bias to allow mirrors to begin to rotate to flat state.
2. Turn bias on to enable mirrors to rotate to addressed states (+10/-10 degrees).
3. Keep bias on to latch mirrors (they will not respond to new address states).
4. Update address states of SRAM array under the mirrors, one line at a time.
5. Repeat sequence beginning at step 1.

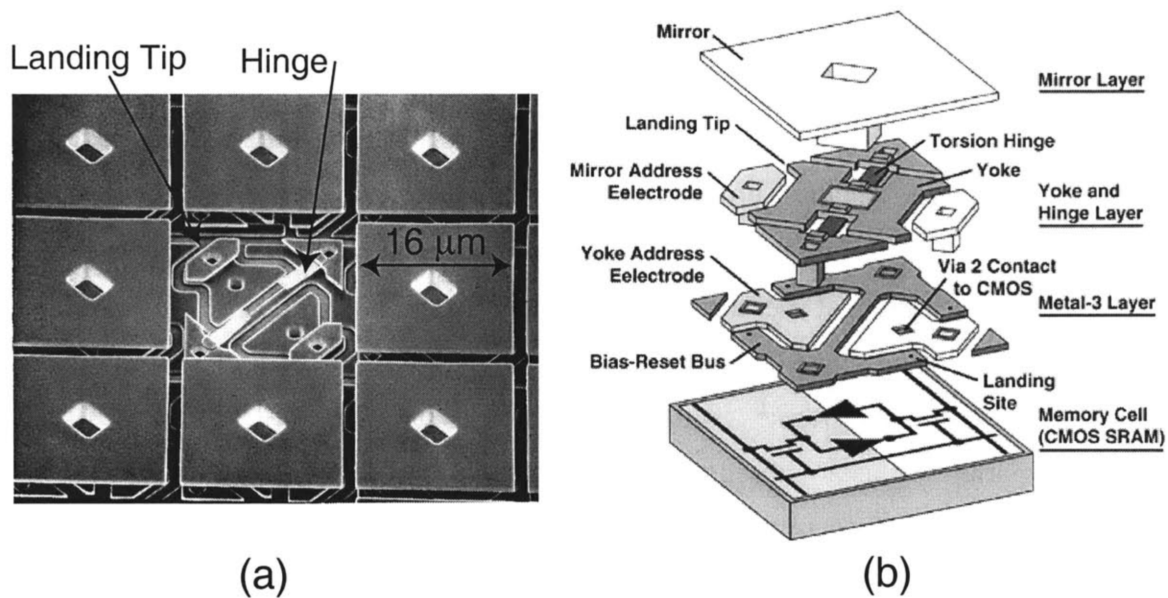

Figure 4- 10. TI DLM Technology. (a) SEM of micromirrors (b) the different layers of the entire micromirror structure

4.3.2 Addressing

Provided we use a CW laser as a source for ZPAL, and given that the mechanical response time of the micromirrors is between 10-20μs (50-100 kHz), the limiting factor in how fast we can write a unit cell with ZPAL is the addressing of the micromechanics. Given a set addressing time, the only way to further increase throughput with ZPAL would be to make a larger array of zone plates. Provided we had a way to manufacture zone plates reliably and all identical to each other, and given that we need one mirror per zone plate, we could have zone-plate arrays in excess of 1 million zones plates (TI currently manufactures a1280x1024 array →1.3 million, and in the future it is likely that they will go to 2048x1536→3.5 million).

Given the importance of addressing for ZPAL performance it is worth analyzing how it is done.

The goal of the TI micromirrors addressing scheme is to be able to transfer information from a memory location on a computer to a memory location underneath the mirrors in the least amount of time possible. TI's first approach to this problem was to place one SRAM memory cell underneath each micromirror that would be sequentially

updated (one line at a time) every frame. The mirrors latched into position until the next frame arrived.

While having an individual SRAM cell underneath each mirror was proven to work, it made the fabrication process less fault tolerant than if one SRAM cell could address a number of mirrors by itself. Texas Instruments took this path and designed an addressing architecture that uses a much smaller number of SRAM cells than mirrors.

The addressing sequence of the micromirrors is shown schematically in Figure 4- 11. Step 1 takes a set of frames that are going to be displayed on the mirrors and stores them on a buffer for faster subsequent addressing. Current technology allows for 1300 frames of 1024x768 pixels to be stored (125 Mbytes of storage). The data is then loaded into the input registers (step 2) in bursts of sixteen 54-bit words and parallel shifted into the static memory cells. For this particular device (other resolutions are analogous) the memory under the 576x864 array of micromirrors has 36 rows by 864 columns of SRAM cells. After the first sixteen 54-bit words have been transferred, the counter is updated (step 3) and row 2 is then active, at which point the next set of 54-bit words is passed. Row addressing is hence sequential. As illustrated in Figure 4- 11, the device is divided into 16 horizontal sections, so the memory must be loaded and transferred to segments of the array of mirrors 16 times to update an entire bit frame displayed by the mirrors. The transferred bits set the state of the micromirrors to either a "1" state or a "0" state. A "1" state corresponds to a +10° and a "0" state to a tilt of -10°. However, in order to have synchronization, the mirrors don't move as soon as their state has been updated. TI refers to this feature as *mechanical latching*. Each micromirror is addressed by two voltages: an *address* voltage (sets the "0" and the "1" state) and a *bias* voltage. If a bias voltage in excess of the address voltage is applied to the array of micromirrors after the "1" or "0" address voltages are set, the mirrors will stay latched (tilted) in the selected state even if the address voltage changes. Only if the bias voltage is removed and then reapplied will the mirrors settle in the newly addressed state. This feature allows multiple mirrors to be addressed by a single SRAM cell in quick succession provided each has a separate source of bias voltage. Once all the data is loaded, the bias voltage is removed and reapplied to tilt the mirrors to their new position [48].

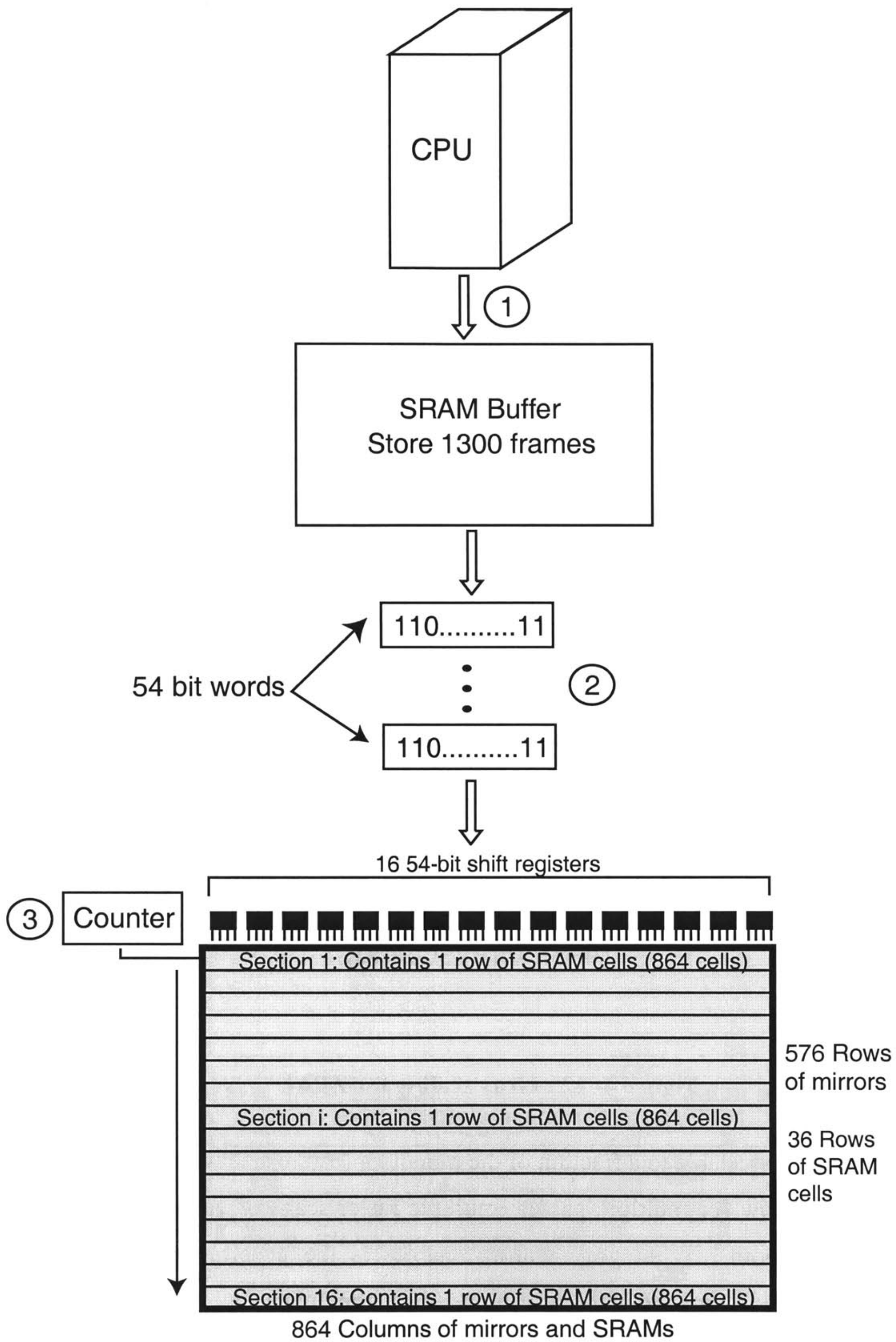

Figure 4- 11 : Addressing of TI micromirrors

4.3.3 Gray Scaling

The concept of gray scaling and its relation to ZPAL is illustrated in Figure 4- 12. A zone plate provided with a unit of energy will focus the energy to a spot size given by the outer zone width. To write patterns we raster scan the substrate under the focused spot. If this was all the control we had, the writing capabilities of ZPAL would be limited to writing features that are either the size of the outer zone width or integer multiples of it (provided we write with a single pass). If we want to have the ability to expose features that can have

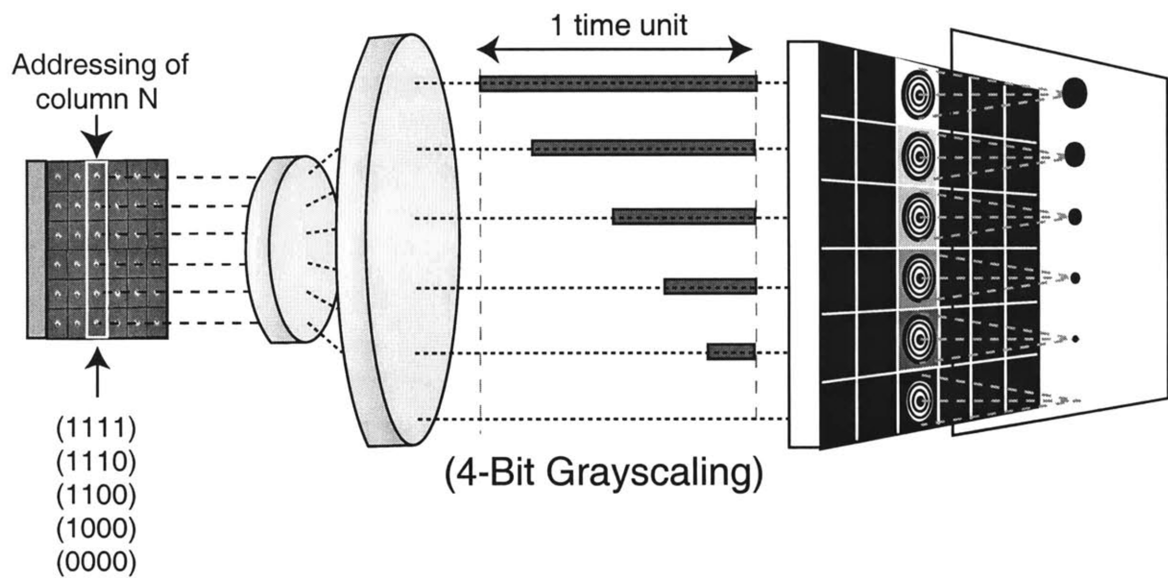

Figure 4- 12 : Gray scaling for ZPAL

widths that are controllable to a fraction of the minimum feature size we must either have grayscaling or allow for multiple passes (multiple raster scans of each unit cell), or a combination of both. What gray scaling enables is the possibility of accurately controlling via electronics the amount of power each zone plate receives. Figure 4- 12 depicts a 4-bit gray scaling implementation. Recall that there is a 1-1 mapping of the micromirrors to the zone plates. To control the amount of light that a zone plate receives all that needs to be done is to control the amount of time that the corresponding mirror

stays latched on the ON position. If we provide an input of (1111) to the top mirror of column N as shown in the diagram, the mirror will be illuminating the zone plate for 1 time unit. If, however, we provide an input (1100) to mirror 3 of column N, the mirror will only be ON for 1/2 a time unit. As illustrated, the shorter the time the mirrors are ON, the smaller the spot size formed at the focal plane of the zone plate array. Clearly, the higher the number of grayscaling levels, the higher the linewidth control that can be achieved. The price that is paid is throughput, as Table 4- 1 indicates.

Grayscaling Levels	1	2	4	6	8	10	12	14
Throughput (arb)	100	50	25	16.7	12.5	10	8.33	7.14

Table 4- 1 : The effect of grayscaling on throughput

The TI micromirrors enable grayscaling through binary Pulse Width Modulation (PWM), which controls the ON-OFF time of a mirror according to a time line, as shown in Figure 4- 13. The intensity level that a mirror is going to provide is sent to the micromirrors in a binary sequence (the number of bits depends on the number of grayscaling levels desired). The most significant bit (MSB) from the digital intensity for each mirror is loaded into each mirror's SRAM cell at the beginning of a video frame. All mirrors remain in the MSB state for half of a frame time. The next most significant bit is then loaded and held for one-quarter of a frame time. Each less significant bit is held for a 2x shorter period until all bits are shown. If for a given frame period we wanted the mirrors to be ON all the time we would send a sequence of 7 ones (1111111 = 127). This is assuming a 7-bit grayscaling implementation. To calculate the bit sequence needed to deliver 60% of the maximum power , we do the following calculation:

$$\frac{60}{100} \cdot 128 \approx 77 \xrightarrow{binary} 1001101$$

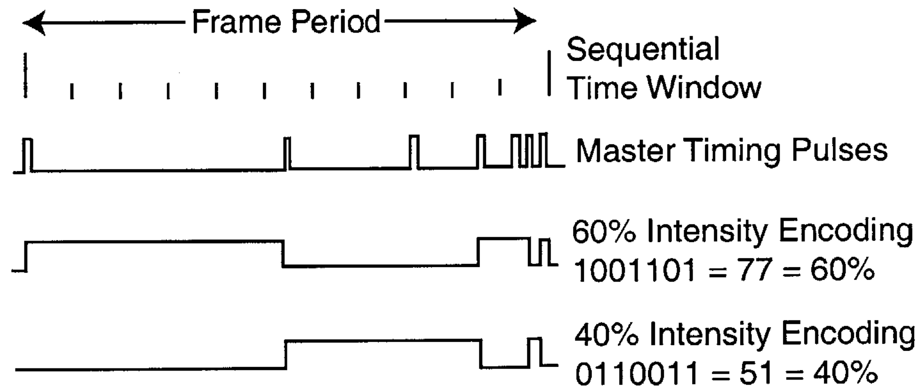

Figure 4- 13 : Pulse Width Modulation (PWM)

In general, for an N-bit gray level scheme, to deliver x% of the maximum power, the sequence is given by

$$\frac{x}{100} \cdot 2^N = Y \xrightarrow{binary} \text{Binary Sequence}$$

TI however figured out a clever scheme to improve the performance of the device by reducing the bandwidth needed to send all the data. The high bandwidth requirement comes from the fact that once we reach the Least Significant Bit (LSB) of the sequence, the MSB of the *next* frame must be loaded into the SRAM cells during the relatively short LSB time period. This requires high bandwidth drivers, even though the data rate is essentially zero throughout the 50% of the frame time represented by the MSB time period. [49].

To avoid this situation the bit order sequence is altered to average out the length of the duration of the last bit of the sequence (no longer necessarily the LSB), as Figure 4- 14 indicates. As described previously in Section 4.3.2 the device is divided into different sections (see Figure 4- 11) that need to be addressed in order to load the desired frame to be displayed by the micromirrors. In Figure 4- 11 there were 16 sections, although this number may vary depending on the array size. Lets analyze with the aid of Figure 4- 14 how the scheme works. For simplicity, lets assume the device was only subdivided in 4 different sections (1 -4) and that we only want to address one mirror in each of the sections (the mirrors are labeled A for the mirror in Section 1, B for the one in

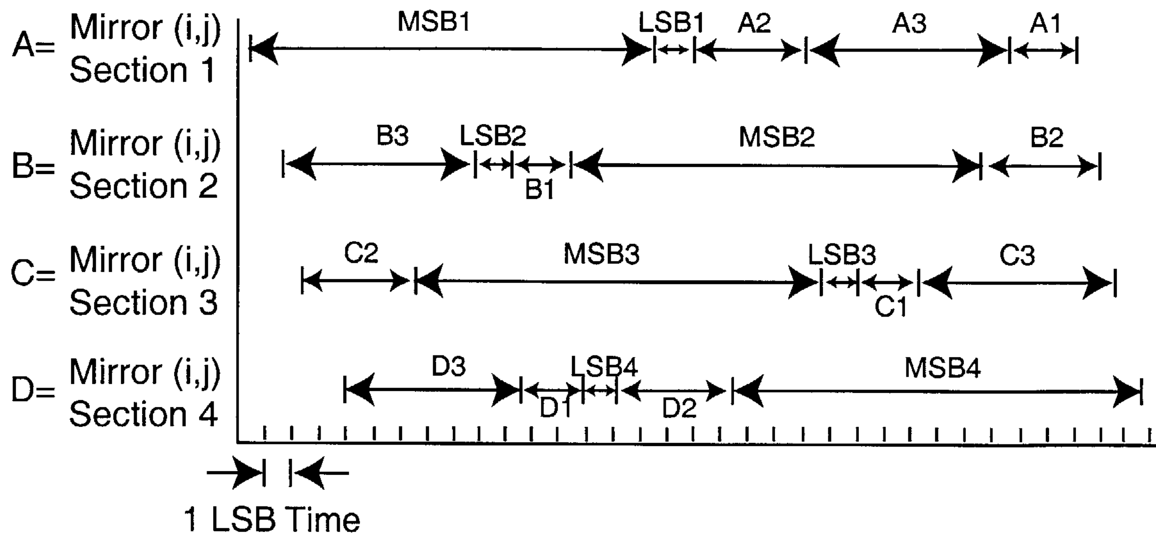

Figure 4- 14 : Low bandwidth PWM scheme for TI micromirrors

Section 2, etc). Again, to simplify matters, lets use a 5-bit grayscaling scheme, so that in order to address each mirror, a string of 5 bits has to be sent (e.g. for mirror A the string is composed of Least Significant Bit 1 (LSB1), A1, A2, A3, and Most Significant Bit 1 (MSB1)). As indicated previously the addressing order of the Sections is sequential, starting first with Section 1 and then proceeding to Section 2, 3, etc.

Notice hence the small lag from the start of the frame for the different sections. However, the most important thing to notice is that the LSB (or any other particular bit for that matter) appears at a different time throughout the frame period in each of the four sections of the device. While one mirror is loaded with MSB data, others are loaded with second MSB data, still others with third MSB data, and so on. The amount of data transferred remains the same; however, the rate of data transmittal is nearly constant. Since some mirrors are updated while others remain latched, a single SRAM memory cell is time-division multiplexed to several mirrors [48].

In summary, one section or another of the device is being updated with one bit or another almost constantly, and, as a consequence, the peak data rate required of the DMD and its drivers has been lowered essentially to the average data rate. No longer does the array have to be updated in its entirety from one frame to the next during the short time duration of the LSB, so effectively the bandwidth necessary for addressing has been significantly decreased. With these improvements, current technology allows

the micromirrors to be driven at a frame rate of 3.5 kHz for an array of 1024x768. The theoretical minimum frame rate is given by the mechanical response time of the micromirrors, and is in the range of 10 to 20 μs, or equivalently, 50-100 kHz.

4.4 Projection Optics: Achieving a 1 to 1 mapping of micromirrors to zone plates

The micromirrors are 16 μm on a side, and the zone plates for UV have a diameter that is typically of the order of 100μm. To achieve a one-to-one mapping, so that only one mirror illuminates one zone plate, projection optics are needed to zoom up the reflection of the individual mirrors to a diameter that fills with light the corresponding zone-plate unit cell. For the experiments performed the unit cell had dimensions of 150x168 μm^2. Therefore, we need a magnification factor of 9.4 to zoom the mirrors from 16μm to 150μm. This magnification was achieved via a zoom lens manufactured by Navitar (10X model).

Figure 4- 15 shows 4 images of the zone-plate array as illuminated from the back with 442 nm light reflected off the micromirror array and imaged onto the zone plates. In the left image, all the zone plates are illuminated. The three images to the right show different combinations of zone plates that are illuminated and not. The right most image shows only the diagonal zone plates illuminated. These patterns demonstrate that with proper magnification and alignment, illumination of individual zone plate can be turned on and off.

4.5 Making the Zone-Plate-Array parallel to and properly spaced from the substrate

We have reached almost the end of the "journey" of the photons that started at the beginning of the chapter when they were generated inside the laser cavity. The photons

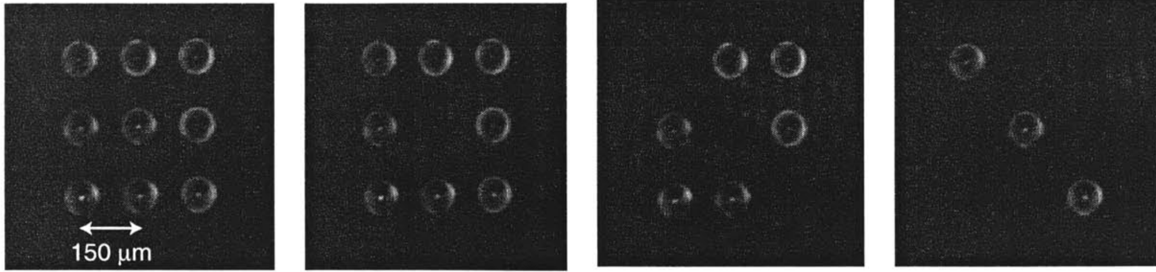

Figure 4- 15 : Images of UV-zone plates as illuminated from the back with 442 nm light reflected off the micromirror array and imaged onto the zone plates. These images demonstrate that illumination to individual zone plates can be turned on or off.

have now reached the zone-plate array and, as described in Chapter 3, they will be focused to a spot at the focal plane of the array. The objective is then to place a photosensitive-resist-coated substrate precisely at the focal plane of the zone-plate array, i.e., to have the two surfaces parallel to each other while maintaining the plane of focus as the substrate is scanned.

Although apparently trivial, these two issues, setting the right distance form the zone plate array to the wafer and making the two surfaces parallel, deserve more attention than one would think *a priori*. Three techniques have been explored for setting the right gap, with a clear and elegant winner. But lets keep the suspense for a moment and not give out the result just yet. Let's first analyze the contenders.

4.5.1 The White light Michelson Interferometer

A standard white light Michelson interferometer was implemented for ZPAL as shown in Figure 4- 16. A white light beam coming out of a fiber is collimated by means of a lens and is then split into two beams by the cube. One of the beams proceeds by transmission toward the zone-plate array and the wafer, while the other proceeds by reflection towards the mirror (this is the reference arm). The waves are reflected at each of the 3 surfaces (the mirror, the chrome pad on the back of the quartz wafer and the Si wafer). The length of the reference arm, d_1, can be changed by translating the reference

mirror with a micrometer-driven stage. Fringes are observable on the screen only if the optical path difference between the arms is less than the coherence length of the light

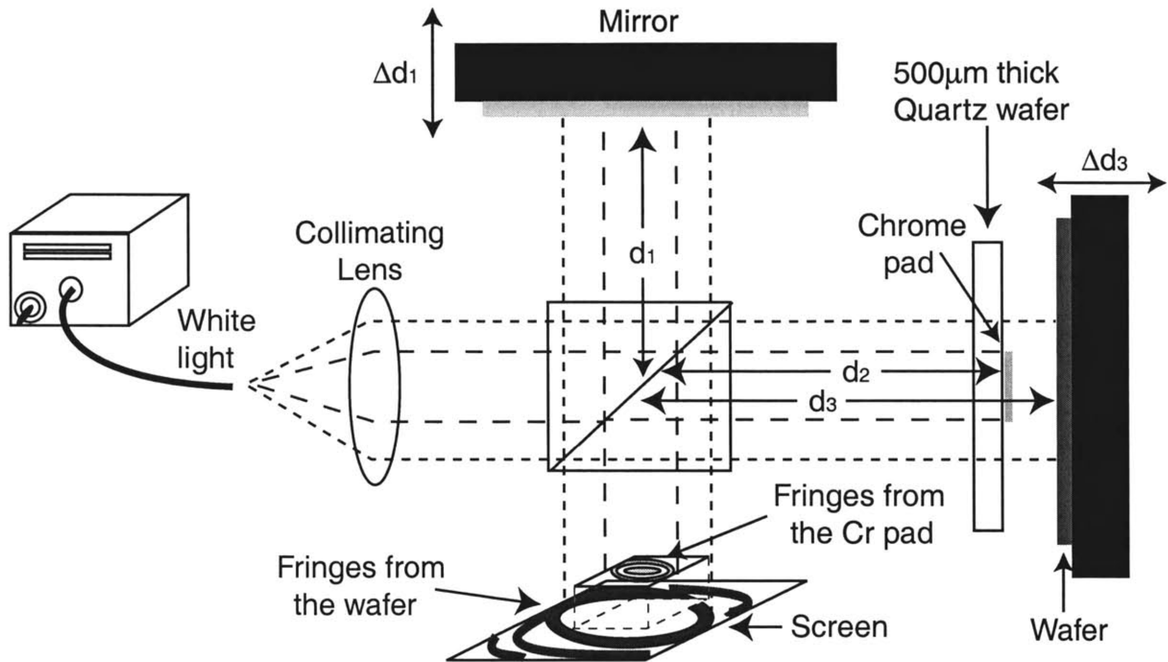

Figure 4- 16 : Michelson interferometer as a gap setting technique

used for the interferometer. The collimated beam of "white" light had spectral components that ranged approximately from 400 to 700 nm.

The coherence length is given by

$$\Delta l_c \approx \frac{\bar{\lambda}^2}{\Delta\lambda} \qquad \textbf{4- 6}$$

where $\bar{\lambda}$ is the mean wavelength and $\Delta\lambda$ is the range of wavelengths in the light used. For white light we then get

$$\Delta l_c = \frac{550^2}{300} \approx 900nm$$

The technique for gapping is hence the following. The reflection off the Si wafer is blocked by placing a card between the two wafers. The reference arm is moved until

fringes are observed at the screen, at which point $|d_1-d_2| < 900$ nm. The objective is to set the gap such that $d_3-d_2 = f$, where f is the focal length of the zone-plate array. To do so, the reference arm mirror is moved away from the beam splitter via a micrometer a distance equal to the focal length (d_1 is now d_1+f). Naturally the fringes will disappear from the screen. The card that was blocking the reflection off the Si wafer is now removed, and the wafer is moved via another micrometer until fringes are observed, at which point the substrate is in the focal plane of the zone-plates. The uncertainty in the gap is at most two times the coherence length of white light (1.8 μm) plus the error introduced by the micrometer displacement (probably under 100 nm). One can do better by trying to gap using a particular location of the Cr fringes, then move the reference arm a focal length away, and then try to find the same location in the Si wafer fringes. Even with a lot of practice it is hard to get the gap error to be under 1 μm. Given that the depth-of-focus of the zone plates used for the experiments was ~750 nm, clearly the technique was not precise enough. The only way to get results with this technique was to do a through-focus experiment every time a pattern had to be written. That is, the gap would be set a couple of μm away from the right focal length, and then the exposures would be repeated as the gap was decreased by increments that were about 1/3 of the focal length, to be certain that through the scan one of the exposures would be within the depth-of-focus of the zone plates. The technique was painfully slow, and also problematic, since it added a lot of background due to the large number of exposures that were performed while not at the right focal length. Despite all its shortcomings this was the technique that was used for all the patterns written with ZPAL that are reported in this thesis.

4.5.2 Capacitive gapping

Because the two surfaces we are trying to gap are conductive (the zone plates are surrounded by a 1.5 x1.5 cm^2 Cr pad), we can configure the system as a parallel plate capacitor by making two metal contacts to the two surfaces. For a parallel plate capacitor the capacitance C is given by

$$C = \varepsilon \cdot \frac{A}{d} \quad \text{4- 7}$$

where ε is the permittivity, A the cross sectional area of the plates and d is the distance between them. Hence, if we measure the capacitance we can extract d. This technique can be extremely accurate if the two plates are identical. It is often used for ultra-high precision mechanical stages. The situation here is little different, since the two surfaces have different areas and are composed of different materials. To test the scheme two mask were made, as shown in Figure 4- 17.

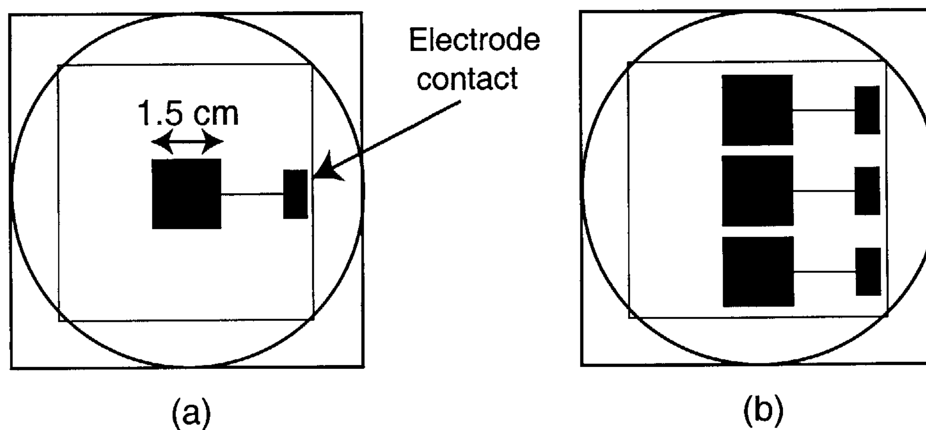

Figure 4- 17 : Mask layout for capacitive gapping technique. (a) One Cr pad (b) 3 Cr pads for establishing parallelism.

Using equation 4- 7, and to a first approximation ignoring fringing fields at the edges of the plates, we expect to get a capacitance of the order of tens of pF in the vicinity of the desired gap (~50 μm). To measure the capacitance a meter manufactured by Boonton (Model 72B) with a measurement range from 1 pF to 3000pF was used. The results are shown in Figure 4- 18.

Figure 4- 18 (a) shows a comparison between what is expected if we use equation 4- 7 versus experiment. The simple model used gives an average error of 2.133 pF from the measured capacitance. Figure 4- 18 (b) takes a closer look at the capacitance values around the desired focal length, 50.9 μm. By taking the derivative of equation 4- 7 with respect to d, we can get an idea of how sensitive this technique is to gap variations. This is what is plotted in graphs (c) and (d) of Figure 4- 18.

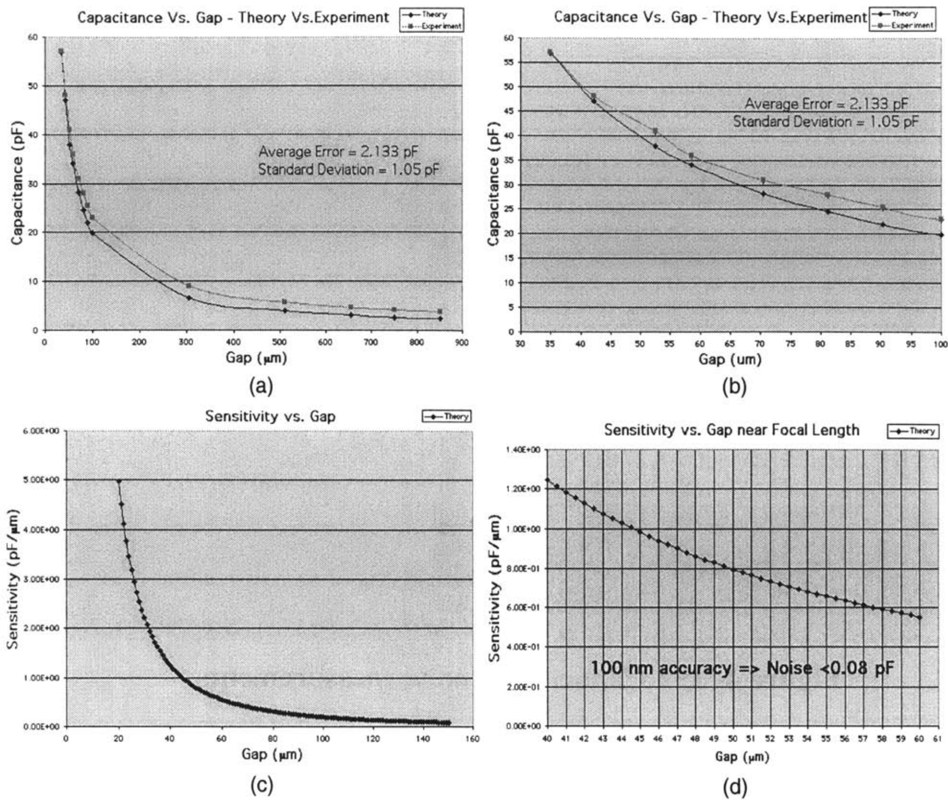

Figure 4- 18: Capacitance gapping results. (a) Comparison of theory to experiment, (b) same as (a) but area close to the focal length is examined, (c-d) sensitivity of the capacitance to gap variation

Taking a closer look at (d) we can see that if we want to have 100 nm accuracy in setting the gap, the uncertainty in the capacitance reading has to be under 0.08 pF. This uncertainty is caused by the noise of the electronics, but with proper design and proper wiring and shielding this value can be achieved, as shown in Figure 4- 19. The figure shows a screen capture of a LABVIEW program that performed measurements for 58 sec at a sample rate of 1000 samples/sec. The key results are highlighted , showing a standard deviation (i.e. noise level) of 0.00221 pF, 36 times better than what was needed to achieve a 100 nm accuracy in gapping. What's even more impressive, taking the max and the min of the 65000 samples, the difference between the max and min was only 0.0091 pF, still ~9 times better than what is needed.

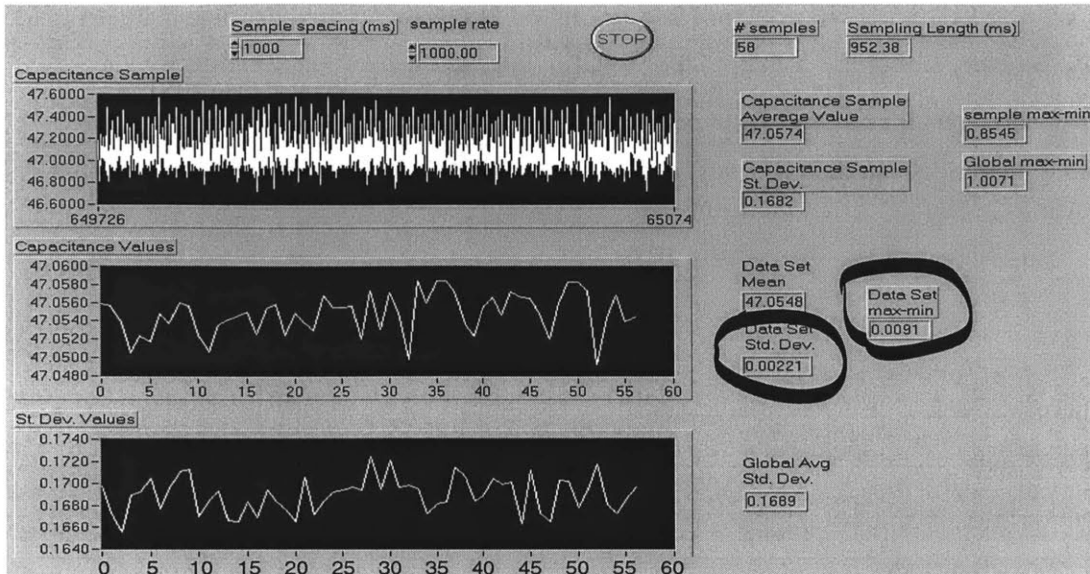

Figure 4- 19 : Capacitance noise measurements

Is capacitance then the winner of the contest, the elegant and simple way to find the optimal gap for the zone plates? Well, not quite. The big problem is repeatability in the capacitance readings from different substrates (with the limitation that the substrate has to be conductive). The unresolved issue was how to provide a solid low-noise repeatable contact to the substrate that is going to be gapped. The wafers are always mounted on a vacuum "pin-chuck" to make them flat, so somehow one would have to contact the wafer through the chuck. While this was tried with a point probe, the readings were not accurate enough to be useful. The results presented in this section were all obtained by making a soldered contact to the wafer. Clearly this is acceptable for proof of concept purposes only, and not for a robust and flexible gapping scheme. Still, the author's opinion is that with some more engineering, capacitance can be made extremely robust, fast, accurate and low cost.

4.5.3 Gapping with Zone Plates

Zone plates have been used for many decades as imaging elements, primarily for x-ray microscopy. In many respects one can think of a zone plate as a lens, and as such,

one should, in principle, be able to image with it. With this concept in mind, if the zone plate is set as the focusing lens of a traditional confocal microscope [50], one would obtain a signal that varies with the gap and that achieves its maximum value exactly at the focal length of the zone plate. The concept is illustrated in Figure 4- 20.

Any confocal scheme is at a minimum comprised of two lenses (an objective lens and a detector lens), a light source, a pinhole and a detector. The mode of operation is

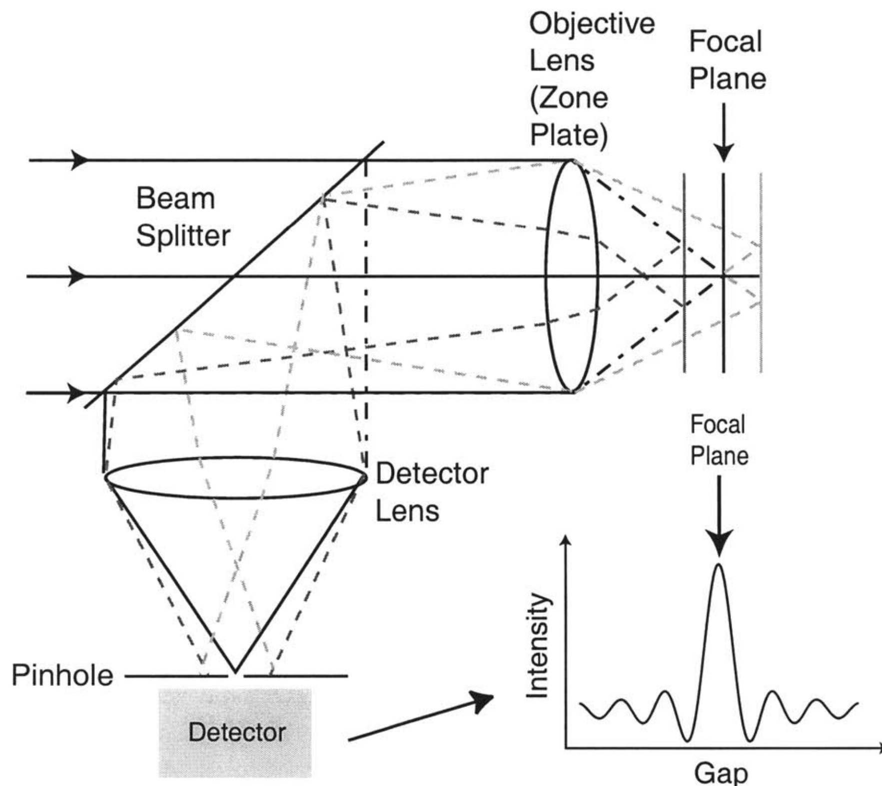

Figure 4- 20 : Confocal gapping technique

very straightforward. Light (typically from a laser) is passed through a beam splitter cube and is the focused by a lens onto a sample. If the sample is exactly at the focal plane of the lens, the light will be focused to a diffraction limited spot at precisely the surface of the sample. Assuming for now a specular reflection at the substrate, the light will travel back through the same lens, come out of it collimated, and then travel to the beam splitter to be reflected and go through a second lens (the detector lens). At the focal plane of this last lens a pinhole is placed, followed by a detector. This path is illustrated with a solid line in Figure 4- 20.

If the sample is not at the focal plane of the objective lens the detector lens will no longer see collimated light, and it will focus the light at a different distance than before. The pinhole's role is now apparent. Its purpose is to improve contrast by only allowing light that comes from the focal plane of the objective lens to go through and reach the detector. The signal obtained as the gap is varied is depicted schematically on the same figure. This technique was implemented with zone plates as the objective lenses with great success; we were able to obtain a confocal signal (axial response) from all the zone plates of the array. The axial response of one of the zone plates of the array is shown in Figure 4- 21.

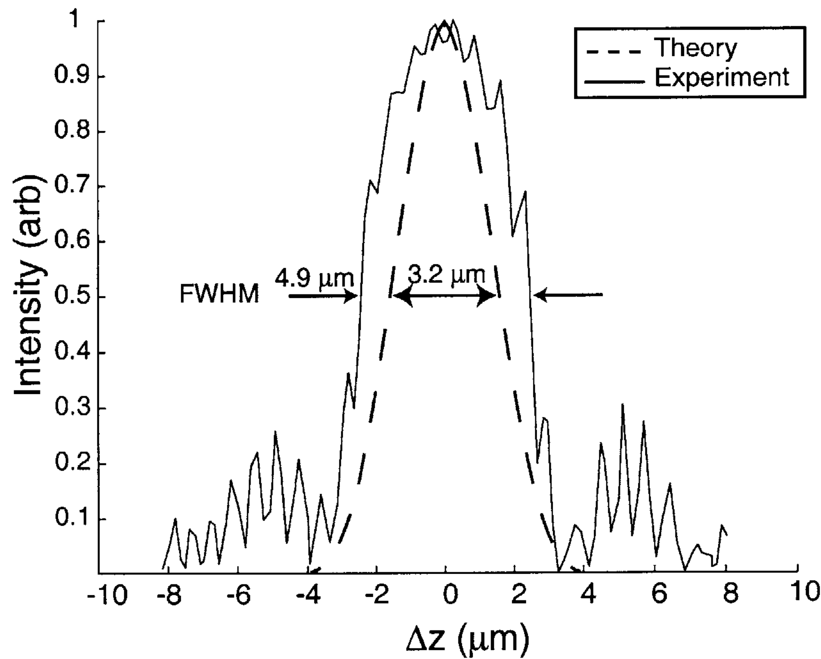

Figure 4- 21. Axial response of a zone plate compared to a theoretical model

The axial response for a confocal system with microlenses can be approximated by the following expression [51]

$$I(u) = \left[\frac{\sin(u/2)}{u/2}\right]^2 \quad \text{with} \quad u = \frac{2\pi}{\lambda}\frac{D}{4f^2}\Delta z \qquad \textbf{4-8}$$

where D is the diameter of the lens (zone plate), f the focal length and λ the illuminating wavelength. Δz describes the displacement of the wafer from the focal plane of the zone plates. This model is only an approximation that treats the zone-plates as microlenses, however, the agreement to experiment is still very good. The zone plates used for testing this gapping scheme had a diameter D = 119.34 μm, a focal length f = 155.6 μm and were designed for λ = 442 nm. With these parameters, the model predicts an axial response with 3.2 μm Full Width Half Maximum (FWHM), versus the 4.9 μm FWHM obtained experimentally, as Figure 4- 21 indicates.

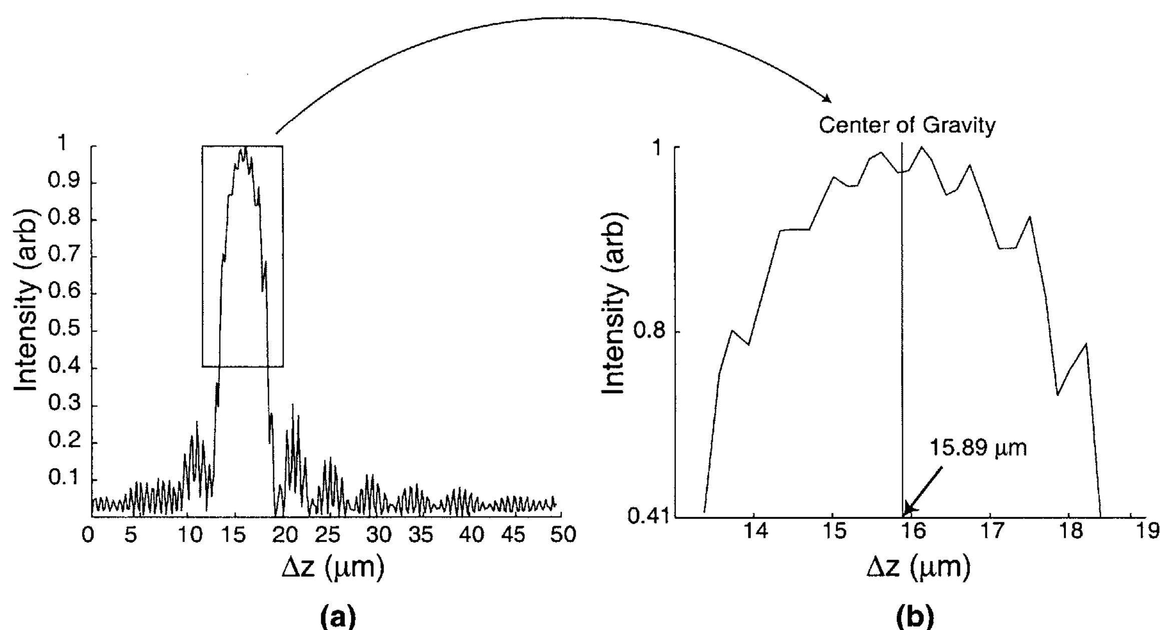

Figure 4- 22. Gap detection by calculating the Center of Gravity (CoG) of the axial response.

The focal length of the array can be found by using a peak detection algorithm to find the maximum intensity of the signal. The focal length determination can be further improved by taking the center of gravity of the axial response (Figure 4- 22) [51]. An algorithm was implemented that scans the wafer through the focal length of the array, selects the region of interest, computes the center of gravity, and then moves the substrate to the right position. With such a scheme sub-100 nm gapping precision can be easily achieved.

Notice the high-frequency component of the signal shown in Figure 4- 22, which results from a beating between the reflection from the exposure substrate and the reflection from the backside of the zone-plate-array fused silica wafer. Despite this minor problem, which should be easily solvable by coating all lenses with an AR coating, this is without question the optimal gapping technique for ZPAL. It is extremely low cost, since few extra optics are needed, fast, accurate and elegant, since it uses the very zone plates that are going to expose the substrate to obtain information about it. There is a small caveat, though. One can not use for gapping the same radiation that is used for exposing patterns, since in the gapping sequence the resist would be exposed. A solution to the problem is to fabricate 4 zone plates at the edges of the zone plate array optimized for HeNe wavelength, but with the same focal length as the zone plates in the array. By matching the intensity readings from each of the 4 zone plates (we really only need 3) the substrate can also be made parallel.

A fascinating extension of this gapping scheme is to take it one step further and build a massively parallel confocal microscope. This can easily be done since each zone plate provides a signal from the substrate, so by processing these signals while scanning the substrate, high-resolution images of the sample can be obtained. Such a microscope was implemented and results will be shown in the next chapter.

4.6 Scanning the substrate

The last of the four major components of ZPAL is a precision movable stage. Its function is to raster scan the substrate over a zone plate unit cell in order to produce the desired patterns. The scanning of the substrate is achieved via a flexure stage manufactured by Physik Instrumente (PI) of Germany. The stage is equipped with low voltage piezoelectric drives (0 to 100 V) integrated into a flexure guiding system. The force exerted by the piezo drive pushes a multi-flexure parallelogram via an integrated motion amplifier [52]. PI claims sub-4 nm accuracy in the displacements, which is certainly more than enough for the requirements of UV-ZPAL

An important issue that's worth noticing at this point is the importance of synchronization between the micromechanics and the stage, a must if we want to obtain

nanoaccuracy in the placement of the features on the substrate. This level of placement accuracy is achieved via careful analysis of the timing sequence, and implemented via software.

4.7 Conclusion

We have finally finished the description of the ZPAL apparatus, and with it the complete journey of the photons, from the time they are generated until they are absorbed by the resist on the wafer. A picture of the system is shown in Figure 4- 23. With this system patterns were exposed, and the results will be shown in the next chapter.

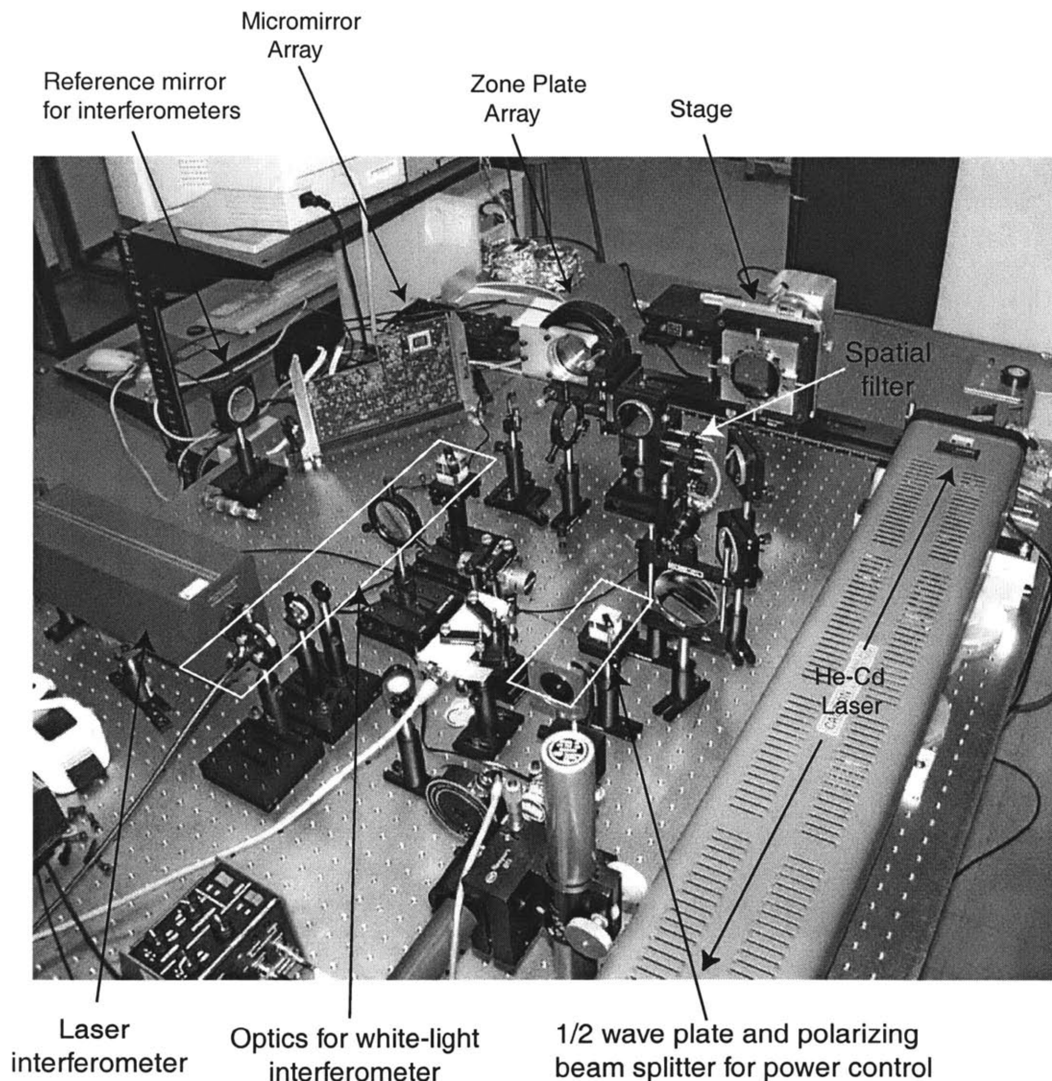

Figure 4- 23. Picture of the UV-ZPAL apparatus

Chapter 5

Pattern Exposures and Microscopy Results

This chapter presents experimental results which demonstrate the patterning capabilities of ZPAL. Patterns were written into resist on a wafer using 442 nm UV-radiation focused with an array of nine zone plates. Nine different patterns were written simultaneously in each of the nine zone-plate unit cells in a quasi-dot-matrix printing scheme.

Also included in this chapter are the images obtained with the zone-plate-array UV confocal microscope that was briefly discussed in the previous chapter.

5.1 Finding the right dose

The initial experiments with ZPAL consisted of exposing single pixels to optimize exposure time, and to determine experimentally the depth-of-focus of the zone plates and the white light gap setting uncertainty. By doing multiple exposures at different gaps while monitoring the gap, the effective depth-of-focus was determined to

be ~0.75 μm. This is slightly smaller than the calculated value of ~1 μm for λ=442 nm and NA=0.66. Figure 5- 1 shows an SEM of a typical exposure to determine the previously mentioned parameters.

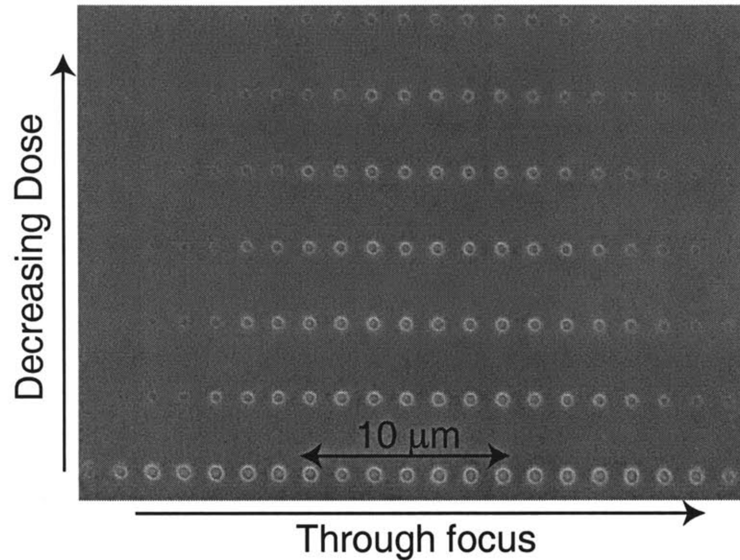

Figure 5- 1. SEM of single spot exposures of a single zone plate for dose optimization

The zone plates of the array chosen for exposures had 76 zones, with a designed outer zone width of 336 nm, and a radius of 44.6 μm. The focal length of the zone plates was 50.9 μm. As explained in Chapter 3, the zone plates should theoretically focus radiation to a spot the size of the outer zone width. By optimizing the dose through a set of through-focus through-dose experiments, as show in Figure 5- 1, one can get very close to the theoretical predictions, as Figure 5- 2 indicates.

5.2 Design and implementation of the experiment to produce arbitrary patterns

A system as described in Chapter 4 was utilized with the following particular configuration. As indicated in Figure 5- 3, the HeCd laser beam is incident at an angle of

~13.5° upon the 640X480 array of micromirrors. The pattern to be written is decomposed into pixel frames that are displayed simultaneously on the micromirror array and on a computer's cathode ray tube screen. For fully black or fully white pixels, the mirrors tilt respectively to ±10° about the diagonal of the mirror face.

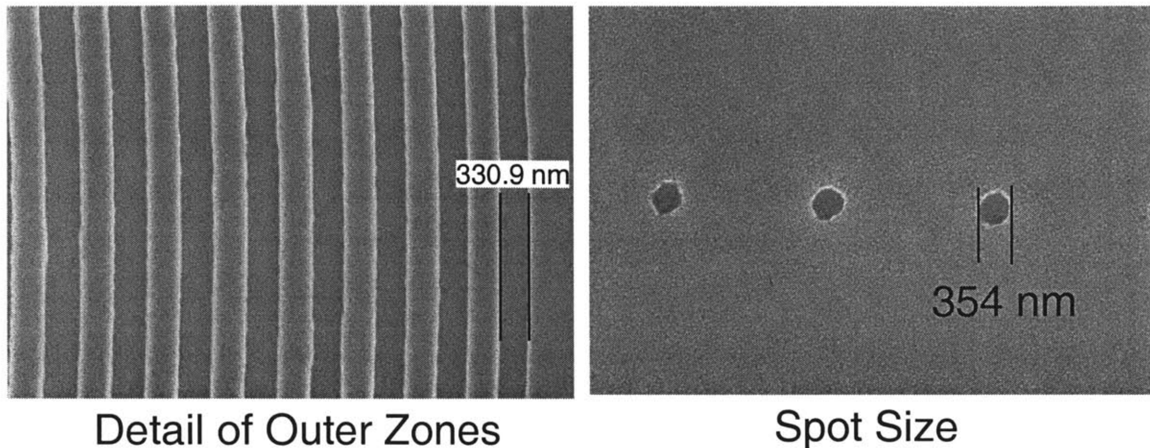

Figure 5- 2. Left- SEM of the outer zones of the zone plates. Right- Spot size at the optimum dose. With careful dose control one can get very close to the predicted resolution (i.e. the outer zone width)

Fully white pixels reflect the laser beam into a lens which images them onto the zone-plate-array, while the reflections from fully black pixels are excluded from the lens aperture. For the exposures that will be shown in the next section, only black and white pixels were written on the screen, and hence displayed by the micromirrors (i.e. no grayscaling was performed). In addition to excluding the fully black pixels, the optical imaging system magnified the micromirror image so that only one mirror illuminated one zone plate. The magnification was 9.8X.

The zone plates were made parallel to the wafer using a gimbal stage. The zone-plate stage also has X, Y, and θ adjustments to allow the zone plates to be aligned to the micromirror image. The alignment is critical to ensure that the intensity is uniform across each zone plate and between zone plates.

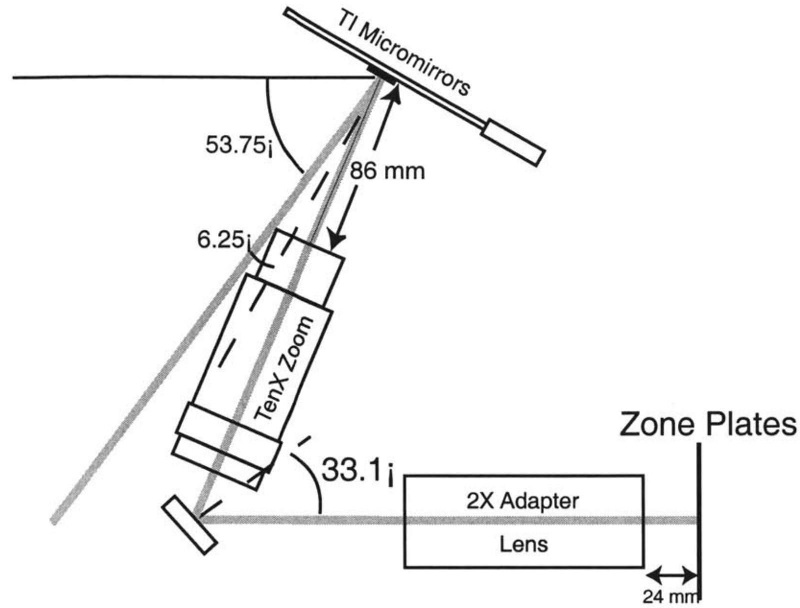

Figure 5- 3: Configuration of optics for illuminating the zone plates with the TI micromirrors

5.3 Exposure results

The gap was initially set smaller than desired (by 2~3 μm) and exposures were repeated as the gap was stepped in small increments. Patterned exposures were done via a modified vector scan. The stage was moved to the first pixel location to be exposed, the mirrors were flashed to a pattern which illuminated the appropriate zone plate, then the stage was moved to the next pixel which needed exposure. Figure 5- 4 shows scanning-electron micrographs of nine different patterns which were exposed in parallel with the UV-ZPAL system. Due to a software error, the actual pattern was the mirror image of the one depicted. The top of the figure shows a large area view of the 3X3 array of patterns. The dotted lines indicate the boundaries between zone-plate unit cells. The bottom half of the figure shows enlarged views of each of the nine patterns. The patterns were exposed in 350 nm of Shipley 1813 resist. The exposure time was 5 ms per pixel.

The image quality was quite good, indicating that the 354 nm single spot shown in Figure 5- 2 was not an artifact due to underexposure of the resist.

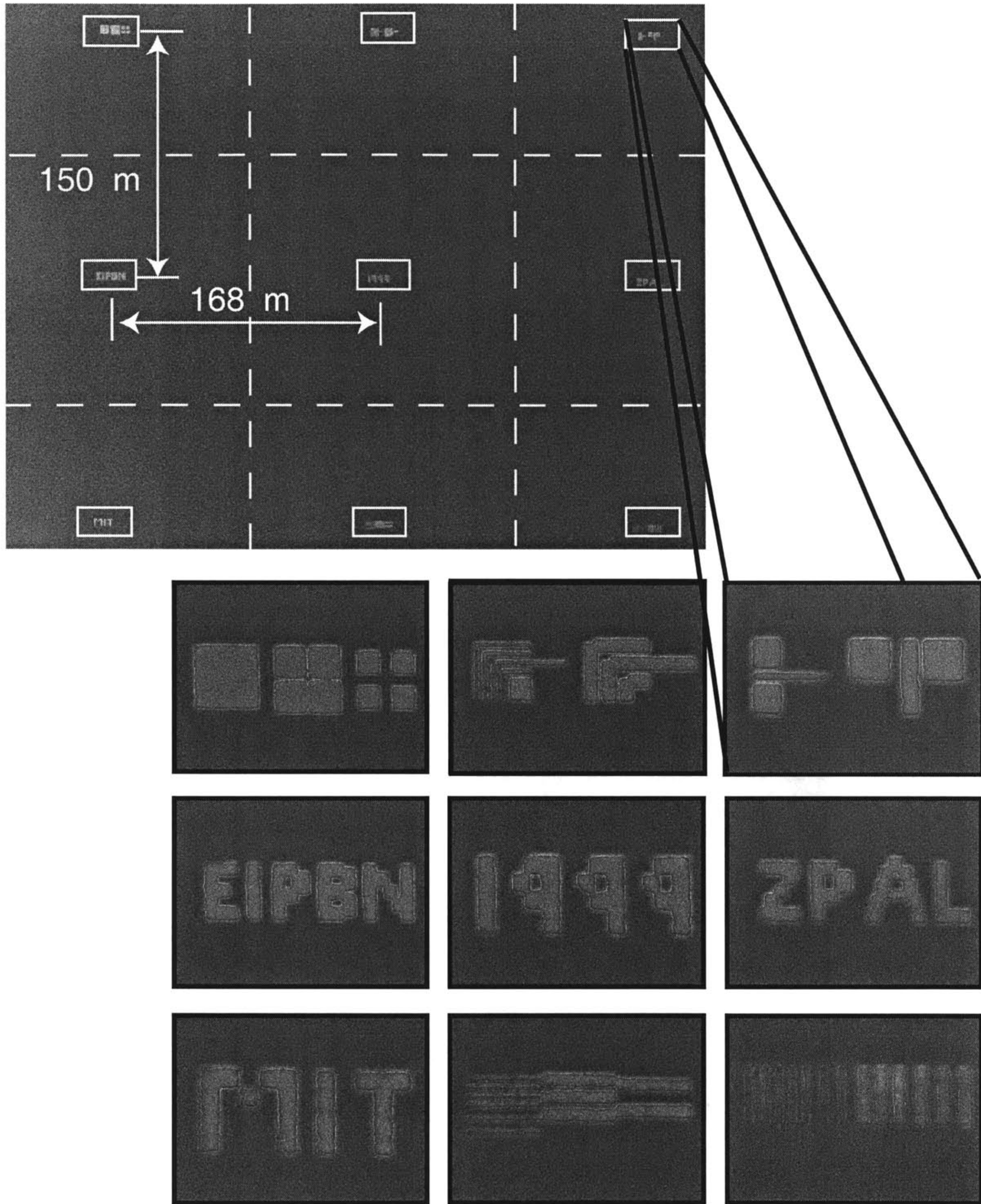

Figure 5- 4. SEM of nine different patterns exposed in parallel with the UV-ZPAL system. Top: Large-area view of 3x3 array. Dotted lines indicate the boundaries between zone-plate unit cells. Bottom: Enlarged views of each of the nine patterns.

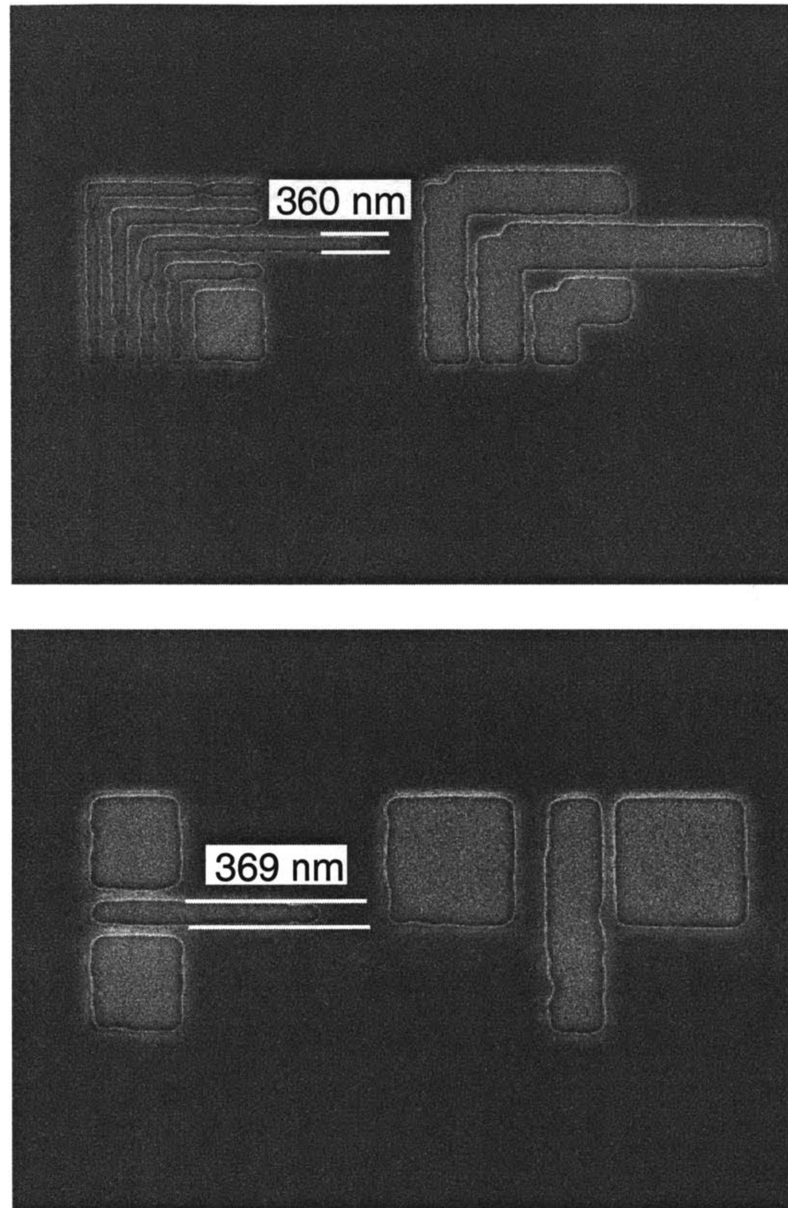

Figure 5- 5. SEMs of top center and the top right patterns from Figure 5- 4.

Figure 5- 5 (top) shows an enlarged view of the single pixel line/space and double-pixel line/space nested-L patterns which were exposed by the top center zone plate in Figure 5- 4. The single-pixel linewidth of 360 nm is very close to the measured spot size from the dose optimization experiments. The single-pixel line/space ratio is approximately 3:2. A notch in the outside corner of the double-pixel nested L's was

faithfully reproduced. The radius of curvature at the corners of the pattern is also comparable to the spot size. Irregularities in the vertical lines are possibly due to noise in the stage motion, which was not optimized.

The bottom of Figure 5- 5 shows a single pixel (left), and a double-pixel (right), line written in between two pads, with the objective of exploring proximity effects. These effects are indeed noticeable, indicating the need of a proximity correction scheme that involves grayscaling. This development is currently under way.

Even without proximity correction excellent patterning capabilities can be achieved, as Figure 5- 6 proves. The image quality is very good, showing dense 350 nm lines at an NA of 0.67 and k_1=0.53.

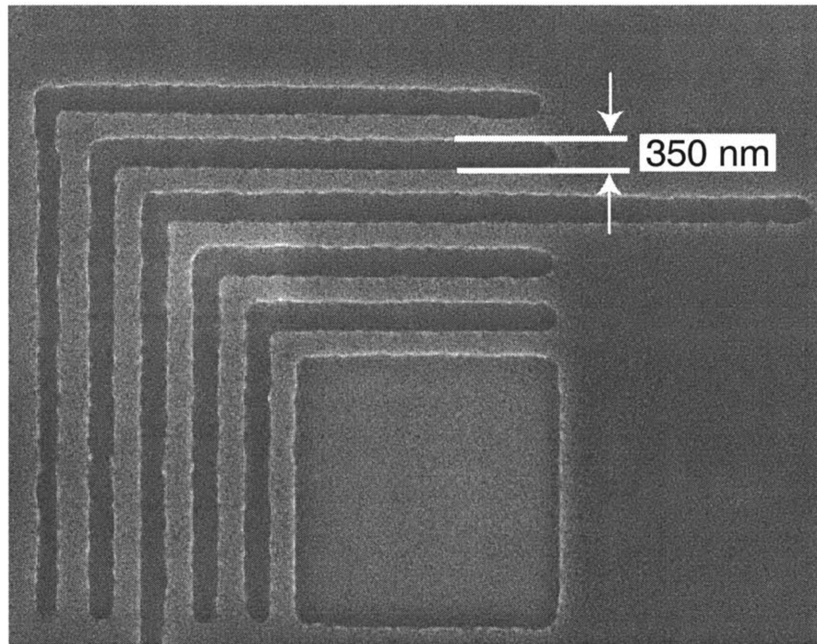

Figure 5- 6: SEM of nested-L pattern. The single pixel line is 350 nm wide. The radius of curvature of the pattern is comparable to the linewidth.

These results are very promising, providing strong support for the soundness of the technology. Many issues are still to be reolved (they will be discussed in more detail in the last chapter), however the author sees no "show stoppers" along the way. By going to shorter wavelengths, fabricating order-sorting apertures, and implementing a proximity correction scheme through gray-scaling, UV and DUV -ZPAL will be able to pattern with great accuracy and contrast all the way down to the 100 nm regime.

5.4 UV-Microscopy with a zone-plate array

In section 4.5.3 of Chapter 4, the confocal principle was explained, and an application involving zone plates was discussed. The setup described enabled gapping between the zone-plate-array wafer and the substrate with great accuracy and precision. It was also mentioned that one could take the configuration one step further and extend the gapping scheme to a massively parallel confocal microscope [53].

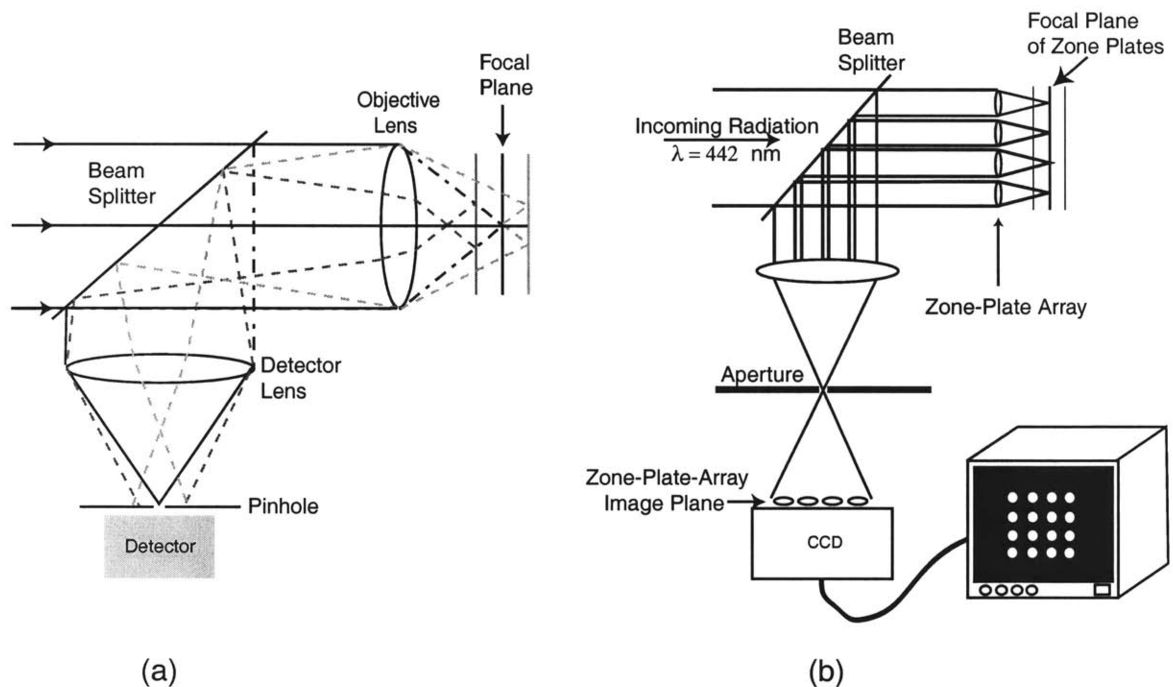

Figure 5- 7. Confocal microscopes. (a) Traditional confocal microscopy (b) Zone-plate-array confocal microscopy. The technique circumvents the inherent problem of traditional confocal microscopy, its speed, by utilizing an array of microlenses (zone plates).

Such a microscope, previously reported by Tiziani et al. [53] was indeed built, and its principle of operation is schematically depicted in Figure 5- 7 (b). Collimated light coming from a laser goes through a beam splitter and is focused by the zone-plate array, forming a 2-D array of diffraction-limited spots at the focal plane of the zone plates. The 2-D array of points get reflected back and pass through the zone plates one

more time, coming out collimated if the substrate is at the focal plane. The array of collimated rays (one for each zone plate) gets reflected off the beam splitter, and is then focused by a lens. After passing through an aperture, the array of light beams reaches the CCD chip of the camera. One signal per zone plate is obtained. The image of the camera is processed by a computer with a frame-grabber. The image is digitized and stored in memory for subsequent processing.

As in traditional confocal microscopy, if the object that is to be imaged is moved out of the focal plane, the array of spots generated by the zone plates will not form collimated rays when they pass through the zone plates for the second time, causing the detector lens to focus the array into a focal plane that is different than when the substrate was at the focal plane of the zone-plate array. The pinhole will hence block most of the radiation. Again, the objective of the pinhole/aperture is to improve contrast by only allowing light from the focal plate of the zone-plates to reach the detector/CCD.

The CCD is placed in the conjugate plane of the zone-plate array, and therefore, the zone plates themselves are imaged with the camera. As a consequence the pinhole can not be arbitrarily small in order to maximize contrast as in traditional confocal microscopy. It must be sufficiently large as to enable the image of each zone-plate to reach the CCD.

5.4.1 Microscopy results

Figure 5- 8 shows the first image obtained with the zone-plate-array confocal microscope. The object scanned was a 25 μm period grating (Cr on glass). The zone-plate array used had a 155.6 μm focal length, and an outer zone width of 620 nm. The substrate was scanned in 0.75 μm increments. As discussed in section 4.5.3, due to a beating pattern between the reflection from the exposure substrate and the reflection from the backside of the zone-plate-array wafer, a fringe pattern will always be convolved with the axial response obtained by each of the zone plates. The problem, which should be easily solvable by coating all lenses with an AR coating, is illustrated in Figure 5- 9.

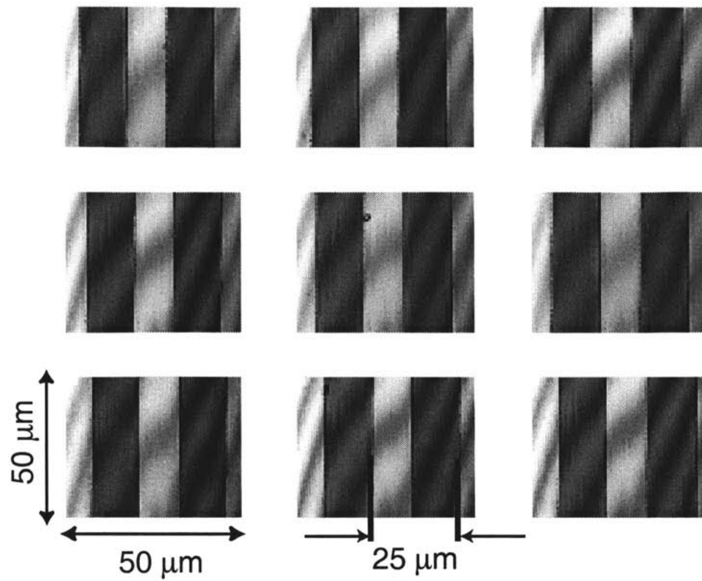

Figure 5- 8. First image scanned with the zone-plate array confocal microscope. The object was a mask with a 25 μm period grating on it. Each zone plate of the array returned an image that was processed via a computer.

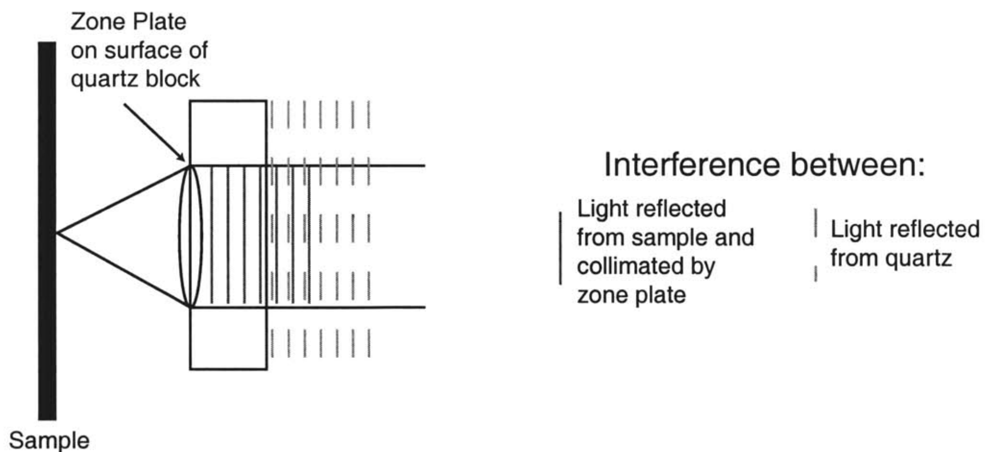

Figure 5- 9. Cause of interference fringes on the images obtained with the zone-plate microscope. The light reflected from the sample and collimated by the zone plates interferes with the light reflected from the quartz substrate.

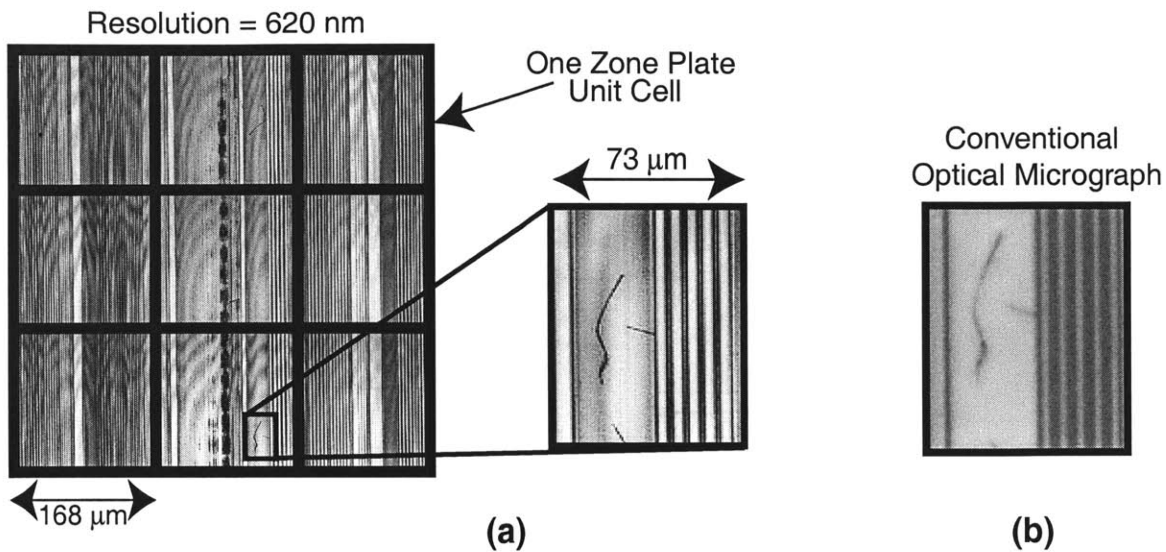

Figure 5- 10. Images of SiO_2 substrate with grating lines of different periods etched 1 µm deep, coated with aluminum. Ragged feature at the center of the image is present in the object. (a) Image taken in confocal mode. The images were taken simultaneously from a 3X3 array of zone plates and stitched together in software. (b) Same detail image of a scratch as shown in (a) taken with a conventional optical microscope.

As an example of a full field scan see Figure 5- 10. The figure shows two images of an SiO_2 substrate with grating lines of different periods etched 1 µm deep, coated with aluminum. The ragged feature at the center of the image is present in the object. The raggedness was caused by the inability of the lithographic stepper used to print the patterns to resolve the features that were to be transferred. In (a), the images were taken in confocal mode, and were obtained simultaneously from a 3X3 array of zone plates and stitched together in software. In (b), the same detail image of a scratch shown in (a), but this time taken with a conventional optical microscope, is shown. This figure illustrates the potential of the scheme. Massive parallelism can be achieved by using an array of zone plates, enabling the possibility of a high-speed, high-resolution microscopy.

A variety of objects with different reflectivities were imaged. A useful technique is to obtain a fast low-resolution image of the substrate to then zoom in on the area that is of most interest at a higher resolution. Figure 5- 11 illustrates such a sequence. The images correspond to an IC pattern on Si. Figure 5- 11 (a) shows a full field low resolution

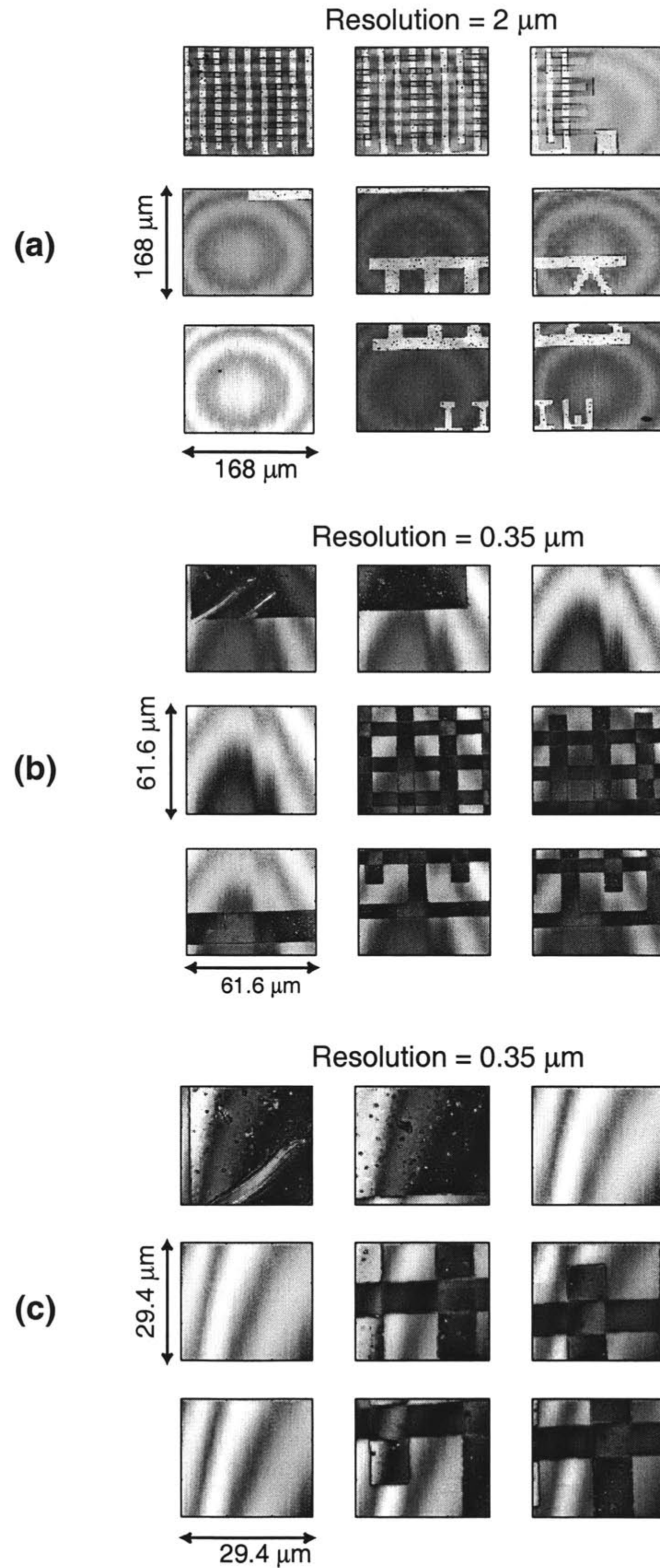

Figure 5- 11. Confocal images of an IC at increasing resolution, from (a) to (c).

image (2 μm pixels). Via software a region of interest can be selected, and by decreasing the pixel size, higher resolution images can be obtained ((b) and (c)).

5.4.2 Speed

The microscope, as of now, is inherently slow. A 100x100 μm unit cell contains 140,000 pixels at 300 nm resolution. To acquire an image a signal is detected for each pixel of a unit-cell by a CCD camera, then a frame grabber acquires the image, and then, via software, the image is analyzed to extract the right information from each lens of the array. This happens 140,000 times in order to acquire the entire image. With the current setup, using a National Instruments frame grabber and a 10-year-old CCD it takes hours to scan a unit cell. This is clearly not good enough.

Let's look at some numbers to get an idea of what kind of hardware would be needed to achieve high imaging speeds. A high precision stage scans the substrate in a raster scan fashion to go over all the pixels of the unit cell. A state-of-the-art stage can move at 300 mm/s with high precision. This means that we can move from one pixel to the next in 1μs. To keep up with this speed we would ideally like to be able to detect, transfer and process the signal coming from any given pixel in a time on the order of 1 μs. This would require CCDs with frame rates in excess of 1 million per second, which is out of the question with current technology. One however needs not go that fast, since that rate would imply that the image would be acquired in 140 ms. Although such a speed is desirable, it's certainly acceptable to wait seconds, even a few minutes, for an image to appear.

As an example, if we wanted to have 0.25 μm resolution while scanning over a 1 cm^2 area, and wanted to obtain an image within 1 1/2 minutes, with a 1000x1000 pixel CCD camera the frame rate would only have to be 20.4 frames/sec. Standard CCD cameras sold by a variety of manufacturers have rates in excess of this number.

5.4.3 Applications of the Zone-Plate-Array Confocal Microscope

The most important application of the microscope as it relates to ZPAL would be to enable level to level alignment. Figure 5- 12 depicts a possible implementation of such a scheme.

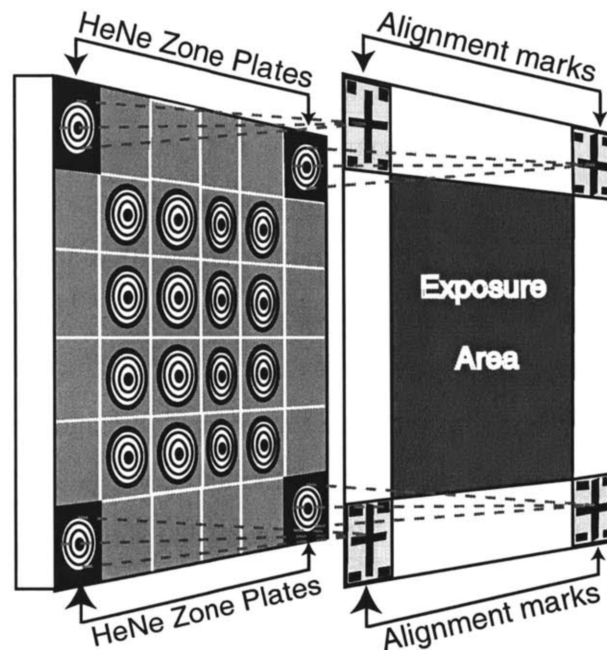

Figure 5- 12. Level to level alignment scheme. This scheme allows gapping, parallelizing and aligning. 4 zone plates optimized for λ=633 nm (HeNe), but with the same focal length as the zone plates in the array are used to image the alignment marks. The image is used to register the zone plates to the substrate.

Four zone plates optimized for λ=633 nm (HeNe), but with the same focal length as the zone plates used for writing patterns, are placed at the edges of the zone plate array. The HeNe zone plates are used to set the right distance,i.e. the focal length, from the zone-plate array to the substrate to be exposed, as well as to make the two surfaces parallel to each other. The later is achieved by gimbaling the wafer until the intensity of the axial response of the HeNe zone plates are matched. The HeNe zone plates are then used to image a set of alignment marks. Because we are using λ=663 nm we don't have to worry about exposing the substrate while we are looking for the alignment marks.

Once the marks are found, the image is processed and the stage is moved to register the zone plates to the substrate. For this alignment scheme to work optimally, it is, of course, crucial that the zone plates are placed with both great accuracy and precision with respect to each other, something that can be achieved by using Spatial-Phas-Locked-Electron-Beam-Lithography (SPLEBEL) [54] when the zone plates are manufactured. By placing the zone plates on an optical flat we can guarantee that, if we make the two wafers parallel with the HeNe zone plates, the exposure-array zone plates will also be parallel to the wafer.

Another important application of the confocal system would be as a tool to characterize the zone plate arrays themselves [55]. It is crucial for ZPAL to have the zone plates matched both in terms of focal length uniformity across the array, and in terms of efficiency. Both errors could be potentially corrected via software, by means of gray scaling. But first the defective zone plates would have to be identified, and to do so by actually writing patterns and the analyzing the results via SEM could be a daunting task. Instead, we could place an extra flat mirror ($\lambda/20$) as the substrate to be imaged, and look for the axial response of each of the zone plates of the array. Provided that the zone plates are illuminated uniformly across the array, and that the zone plate-wafer and the mirror are parallel, we would expect to get identical axial responses if the zone plates are all identical to one another. The responses can be easily processed via a computer, and the defective zone plates could easily be identified. With proper calibration the defective zone plates could be characterized to determine exactly the percentage error in terms of efficiency with respect to fully functional zone plates. As an example, if zone plate (i,j) of the array was found to have a 5% drop of efficiency with respect to the rest of the zone plates, then, at the time of the exposures, we could take this onto account and provide zone plate (i,j) with and extra 5% of power by dwelling a longer time in the ON position of its corresponding multiplexing element.

In summary, the microscope will provide increased versatility to ZPAL, in terms of facilitating both the usability of the tool (enabling gapping, parallelization and alignment) and the manufacturability (zone plate array testing). In addition, the zone-plate-array confocal microscope has enough merits to be a stand-alone technology, with uses that could range from biological imaging to semiconductor wafer inspection.

Chapter 6

Optimization and Extendibility of ZPAL

This chapter explores the limits, as well as the extendibility, of Zone-Plate-Array Lithography. In particular, ZPAL's throughput is analyzed as a mean of understanding what the limiting components of the apparatus are. Alternative micromechanics for ZPAL are also briefly discussed, as they could potentially allow the system to be extended all the way down to the x-ray regime.

6.1 Modeling the throughput of ZPAL

For a ZPAL system operating with CW radiation the only input parameters needed to model the entire behavior of the system are:

- λ, the wavelength of the radiation used
- OZW, the Outer Zone Width of the zone plates of the array. This parameter sets the minimum feature size that the system will be able to resolve.
- f_m, the operating frequency of the micromechanics.

- The number of grayscaling levels.
- V_{stage}, the stage velocity
- #ZPs, the maximum number of zone plates that can be manufactured with nearly indentical characteristics.

Subject to the constraints:

- Focal length of zone plates > Minimum tolerable gap
- Number of Zones > 40. Fewer than 40 zones seriously degrades the zone plate performance.

As discussed in Chapter 3, the Radius of a zone plate is given by

$$R_n^2 = n \cdot \lambda \cdot f + \left(\frac{n \cdot \lambda}{2}\right)^2 \tag{6-1}$$

where n is the total number of zones, λ is the wavelength, and f is the focal length of the zone plate. The area of a unit cell (this is the area each zone plate is responsible for exposing on the substrate) is then given by

$$\text{Unit Cell Area} = (2 \cdot R_n)^2 \tag{6-2}$$

which corresponds to the following number of pixels per unit cell

$$\text{\#Pixels/unit cell} = \frac{UnitCellArea}{PixelArea} = \frac{(2 \cdot R_n)^2}{\pi \cdot \left(\frac{OZW}{2}\right)^2} \tag{6-3}$$

where OZW is the outer zone width of the zone plates of the array. The time needed to expose one pixel is set primarily by the micromechanics response time. The real limit is the addressing time of the mirrors, as discussed in Chapter 4. To a smaller extent, the time needed per pixel is also determined by the stage velocity, since it takes some finite amount of time to travel from one pixel to the next. However, since the distance to be

traveled is of the order of hundreds of nanometers for UV-ZPAL, and given that stages today can travel at speeds in excess of hundreds of mm/s, the contribution of the stage response to the time needed to expose a pixel is negligible compared to the micromechanics addressing time. The total time per pixel, with the above approximation is

$$Time/_{Pixel} = \left(\frac{1}{f_{Micromirrors}}\right) \cdot \# \, of \, Grayscaling \, levels \qquad \textbf{6-4}$$

The total time to write the area underneath the zone plate array is given by

$$T_{ArrayArea} = \left(Time/_{Pixel}\right) \cdot \left(\# \, pixels/_{UnitCell}\right) \qquad \textbf{6-5}$$

Hence, to write an entire wafer of area A with a zone plate array that covers an area B of the wafer with its unit cells, the total time needed is

$$T_{Total} = T_{ArraySize} \cdot \frac{A}{B} \qquad \textbf{6-6}$$

The final expression for the total exposure time can be written as follows

$$T_{Total} = \left(\frac{\# GrayScalingLevels}{f_{Micromirrors}}\right) \cdot \left(\frac{4 \cdot \left(n\lambda f + \left(\frac{n\lambda}{2}\right)^2\right)}{\frac{\pi}{4} \cdot OZW^2}\right) \cdot \frac{WaferArea}{ArrayArea} \qquad \textbf{6-7}$$

but, given that

$$ArrayArea = \# ofZonePlates \cdot (2R_n)^2$$

and

$$WaferArea = \frac{\pi}{4} \cdot (WaferDiameter)^2$$

Equation 6- 7 can be simplified to

$$T_{Total} = \left(\frac{\#GrayScalingLevels}{f_{Micromirrors}} \right) \cdot \frac{WaferDiameter^2}{(OZW^2) \cdot (\#ofZonePlates)} \qquad \textbf{6-8}$$

The throughput in terms of wafers per hour is simply

$$Wafers/_{Hour} = \frac{3600}{T_{Total}} \qquad \textbf{6-9}$$

provided T_{Total} is in seconds.

By inspecting Equation 6- 8 it is easy to get a feeling of how the different parameters affect ZPAL's throughput. The frequency of the micromechanics and the number of zone plates both exhibit a linear behavior. Doubling them doubles the throughput, and so on. The number of grayscaling levels is inversely related to throughput. The remaining two parameters, the OZW (min. feature size) and the wafer diameter, are both quadratic. Decreasing the minimum feature size by a factor of 2 decreases the throughput by a factor of 4.

Figure 6- 1 analyzes the performance of a ZPAL system with some realistic numbers. The figure contains two contour plots of the number of wafers/hour that the system is capable of, as a function both the minimum feature size and the number of zone plates used. The only difference between figure (a) and (b) is the wafer size, which is 8" and 12" respectively. The numbers reflect a 4-bit grayscaling scheme and micromechanics with a 3.5 kHz frequency.

In reality there are only two parameters we can vary to increase the throughput of the tool, since the wafer size, the minimum feature size and the number of gray scaling level are fixed for a given technology node. If ZPAL is introduced into the semiconductor industry market to compete with other tools for the 180 nm feature size

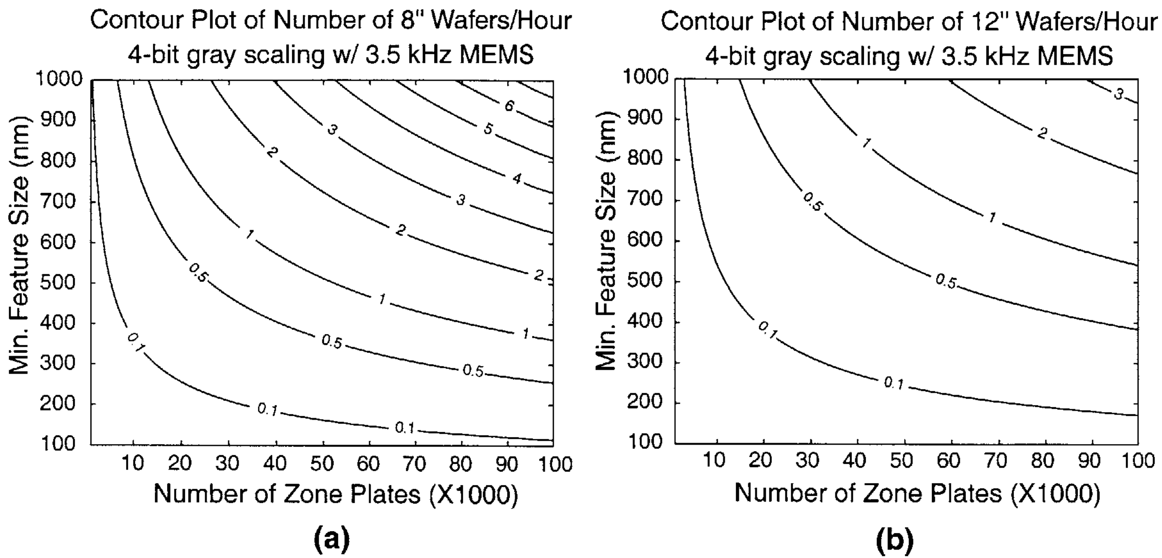

Figure 6- 1. ZPAL's throughput. (a) Contour plot of the number of 8" wafers per hour for a variety of feature sizes and number of zone plates. The numbers reflect a 4-bit grayscaling scheme and micromechanics with 3.5kHz frequency.(b) Same as (a) but wafer size is 12".

node, and current wafer sizes are 12", these parameters can not be varied to increase the throughput. The number of gray scaling levels could be varied only if the pattern that is to be written is exclusively composed of features that are either the OZW or multiples of it. In this particular case the number of levels would be one, and the throughput would increase by a factor of 4 compared to the numbers presented in Figure 6- 1. In general, at a minimum, 4 gray scaling levels will be needed.

All we can really do to increase the throughput is to either increase the number of zone plates, increase the addressing speed of the micromechanics, or a combination of both. Both of these parameters have the same linear effect on throughput, so a priori there is no clear path to follow. More careful analysis of what increasing these two parameters implies is needed to both understand the ultimate limits of the system, as well as to optimize the system performance based on the engineering cost of achieving these limits.

6.1.1 Increasing throughput by increasing the number of zone plates

It is apparent from Equation 6- 8 that for a given technology node we should always have the largest number of zone plates possible. The upper limit will be dictated by the need to have one micromechanical element per zone plate. The limit on the number of micromechanical units with current technology is close to 3 million (QXGA resolution). If we had such an array of zone plates with their corresponding micromechanics, at 0.25 μm resolution three 8" wafers/hour could be written. This would be an extremely attractive system if employed as a mask writer, since current systems take approximately 4 hours to write the equivalent of an 8" wafer. So why not do it?

The problem lies in the way zone plates are manufactured. In Chapter 3 the fabrication of zone plates was described in detail, explaining that the zone plate array had to be manufactured via e-beam lithography. While the ebeam is a versatile tool, it is inherently slow. State-of-the-art e-beams (MEBES systems manufactured by ETEC) can write at 160 MHz frequencies. The zone plates used for the results shown in this thesis were written with an ebeam that operated at a frequency of 0.2 MHz. The approximate writing time per zone plate was 5 minutes. If we used a MEBES system we could write them 200 times faster, in about 1.5 seconds (allowing for 4 passes to optimize linewidth control). Even at this speed, 3 million zone plates would take ~52 days to write. Were we to outsource the writing, at an approximate cost of $1000/hour of writing time, the zone plate array would cost ~$1.2M!. These numbers assume we are using PMMA as a resist, and although much faster resists could be used, the increase in throughput due to the use of such resists probably cancels out with the overhead needed to align each zone plate, which is being neglected. It is clear that these numbers are only very rough estimates, however, even if they are off by a factor of 2 or 3, the cost and writing time are still very high.

If the zone plates are to be written with an ebeam, arrays of 100x100 are probably the limit, with an estimated writing time of 48 hours. To increase the sizes of the array a

replicating technique is needed. A possibility is to have self-replicating arrays, that is, to write zone plate arrays with ZPAL using zone plate arrays. This will certainly be possible in the future, once the system is sufficiently characterized and proximity correction schemes done with gray scaling are implemented.

Another option that may be attractive is to make a mask and try to replicate it with contact printing or near field printing. Particle contamination is a great concern with this technique, since any particle trapped in between the mask and the wafer will distort the transferred pattern, making the array unusable. However, even with low yield, the cost could be sufficiently low as to make these techniques worthwhile. X-ray lithography is also a possibility, particularly when finer features are needed. However, the masks in x-ray lithography can be subject to significant distortions, especially if the area to be printed is large.

6.1.2 Increasing throughput by faster addressing of the micromechanics

Sections 4.3.1 and 4.3.2 of chapter 4 described in detail the electronic operation and the addressing scheme of the micromechanics of choice for ZPAL, the TI micromirror array. As a result of an improved addressing scheme, it was reported at the end of section 4.3.2 that soon a 3.5kHz array of 1024x768 mirrors will be released. The maximum rate at which the micromechanics could be operated is given by the mechanical response time of the mirrors, around 10 μs (100kHz frequency). This would correspond to a 28X increase in throughput for the numbers presented in Figure 6- 1.

An interesting idea is to realize that we might not need to wait for faster addressing schemes to be developed to get close to the limits of the micromirror's performance. The key to achieve this rather peculiar claim is to separate what the micromirrors are designed for, and what we intend to use them for in ZPAL. For the reasons explained in the previous section, it might be, at present, unreasonable to fabricate arrays of zone plates in excess of 100 by 100. TI manufactures the mirrors for displays, were the larger the number of mirrors, the better. Although ZPAL could

potentially, in the not so distant future, catch up with the array sizes manufactured by TI, for the moment a much smaller array of mirrors would suffice. As a matter of fact, an array of 100 by 100 would be as useful to ZPAL as an array of 1024 by 768. However, since we are not manufacturing the micromechanics, the later array is the only one that is available to us, even though we only plan to use a tiny part of it.

A possibility to drastically increase the throughput of ZPAL is the following. TI claims a 3.5 kHz rate provided you address the *entire array*. Since only $1/78^{th}$ of the array needs to be addressed (10,000 out of 786,000), if the addressing of the micromirrors could be sufficiently controlled as to deactivate the unused mirrors so that no data would have to be sent to them, the data rate for the 100x100 sub-array would increase dramatically. Rather simplistically, it could be argued that the addressing time would be 78 times faster than when the full array was being addressed. But even if this is not so due to the system architecture that loads the data of many areas of the array simultaneously, a 28 times increase is all that is needed to reach the limit of the micromechanics, so even if the increase is a factor of 3 slower than what is being assumed it would still be sufficient to reach the ultimate limit of the current micromirror technology.

The key point to realize is that the gain is the same in terms of throughput whether the number of zone plates are doubled or the addressing speed is doubled. However, doubling the number of zone plates is an enormous technological challenge, whereas doubling the addressing speed of the mirrors might be easily achieved with the idea just discussed above.

The remaining issue that needs to be solved prior to employing a scheme that drives the micromechanics close to the mechanical limit is the uniformity of the illumination of each zone plate as the mirrors are turned ON and OFF (Figure 6- 2). The ideal shape of the light pulse that illuminates a given zone plate is a square. A square pulse would imply that the percentage area of the zone plate receiving optical power would go from 0 to 100% instantaneously. However, because the mirrors reach the ON position gradually, through tilting, the shape of the pulse looks trapezoidal, as shown in Figure 6- 2 (a). As long as the time the zone plates sees a gradient of illumination across its area remains small compared to the time the mirror stays latched in the ON position,

there is nothing to worry about. However, as the addressing of the micromechanics becomes faster and faster, while the mechanical response remains constant, the light pulse that the mirror produces will look more and more triangular, as show in Figure 6- 2 (b). As a consequence, the zone plate's area is only 100% illuminated a very short amount of time, and the time duration for which the zone plates only sees partial illumination can no longer be ignored. The focused spot of a zone plate under such illumination is likely to be highly astigmatic, if a spot is produced at all.

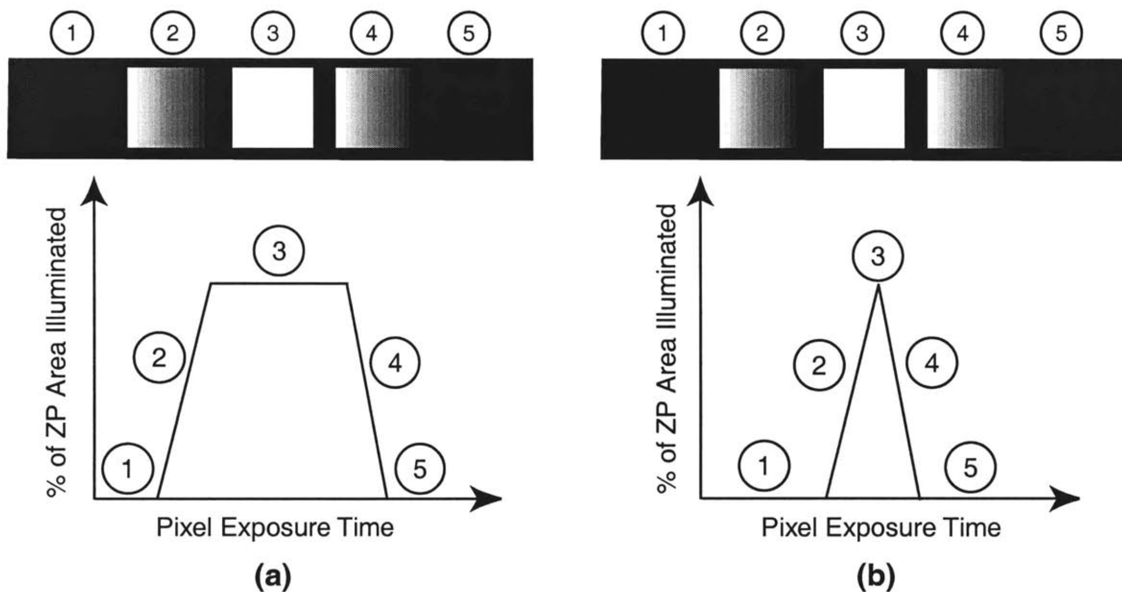

Figure 6- 2. Zone plate illumination uniformity. (a) Micromechanics are not driven close to the limit. The time it takes for the mirrors to reach the ON position is small compared to the time it stays ON. The non-uniformity of the illumination as the transition occurs has little impact on the zone plate's performance. (b) Micromechanics driven to the limit. The zone plate only sees uniform illumination (3) for a very brief period of time. The shape of the light pulse no longer looks square, producing deleterious effects on the zone plate's performance.

The fact that the mirrors stay ON for a very short amount of time is not really problematic, provided we have a laser powerful enough to provide enough photons to expose the resist when focused by the zone plate. It is very unlikely that with current laser technology this will ever become a problem for ZPAL. The problematic issue that

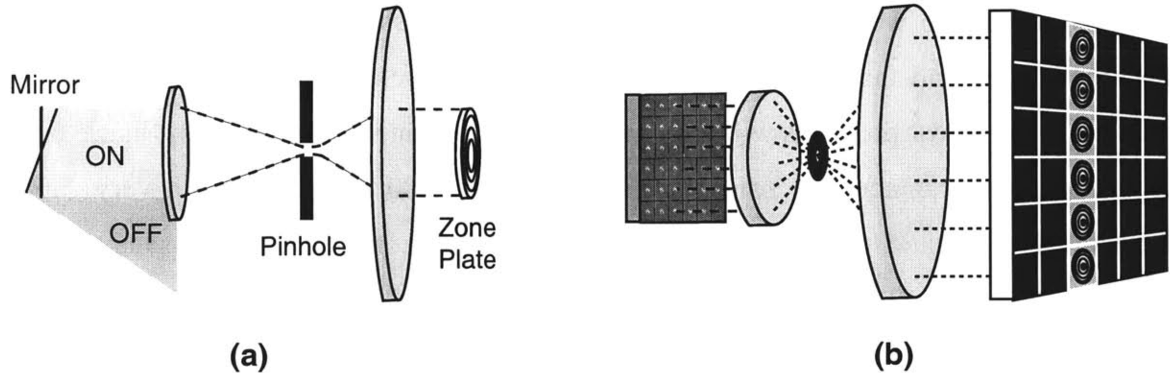

Figure 6- 3. Optical solution to zone plate illumination non-uniformities. (a) A pinhole placed in the optical axis of the system prevents radiation from all but the ON positions of the micromirrors to reach the zone plate array. (b) Implementation for an entire array of micromirrors.

needs to be resolved is the slope of the pulse shape, since it causes the zone plates to be partially illuminated during ON-OFF transitions. Figure 6- 3 illustrates a possible solution to this problem. The idea is to place a pinhole between the micromirrors and the zone plates, so that only when the mirrors latch completely to the ON position (point 3 in Figure 6- 2) will the light reflected off them pass though the pinhole. Figure 6- 3 (a) depicts such an implementation for a single mirror to zone plate system. It is clear that while the mirror is traveling from the OFF to the ON position the lens will focus the radiation to a spot that is off the optical axis. Hence, the pinhole will block the light. Only light reflected from the ON position of the mirrors will make it through the pinhole, allowing the light pulses reaching the zone plates to recover the desired square shape .

6.2 Extendibility of ZPAL: The move to shorter wavelengths

An exciting feature about zone plates is that, with proper design and fabrication, they will work at *any* wavelength. This fact could potentially extend the technology all the way down to x-ray wavelengths, allowing ZPAL to print features as small as 25 nm. This is, of course, provided the rest of ZPAL's components are compatible with radiation of such short wavelength. Leaving aside the issue of EUV and x-ray sources with enough

power to achieve decent throughput, the limiting component will once again be the micromechanics.

X-rays exhibit very strong absorption for all materials, and will only be able to be reflected off multilayer coatings (as in EUV lithography) or mirrors at glancing angle. If the micromechanics of choice are the micromirrors manufactured by TI, the protecting packaging in which they are enclosed will have to be removed, decreasing the reliability of the micromechanics due to stiction and particle contamination. There are other products in the market that would make the issue of packaging less relevant. In particular, the Daewoo Electronics manufactures a Thin-film Micromirror Array (TMA) [56] that is piezoelectrically actuated, circumventing the packaging problem, since the activation mechanism allows enough force to be provided to each mirror to overcome the stiction force that all MEMS structures exhibit when in contact with another surface.

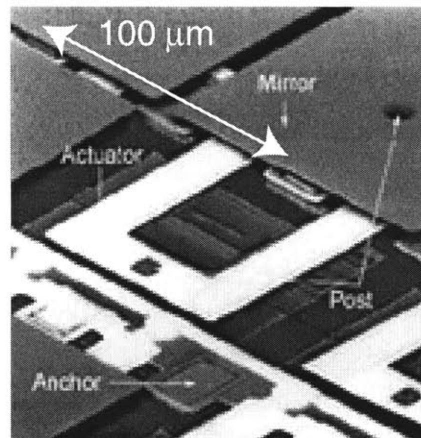

Figure 6- 4. Thin-film micromirrors manufactured by Daewoo Electronics

The micromachined thin-film piezoelectric actuators (Figure 6- 4) allow for the control of the tilt angle of each micromirror. Although the Daewoo mirrors might solve the packaging problem, making them a better choice for x-ray ZPAL, there is still the problem of aligning the micromirrors to the zone plates. This alignment would prove to be daunting, since there is no easy way to check when the radiation reflected off the mirrors is hitting the zone plates.

A much more desirable approach would be to have shutters directly above the zone plate array, as depicted in Figure 6- 5. Shutters would make the alignment problem

much easier, since they simply would have to be placed on top of the zone plate array once and for all. Since the features to be aligned have sizes in excess of 10 μm, the alignment could probably be done even with a simple setup comprised of an optical microscope and some good translation stages.

Such microshutters have been manufactured at Lincoln Laboratory by Dr. Carl Bozler [57], and like the micromirror arrays, the objective is to use them for displays.

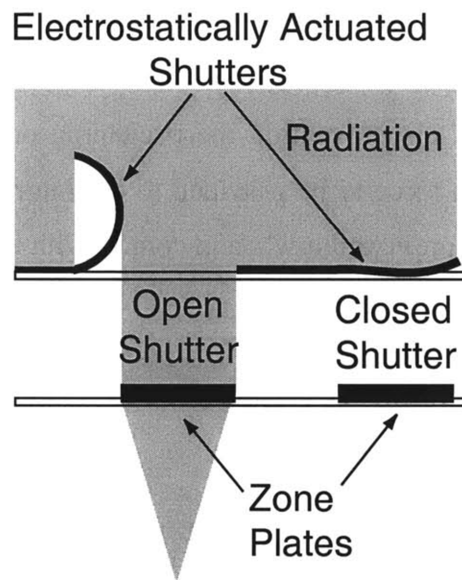

Figure 6- 5. Shutters for ZPAL as multiplexing elements

The principle of operation of the shutters is the following. A thin transparent conducting layer is formed on top of a transmissive substrate (glass or quartz). After defining the electrodes that will activate each shutter, an overlying coilable electrode is formed (the shutter). This electrode is formed by depositing and patterning successive layers of: 1) a low stress insulating film, 2) a conductive film having compressive stress and 3) a compressive film having tensile stress. The difference in stresses of the three layers causes the electrode to curl in a preferential direction. In a sense the coiling can be thought as a mechanical bias, a position of minimum energy. If a voltage is applied between the coilable electrode (shutter) and the electrodes placed on the substrate, the shutter will uncoil itself and lie flat on the substrate, as a result of a capacitive force.

The voltage needed to activate the shutters ranges from 1 to 50 V. Figure 6- 6 shows two scanning electron micrographs of the shutters built by Dr. Bozler.

The shutters would need a certain number of modifications were they to be utilized for ZPAL at x-ray wavelengths. First, the substrate on which they are fabricated would either have to be a thin membrane, or holes would have to be made under the area

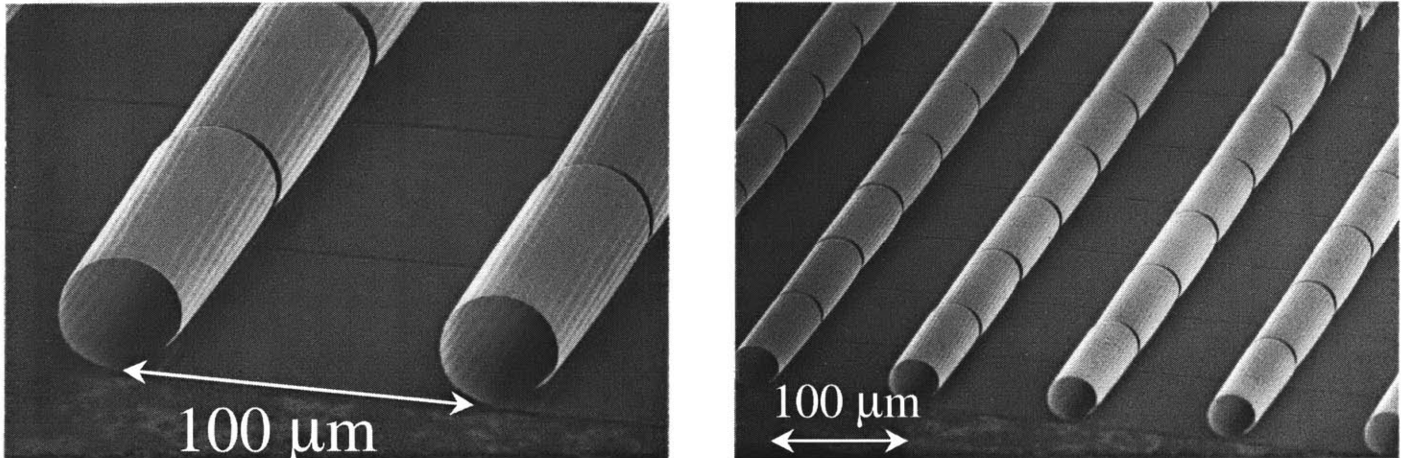

Figure 6- 6. Scanning electron micrographs of MIT Lincoln Labs Shutter Arrays.

the shutters cover to allow the radiation to propagate without extreme attenuation. In addition, to close pack the zone plates as much as possible, the shutters would have to be reduced in size from 100 μm to approximate 10 μm, the typical diameter of an x-ray zone plate.

In conclusion, if appropriately modified to allow for x-ray transmission, the shutters present an exciting possibility that will allow maskless parallel patterning with ZPAL to be extended all the way down to the limits of the lithographic process.

Chapter 7

Conclusions and Future Work

The objective of this thesis was to design and build a fully functional Zone-Plate-Array-Lithography setup that would operate with UV radiation. Four different arrays of 3x3 zone plates were designed for λ=442 nm, and manufactured in house via electron-beam lithography. The zone plates were tested and integrated in a ZPAL system that included the micromechanics needed to provide independent illumination to each zone plate of the array. Extensive optimization of the system was performed to integrate all the four major components, the laser, the micromechanics, the zone plates and the scanning stage, to successfully write patterns at the expected resolution. For the first time, maskless parallel patterning of features of arbitrary geometry was achieved with an array of zone plates [58]. Excellent patterning capabilities were demonstrated, proving the soundness of the technology. In addition, a parallel confocal microscope employing the same array of zone plates used for exposing patterns was built, and images were taken with it. The microscope adds great functionality to the system, enabling accurate gapping and parallelization of the zone-plate array to the wafer, as well as providing the possibility of level-to-level alignment.

ZPAL has the potential to truly revolutionize lithography. It could do so by departing from century-old optical technologies that rely on massive, expensive, lens stacks. ZPAL, as a substitute, offers *optics on a chip*. Arrays of diffractive optical elements that can be fabricated with planar technology, and hence with great accuracy, will allow the replacement of multimillion dollar optical columns currently used in lithography steppers. Equally exciting is the fact that masks will no longer be needed with such a system.

Despite all the current hype, it is important to realize that there is nothing new about maskless lithography. Electron beam lithography is maskless too, and it has been around for many decades. It is used by researchers all over the world to produce fascinating devices that lead the way into important advances in technology. However, it is slow and costly. Apart from ebeam, researchers at universities generally only have traditional optical aligners to do lithography, which not only require masks, but usually have severe limitations in terms of resolution, rarely getting below 1 μm. And then there is the semiconductor industry, with its incredible resources. They can build devices all the way down to 180 nm, a number that will be outdated probably by the time this thesis is finished. However, since the concern is to a great extent throughput, the cost of the tools have skyrocketed, making them completely inaccessible to all but a handful of mega-corporations.

At the same time the field of nanotechnology is exploding, with many people believing it is the wave of the future. It is almost impossible to define what is meant by such a vague term as nanotechnology, since it ranges from work done in chemistry, to molecular biology to electrical engineering. However, almost philosophically, one has the conviction that being able to control the nanometer domain of the world we live in will prove itself to be extremely useful. Lithography provides an excellent means to control such dimensions.

To explore applications at the sub-micron regime researchers will need the tools to do so, but they can *not* be at any cost. Prohibitive costs of tools hinders innovation, and that is the biggest price to be paid. ZPAL has as its objective to bridge the existing gap, by providing a fast, high resolution, economical solution.

Much work needs to be done for this worthy goal to be achieved. There are some key elements of the technology that need to be tested, in particular the fabrication of order-sorting apertures to improve contrast, and the implementation of a proximity correction scheme by means of gray scaling. Large array of zone plates need to be fabricated by means of Spatial-Phase-Locked-Electron-Beam Lithography (SPLEBEL) [54], and mass fabrication techniques for reproducing zone plate arrays should be explored.

At the same time, it seems logical to move to shorter wavelengths to increase the resolution of the system. Below 260 nm there is no source of CW light, so the radiation employed will have to be pulsed if a laser is to be used. A whole different set of issues might arise then, particularly due to the power fluctuations between pulses. In terms of proving the absolute limits of the technology, the x-ray setup that is currently being built should enable us to prove the extendibility of ZPAL, even if currently there is no micromechanical solution for such short wavelengths.

There is plenty of exciting and very meaningful work to be done with ZPAL in the following years. The author can not feel but privileged to be a part of it.

Appendix A

UV Zone Plate Fabrication

Equipment Needed

- Hood Space for Solvent and Aqueous Processing
- Spinner
- Ebeam evaporator
- Oven at 180° C
- Electron Beam Lithography System - VS-2A
- Plasma Asher
- UV-Ozone cleaner station
- Reactive Ion Etcher
- Scanning Electron Microscope and Optical Microscope

A.1 Preparing the substrates

- Choose the substrate in which the zone plates are going to be written. The substrate obviously has to be transmissive for the wavelength the zone plates are going to be used for. At UV wavelengths quartz works really well. A double side polished 3" - 1/2 mm thick quartz wafer was used for the experiments presented in this thesis. It is a good idea to run the process with at least 3 quartz wafers and a Si monitor wafer.

One of the quartz wafers will be used to test etch rates, and the other will serve as a backup.

- Clean the wafer surfaces by immersing them in RCA organic clean solution (5:1:1 DI water:hydrogen peroxide:ammonium hydroxide, at 80°C) for 15 min.

- Calculate how much Cr will be needed to attenuate all the undesired radiation (see Chapter 3 -Section 3.3.1). For 442 nm radiation, 87 nm of Cr is sufficient. Evaporate the Cr via an e-beam evaporator onto two of the quartz wafers and the Si wafer.

- Spin coat 250 nm of 3.5% PMMA on all three quartz wafers. A spin curve for 3.5% PMMA is shown in Figure A- 1

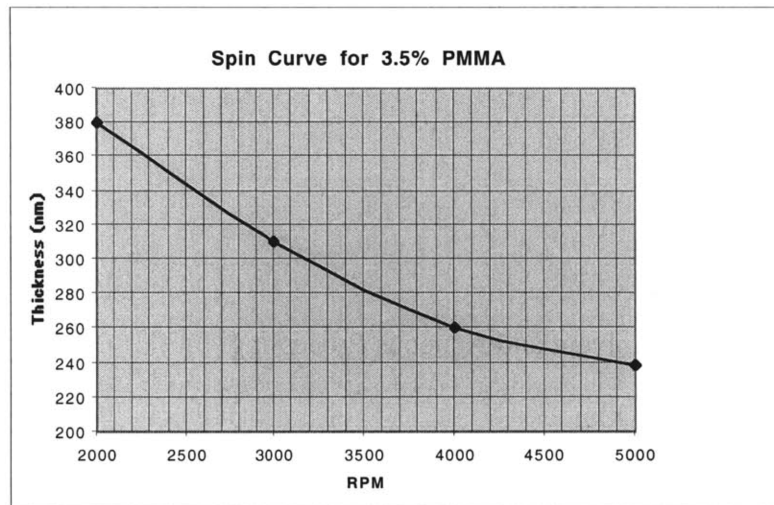

Figure A- 1. Spin curve for 3.5% PMMA

- Bake the wafers in an oven for 60 min at 180°C

A.2. First Ebeam write

- Login Nanoweb via **trajan.mit.edu** and access the following directory: ~/dgil/Zoneplates. Have ready the design parameters of the zone plates. In particular, the wavelength λ, the number of zones N, the outer zone width (OZW) and the E-beam field size will be needed. The ebeam field size should be big enough to accomodate one zone plate. It also depends on how close packed the zone plates are going to be in case an array is being fabricated. The program that generates the code to write the zone plates on the ebeam is **zp.c**. To compile it type:

    - >cc -o zp zp.c

This will generate an executable called **zp.** Run the program by typing

- >./zp

Provide the inputs demanded. As an example, lets run it for a zone plate with λ=442nm, N=76, OZW=336 and e-beam field size = 150 μm. It will look as follows.

Input wavelength lambda (nm)? 442
Input outer zone width (nm)? 336
Input number of zones N? 76
f = 50.935745 um, RN = 44.644585 um, dof = 382.533630 nm

Is this ok? 1 (Type 1 if satisfied or 0 if not)
Input field size(um)? 150

At this point the program has generated two files. One is called **ap.pat** and the other **zp.pat**. **ap.pat** generates the outer circles where the zone plates will later be placed. This step is needed to be able to selectively cover with Cr the areas of the wafer that don't have zone plates (see Chapter 3 Section 3.3.1). **ap.pat** will generate the commands for the ebeam to write 1 big circle at the center of the field whose size is the diameter of the zone plates, and 4 alignment marks (squares) at the edges of the ebeam field. **zp.pat** will be used later, and contains the commands to write the actual zones of the zone plates.

For the first ebeam write only **ap.pat** is needed. Convert to **vsx** file format by typing

- >./pat2vsx ap.pat ap.vsx

Take the file **ap.vsx** to the VS-2A and use **Ihsan's** version of the code. This is VERY important, since the other versions can NOT write circles. The VS-2A is maintained by Mark Mondol.

- Layout in VS-2A the dimensions of the array. Write the file on one of the quartz wafers with Cr + PMMA on it.

- Develop PMMA. Mix the developer (1:2 MIBK:IPA) in a beaker big enough to fit the wafer. The temperature should drop to 16°C upon mixing. The developing temperature is 21°C. To get to this temperature warm beaker with hands while monitoring the temperature. Have the beaker covered to prevent the evaporation of MIBK. Develop for 90 sec.

- Rinse for 60 sec with IPA + 60 sec H_2O.

- UV-ozone clean the wafer. Warm the cleaner for 60 sec, put wafer in for 10 sec.

- Rinse with H_2O for 60 sec.

- Remove the Cr that is inside the circles just created via a wet etch (CR-7 - Chromium photomask etchant). To calculate the time needed, test it with the Si wafer that has the Cr on it. ~45 sec should be sufficient for the quartz wafer. Agitate while etching.

- Strip PMMA. Soak for 10 min in Acetone (or 5 min on the Plasma Asher). Rinse with IPA for 1 min, then H_2O for 1 min.

A.3 2nd ebeam write

- Spin 250 nm of PMMA as previously indicated.

- Evaporate 5 nm of Cr. Needed to provide a conductive layer for the ebeam write.

- Use the file previously generated, **zp.pat**, to write the zones of the zone plates. This is an aligned ebeam write. To convert the **zp.pat** to **vsx** format, from the same directory in Trajan previously mentioned type:

  - >./pat2vsx zp.pat zp.vsx

  Take the file **zp.vsx** to VS-2A and write the file.

- Remove the 5 nm of Cr via a wet etch (CR-7 - Chromium photomask etchant). 15 s should suffice.

- Develop PMMA as previously described.

- Rinse for 60 sec with IPA + 60 sec H_2O

- With the spare quartz wafer do test runs on the RIE to calculate how much power is needed to etch the desired depth for a π phase shift (see Chapter 3, Section 3.3.1) if phase zone plates are being fabricated. The etchant is $CH\ F_3$, and there is a process for it in Ihsan's directory (the only one in there) on the inner lab RIE. To test it, put some pattern on the dummy quartz wafer and monitor the etch. Table A- 1 and Figure A- 2 show the etch rates obtained. The process will etch in 35-sec steps, then cools down, then etch again for 35 sec, and so on. The power numbers given are the sum of the average power that was delivered on each of the etching steps.

Power	Etch Depth (nm)
5027	325
7319	425
8267	548

Table A- 1. Etch depths for quartz w/ $CH\ F_3$

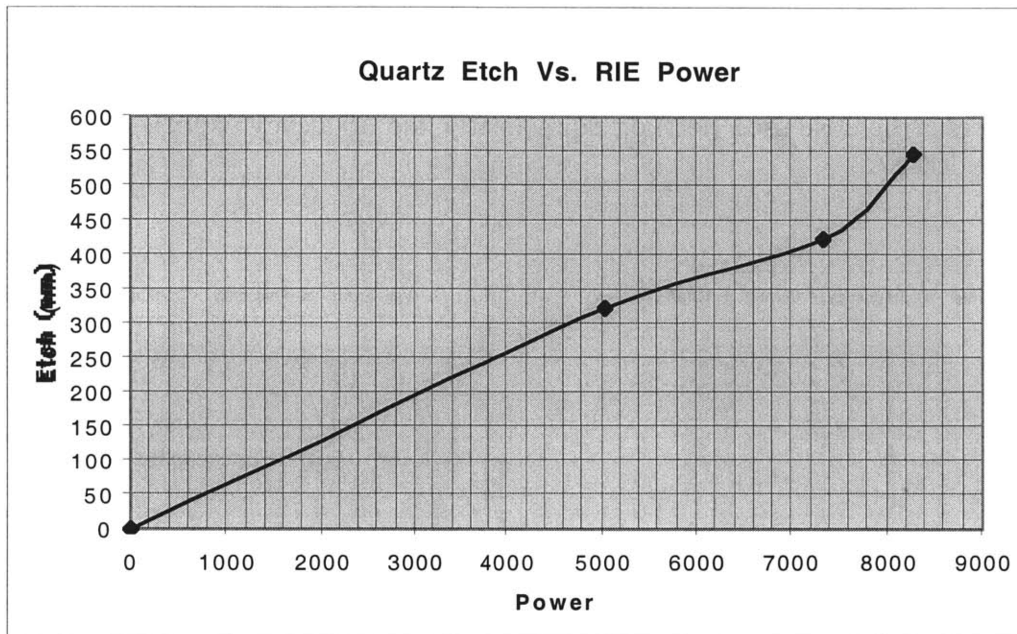

Figure A- 2. Quartz etch depths w/ CHF_3 for inner lab RIE

- Etch the real sample. Run a warm up dummy Si wafer prior to the real run.
- Remove the PMMA as previously indicated.

A.4. Covering the alignment marks

- The alignment marks used for the aligned ebeam write need to be covered. Spin resist (Shipley 1813 for example) on the sample. Selectively expose with the optical microscope the areas that need to be covered (4 squares per zone plate).
- Develop resist. Check with microscope (use filter to avoid exposure) to see if the exposure was successful.
- Evaporate 87 nm of Cr to cover the alignment marks.
- Liftoff to get rid of the resist with the unwanted Cr on top of it.

A.5 Ebeam errors statistics

- Prior to doing the real run, the ebeam writing of the zones of the zone plates needs to be characterized. This characterization will involve choosing the e-beam frequency, and the biasing of the zones. Close to 100 zone plates were measured with different zone widths and written with different doses. As a summary, Figure A- 3 plots the average errors (deviation from the desired zone widths to the measured widths via SEM) versus the dose used (left) or, equivalently, the frequency (right). The current used was 100 pA.

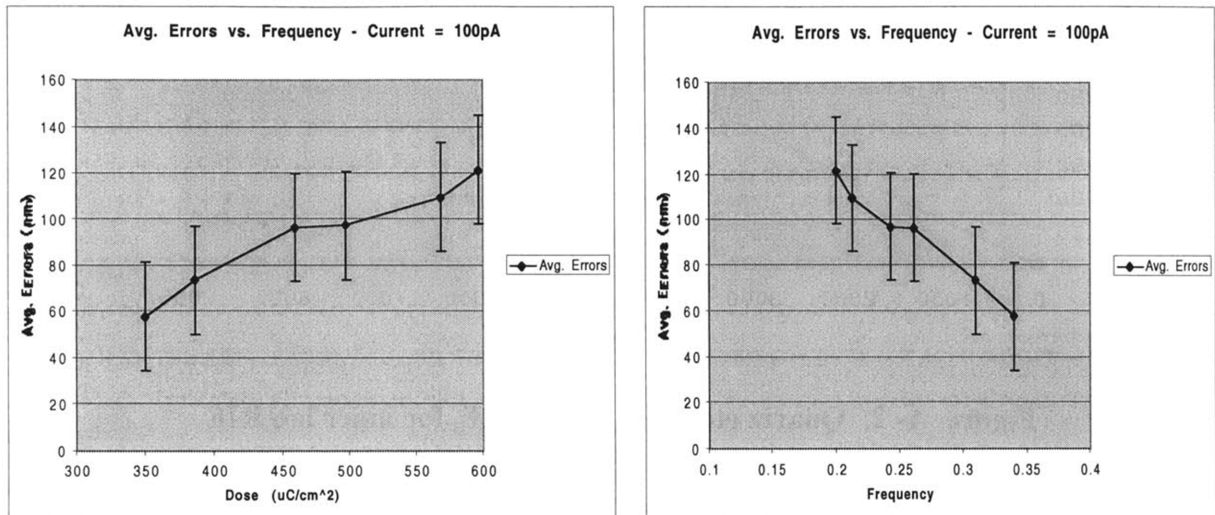

Figure A- 3. Average ebeam errors encountered while writing zone plates

References

[1] H.I,Smith. "Robust Sub-100 nm Maskless Lithography with Sub-1nm Accuracy", Proposal to The Army Research Office, 1998

[2] H.I. Smith, "A Proposal for Maskless, Zone-Plate-Array Nanolithography," J. Vac. Sci. Technol. B 14, 4318-4322 (1996).

[3] M.L. Schattenburg, E.H. Anderson, and H.I. Smith, "X-ray/VUV Transmission Gratings for Astrophysical and Laboratory Applications", Physica Scripta 41, 13-20 (1990).

[4] M.H. Lim, T.E. Murphy, J. Ferrera, J.N. Damask and Henry I. Smith, "Fabrication Techniques for Grating-Based Optical Devices", J. Vac. Sci. Technol. B, 17(6), 3208-3211 (1999).

[5] National Institute of Standards and Technology (NIST), Advanced Technology Program. http://www-15.nist.gov/atp/97wpm212.htm

[6] G.E.Moore, "Cramming More Components onto Integrated Circuits", Electr.Mag., 114 (19 April 1965)

[7] Semiconductor Industry Association, National technology roadmap for semiconductors. Available at: http://www.itrs.net/ntrs/publntrs.nsf

[8] E.Spiller, Soft X-Ray Optics, pg. 5, SPIE, Bellingham, WA, 1994.

[9] E.Spiller, Soft X-Ray Optics, pg. 140, SPIE, Bellingham, WA, 1994.

[10] J.Bjorkholm, "EUV Lithography-The Successor to Optical Lithography?", Intel Technology Journal Q3, 1998.

[11] E.Spiller, Soft X-Ray Optics, pg. 185, SPIE, Bellingham, WA, 1994.

[12] Semiconductor Industry Association, Next Generation Lithography Workshop, Colorado Springs, Colorado. December 8-10, 1998. Available at: http://www.sematech.org/public/resources/coo/index.htm

[13] Sandia National Laboratory Lab News, Sept. 26,1997.

[14] Gwyn CW, Stulen R, Sweeney D, Attwood D, " Extreme ultraviolet lithography", J. Vac Sci. Technol. B,16: (6) 3142-3149 NOV-DEC 1998

[15] J.M. Gibson and S.D.Berger, Appl.Phys.Lett. 57, 153 (1990)

[16] M. McCord, "Electron beam lithography for 0.13μm manufacturing", J.Vac Sci. Technol. B 15(6), Nov/Dec 97

[17] H.Yasuda, S.Arai,J. Kai, Y. Ooae, T. Abe, S. Maruyama, and T.Kiuchi, J.Vac. Sci. Technol. B 14, 3813 (1996)

[18] T.H.P. Chang, M.G.R. Thomson, E. Kratschmer, H.S. Kim, M.L. Yu, K.Y. Lee, S.A. Rishton, and B.W. Hussey,"Electron-beam microcolumns for lithography and related applications", J.Vac. Sci. Technol. B 14, 3774 (1996)

[19] D.L. Spears and H.I. Smith, "High-Resolution Pattern Replication using Soft X-rays", Electronics Lett. 8, 102-104 (1972).

[20] D.L. Spears and H.I. Smith, "X-ray Lithography: A New High Resolution Replication Process", Solid State Technol. 15, No. 7, 21-26 (1972).

[21] D.Attwood, *Soft X-rays and Extreme Ultraviolet Radiation*, pg. 408, Cambridge University Press, 1999.

[22] H.I. Smith, M.L. Schattenburg, S.D. Hector, J. Ferrera, E.E. Moon, I.Y. Yang, and M. Burkhardt, "X-ray Nanolithography: Extension to the Limits of the Lithographic Process", Microelectronic Engineering 32, 143-158 (1996).

[23] L.E.Ocola and F.Cerrina, J.Vac. Sci. Technol. B 12, 3986 (1994)

[24] H.I.Smith, J.Vac. Sci. Technol. B 13, 2323 (1995)

[25] D.Attwood, *Soft X-rays and Extreme Ultraviolet Radiation*, pg. 410, Cambridge University Press, 1999.

[26] S.Subbana et al., IEDM Tech.Digest, 695 (1994)

[27] R.DellaGuardia et al.,Proc. SPIE 2437, 112 (1995)

[28] Y.Nishioka et al., IEDM Tech Digest, 903 (1995)

[29] S.J.Wind et al., J.Vac. Sci. Technol. B 13, 2688 (1995)

[30] K.Sunouchi et al., IEDM Tech Digest, 601 (1996)

[31] I. Djomehri, T. Savas, and H.I. Smith, "Zone-Plate-Array Lithography in the Deep Ultraviolet", J. Vac Sci. Technol. B, 16(6), 3426-3429, Nov/Dec. (1998).

[32] I. Djomehri, "Zone Plate Array Lithography in the Deep UV", M. S. Thesis, Department of Electrical Engineering and Computer Science, MIT, September,1998.

[33] Kearney P.D., Klein A.G., Opat G.I., Gahler R, Nature, Vol. 287, pp 313-314, September 25, 1980.

[34] H.I.Smith and D.C.Flanders, "X-ray lithography- A review and assessment of future applications," J.Vac.Sci.Technol. 17, pp. 533-535, 1980.

[35] H.I.Smith and D.C.Flanders, "X-ray lithography- A review and assessment of future applications," J.Vac.Sci.Technol. 17, pp. 533-535, 1980.

[36] *Euvres Completes d'Augustin Fresnel*, Vol. 1, Note 1, pp. 365-372 (1886)

[37] E.Hecht, Optics, Addison-Wesley Publishing (1987)

[38] Myers Jr, Ora E., American Journal of Physics, Vol. 19(6), pp. 359-365 (1951).

[39] Baez, Albert V., Journal of the Optical Society of America, Vol. 51(4), pp. 405-412, April 1961

[40] Spiller, E, Soft X-Ray Optics, pp 90-91,SPIE Press, 1994

[41] D. Carter, "Sub-50 nm X-ray Lithography with Application to a Coupled Quantum Dot Device", pp.51, Ph.D. Thesis, EECS, MIT, June 1998.

[42] C.J.Buckley, A.G.Michette, X-Ray Science and Technology, pp 335-336, Inst. Of Physics Pub, 1993

[43] C.J.Buckley, A.G.Michette, X-Ray Science and Technology, pp 312-313, Inst. Of Physics Pub, 1993

[44] E.H.Anderson, "Fabrication and Electromagnetic Applications of Periodic Nanostructures", pp 100-104, Ph.D. Thesis, 1988, MIT.

[45] Digital Light Processing World Wide Web site: http://www.ti.com/dlp

[46] TI Technical Journal, White Papers. Available at: http://www.ti.com/dlp/resources/whitepapers/tech/dlpmems.shtml

[47] TI Technical Journal, White Papers. Available at:
http://www.ti.com/dlp/resources/whitepapers/pdf/ieeeir.pdf

[48] C. Tew et al., "Electronic control of a digital micromirror device for projection displays," 1994 IEEE Solid-State Circuits Digest of Technical Papers, Vol. 37, p.130 (1994)

[49] TI Technical Journal, White Papers. Available at:
http://www.ti.com/dlp/resources/whitepapers/tech/over.shtml

[50] M.Minsky, US patent 3,013,467 (19 Dec 1961, filed 7 Nov. 1957).

[51] H.J.Tiziani, R.Achi, R.N.Kramer and L.Wiegers, "Theoretical analysis of confocal microscopy with microlenses." *Appl. Opt.* **35**(1). 120-125 (1996).

[52] Phisik Instrumente.
http://www.physikinstrumente.com/pztflexurenanopositioners/index.html

[53] H.J.Tiziani, M. Wegner, D. Steudle, "Confocal principle for macro and microscopic surface and defect analysis", Opt.Eng ,39(1) 32-39, Jan 2000

[54] H.I.Smith, S.D.Hector, M.L Schattenburg, and E.H.Anderson," A New Approach to High Fidelity E-Beam Lithography Based on an In-Situ, Global Fiducial Grid", J.Vac.Sci.Technol. B 9, 2992-2995 (1991)

[55] H.J.Tiziani, R.Achi, R.N.Kramer, T.Hessler, M.T.Gale, M.Rossi, and R.E.Kunz."Microlens arrays for confocal microscopy," *Opt.Laser. Technol.* **29**(2), 85-91 (1997)

[56] S.G.Kim, K.H.Hwang, Y.J.Choi, Y.K.Min, and J.M.Bae, "Micromachined Thin-Film Mirror Array for Reflective Light Modulation," *Annals of the CRI,* Vol.46, No.1, pp.455-458, 1997

[57] Carl O. Bozler, Steven Rabe, U.S.Patent 5,959,763, September 28, 1999

[58] D.J.D. Carter, D. Gil, R. Menon, M. Mondol and Henry I. Smith, "Maskless, Parallel Patterning with Zone-Plate Array Lithography (ZPAL), J. Vac. Sci.Technol. B 17(6) 3449-3452 (1999).